

UC Riverside

UC Riverside Electronic Theses and Dissertations

Title

The Dynamic Influence Toxoplasma Gondii has on the CNS, and the Recruitment of Protective T Cells to the Inflamed Brain

Permalink

<https://escholarship.org/uc/item/2kv0k86p>

Author

Vizcarra, Edward Alexander

Publication Date

2022

Peer reviewed|Thesis/dissertation

UNIVERSITY OF CALIFORNIA
RIVERSIDE

The Dynamic Influence *Toxoplasma Gondii* has on the CNS, and the
Recruitment of Protective T Cells to the Inflamed Brain

A Dissertation submitted in partial satisfaction
of the requirements of the degree of

Doctor of Philosophy

in

Biomedical Sciences

by

Edward Alexander Vizcarra

September 2022

Dissertation Committee:

Dr. Emma H Wilson, Chairperson

Dr. Meera Nair

Dr. Marcus Kaul

Copyright by
Edward Alexander Vizcarra
2022

The dissertation of Edward Alexander Vizcarra is approved by:

Committee Chairperson

ACKNOWLEDGMENTS

Chapter 2 includes data and analysis from an unpublished manuscript that was generated by myself, Dr. Arzu Ulu, and by Dr. Michael White and his lab members. For this project I would also like to acknowledge the Le Roch lab for providing us equipment and guidance in the generation of the single cell RNA-sequencing data.

I would like to thank and acknowledge Dr. Tyler A. Landrith for setting the foundations of the T cell aspect of my thesis. He discovered that a population of mGluR-expressing T cells exist in the *T. gondii* infected brain. Although the paper is in the process of being submitted, I would like to thank and acknowledge all of my co-authors for their contributions to this manuscript: Dr. Tyler A. Landrith, Xinru Qiu, Dr. Adam Godzik, and Dr. Emma H. Wilson

Chapter 4 includes unpublished work focusing on an aspect of addressing the question, “What leads to astrocytic glutamate transporter-1 downregulation?” I would like to thank and acknowledge our undergraduate researcher, Mike Akaraphanth, who provided substantial support in generating figures, analysis, and writing of the manuscript. I appreciate all of the time and effort he put into helping me in grad school.

DEDICATION

This dissertation is foremost dedicated to my ancestors who all wanted nothing but the best for the subsequent generations. I want to thank all of my family who has supported me throughout my life, but especially during the “grad school years.” I would not have finished without your encouragement.

I want to thank my beautiful wife, Dr. Esteffi Guardado, for all of the love and therapy sessions she has given me. Especially during the hardest times of grad school. I look forward to a fruitful future with you!

I want to thank my mentor Dr. Emma Wilson for her mentorship during my time in her lab. I am a better scientist and lab member for having been guided by you. You created a safe and nurturing place for me to grow as a scientist, and for that, I will be a better mentor to the next generation of scientists.

To Dr. Nair, thank you for being a great co-sponsor and investing time into my future. I also appreciated our random unscheduled meetings in the hallway catching up.

To Dr. Kaul, thank you for the guidance you have provided me over the years, and your insightful questions. Also, thank you for being a huge supporter of students.

Thank you to all of the supportive students I have met while at UCR, but especially to Dr. Joe Valdez and Paula Da Silva Frost. I enjoyed starting “Welcome to Grad School” with you. Those experiences go into the grad school memory box.

Finally, I would like to thank UCR’s SOM/ BMSC Program for giving me resources to make my science better, and the opportunities to grow as a person at both a personal and professional level. What I have learned at UCR will allow me to be successful wherever I go.

ABSTRACT OF THE DISSERTATION

The Dynamic Influence *Toxoplasma Gondii* has on the CNS, and the Recruitment of Protective T Cells to the Inflamed Brain

by

Edward Alexander Vizcarra

Doctor of Philosophy, Graduate Program in Biomedical Sciences
University of California, Riverside, September 2022
Dr. Emma H. Wilson, Chairperson

Toxoplasma gondii (*T.gondii*) is the most prolific parasites in the world infecting 30% of the human population. The encystment of the parasite in CNS-neurons results in a lifelong chronic infection. Infection with this pathogen poses the greatest risk-threat to immunocompromised individuals, where parasite recrudescence can lead to lethal toxoplasmic encephalitis. However, it is unclear what is the developmental biology of the parasite upon reawakening from its dormant state, and if infected host cells influence their differentiation process.

Within the brain, a pro-inflammatory response is essential to prevent parasite reactivation. However, an anti-inflammatory response is also required to prevent inflammation-induced mortality, suggesting a balanced immune response. Additionally, infection in the immunocompetent experience asymptomatic infection, further pointing to a tightly regulated immune response in the CNS. However, it is unclear what are the tissue-derived signals that maintain this

delicately balanced immune response. This dissertation investigates these unknowns in the follow ways:

Chapter 1 is an introduction to *T. gondii* infection and the effects the parasite has on the host. Topics covered in this section include the life cycle and the immune response to *T. gondii*. This encompasses evasion strategies by the parasite, and signals that are required for protective immune cells to traverse the blood brain barrier. This chapter ends on describing the role astrocytes play in the CNS, and the implications of *T. gondii* infection on glutamate regulation. Chapter 2 describes the attempts that have been made to study recrudescence of tissue cysts. This chapter poses a new *ex vivo* model of bradyzoite-initiated development that better preserves the key attributes of the parasite's intermediate life cycle. In chapter 3, we discuss elements found in the CNS-microenvironment during chronic *T. gondii* infection, and consider how tissue-derived signals, such as high extracellular glutamate, influence protective CD8 T cells. Chapter 4 explores a potential mechanism that leads to the downregulation of astrocytic GLT-1 in *in vitro* cultures. Finally, chapter 5 summarizes topics discussed in previous sections, and highlights my contributions to the fields of neuroimmunology and parasitology. Furthermore, this chapter emphasizes work that still needs to be done and avenues that are yet unexplored.

TABLE OF CONTENTS

LIST OF FIGURES	ix
CHAPTER ONE	1
1.1 The Life Cycle of <i>Toxoplasma Gondii</i>	2
1.2 The Immune Response to <i>Toxoplasma Gondii</i>	3
1.3 CD8 ⁺ T Cell Entry Into the CNS.....	4
1.4 Figures & Legends.....	5
CHAPTER TWO	7
2.1 Abstract.....	8
2.2 Introduction.....	9
2.3 Materials and Methods.....	11
2.4 Results.....	17
2.4.1 ME49EW Bradyzoites in Mature Tissue Cysts are a Dormant and Diverse Population.....	17
2.4.2 Bradyzoite-Initiated Recrudescence in Fibroblast and Astrocytes...19	
2.4.3 Bradyzoite-to-Bradyzoite Development.....	20
2.4.4 Resolving Parasite Development by Single Cell Transcriptomics...21	
2.5 Discussion.....	24
2.6 Figures & Legends.....	34
CHAPTER THREE	43
3.1 Abstract.....	44
3.2 Introduction.....	45

3.3 Materials and Methods.....	48
3.4 Results.....	54
3.4.1 Expression of Group 1 Metabotropic Glutamate Receptors are Enriched on CD8 ⁺ T Cells in the <i>Toxoplasma</i> -Infected Brain.....	54
3.4.2 Glutamate Receptor Expression Identifies a Transcriptionally Distinct Population of CD8 ⁺ T cells in the Brain.....	56
3.4.3 mGluR ⁺ CD8 ⁺ T cells Exhibit a Memory Phenotype.....	58
3.4.4 mGluR ⁺ CD8 ⁺ T cells Recruited to the <i>T. gondii</i> -Infected Brain are a Proliferating Population.....	61
3.4.5 Production of IFN- γ is Partially Dependent on mGluR ⁺ Stimulation..	66
3.5 Discussion.....	68
3.6 Figures & Legends.....	75
CHAPTER FOUR	94
4.1 Abstract.....	95
4.2 Introduction.....	96
4.3 Materials and Methods.....	99
4.4 Results.....	102
4.4.1 Direct Parasite Invasion of Astrocytes Downregulates GLT-1.....	102
4.4.2 <i>Toxoplasma</i> Virulence Factors Contribute to GLT-1 Downregulation.....	104
4.4.3 Downregulation of GLT-1 in Primary Cultured Astrocytes is Mediated by a Degradative Pathway.....	104

4.5 Conclusions and Future Direction.....	106
4.6 Figures & Legends.....	108
CHAPTER FIVE	118
5.1 Summary and Conclusions	119
5.2 References.....	123

LIST OF FIGURES

1.1.1 The Life Cycle of <i>Toxoplasma Gondii</i>	5
2.4.1 ME49EW Bradyzoites in Mature Tissue Cysts are a Dormant and Diverse Population	34
2.4.2 Bradyzoite-Initiated Recrudescence in Fibroblast and Astrocytes	36
2.4.3 Bradyzoite-to-Bradyzoite Development	38
2.4.4 Resolving Parasite Development by Single Cell Transcriptomics	41
3.4.1 Expression of Group 1 Metabotropic Glutamate Receptors are Enriched on CD8 ⁺ T Cells in the <i>Toxoplasma</i> -Infected Brain	75
3.4.2 Glutamate Receptor Expression Identifies a Transcriptionally Distinct Population of CD8 ⁺ T cells in the Brain.....	77
3.4.3 mGluR ⁺ CD8 ⁺ T cells Exhibit a Memory Phenotype	79
3.4.4 mGluR ⁺ CD8 ⁺ T cells Recruited to the <i>T. gondii</i> -Infected Brain are a Proliferating Population	81
3.4.5 Production of IFN- γ is Partially Dependent on mGluR ⁺ Stimulation	74
4.4.1 Direct Parasite Invasion of Astrocytes Downregulates GLT-1.....	108
4.4.2 <i>Toxoplasma</i> Virulence Factors Contribute to GLT-1 Downregulation.....	111
4.4.3 Downregulation of GLT-1 in Primary Cultured Astrocytes is Mediated by a Degradative Pathway.....	114

CHAPTER ONE

Introduction

1.1 The Life Cycle of *Toxoplasma Gondii*

The obligate intracellular parasite, *Toxoplasma gondii* (*T. gondii*), is one of the world's most successful protozoan pathogens where it is estimated that over two billion people are infected. *T. gondii* poses the greatest health-threat to immunocompromised individuals, such as those undergoing immune suppressive therapies, or HIV/AIDS patients (**Fig 1.1.1, panel 5-6**) [1]. As *T. gondii* is one of the few pathogens that can cross the blood-placenta barrier, infection also poses a concern for pregnant mothers. Congenitally-acquired toxoplasmosis can lead to hydrocephalus, intracranial calcification, mental retardation, or loss of life [2]. Severity of these clinical manifestations is dependent on which trimester the mother becomes infected, and if she has had previous exposure to this apicomplexan. It is also important to stress that treatment options only target the fast-replicating tachyzoite form of the parasite (i.e. sulfonamides and pyrimethamine), but no viable way to clear the tissue cyst state [2]. This is in part due to a lack of *in vitro* models that can recapitulate the recrudescence process.

Initial infection begins with the consumption of oocysts from contaminated food/water sources, or tissue cysts from undercooked infected meat (**Fig 1.1.1, panel 2**). This mode of transmission leads the encysted pathogen to the GI tract where it will rupture and release sporozoites or bradyzoites, respectively (**Fig 1.1.1, panel 3**). Although both forms will initially invade enterocytes that line the intestine, the forms the parasites can differentiate into is host-dependent. For example,

replicating parasites in the intestine of the feline definitive host will convert to merozoites which are the precursors to the sexual sporozoite form [3, 4]. Eventually, the highly resistant oocysts will be shed into the environment to be consumed by another host (**Fig 1.1.1, panel 1**). When an intermediate host becomes infected, such as a rodent or human, *T. gondii* will convert to tachyzoites [4]. This form has the capacity to invade any nucleated cell, but tends to infect and spontaneously form tissue cysts in muscle tissue in the periphery, and neurons in the brain (**Fig 1.1.1, panel 4**) [5, 6]. In the event an infected rodent is ingested by a felid, the life cycle of *T. gondii* is complete.

1.2 The Immune Response to *Toxoplasma Gondii*

The genesis of this pro-inflammatory response against *T. gondii* begins with recognition by innate immunity. As parasite disseminates within a host, conserved foreign sequences, will be recognized by pathogen recognition receptors, such as Toll-like receptors (TLRs) expressed on innate immune cells. Parasitic profilin will bind to TLR11 which triggers the MyD88-dependent pathway to produce IL-12 [7, 8]. It is important to mention that humans do not express TLR-11. Nonetheless, TLR-2 and 4 work collectively to recognize parasitic glycosylphosphatidylinositol-anchored proteins which also results in downstream IL-12 production [9]. During acute infection, IL-12 will signal to natural killer cells to secrete the protective cytokine, IFN γ [10]. As adaptive immunity sets in, both CD8 and CD4 T cells become the dominant producers of IFN γ [11].

IFN γ signaling stimulates STAT1-mediated phosphorylation, which results in dimerization and translocate to the nucleus where interferon stimulated genes are upregulated. This leads to the upregulation of immunity related GTPases to bind to and disrupt the parasitophorous vacuole, making the tachyzoite form of *T. gondii* susceptible to lysosomal degradation [12]. However, tissue cysts remain. Additionally, IFN γ leads to the upregulation of dioxygenases (Indole amine 2,3, dioxygenase and Tryptophan 2,3, dioxygenase) which degrade the essential amino acid for *T. gondii*, tryptophan, resulting in parasite starvation [13]. Furthermore, work has demonstrated if IFN γ signaling is inhibited at any level, mice become susceptible to infection [5, 11, 12, 14, 15]. Although IFN γ is required to prevent clinical disease, an anti-inflammatory response is also vital to avert inflammation-induced mortality [15, 16]. In particular, the presence of IL-10 and IL-27 are important to dampen the immune response by inhibiting IL-12 production, and by promoting the downregulation of co-stimulatory and antigen presentation molecules [11, 16-18]. As *T. gondii* is never fully cleared, the presence of cognate antigen perpetuates a well-controlled inflammatory response.

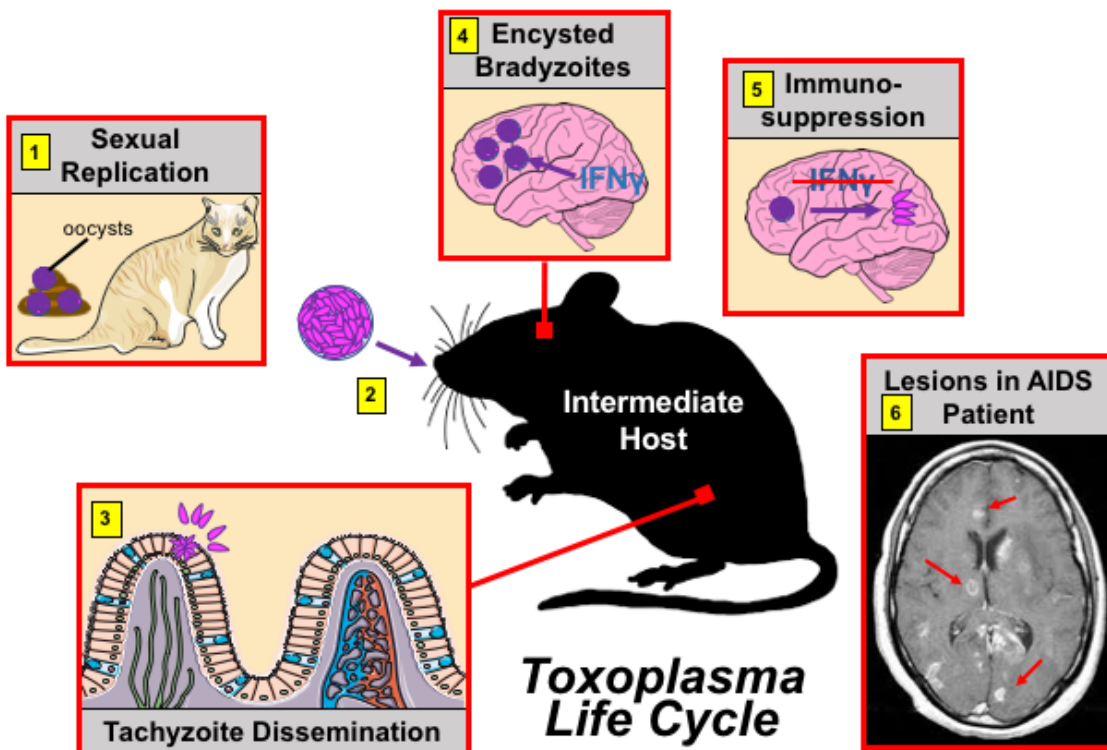
1.3 CD8⁺ T Cell Entry Into the CNS

As the central nervous system (CNS) is an immune-privileged site, there are a specific set of rules that dictate CD8⁺ T cell access. A key element that governs CNS entry is the presence of cognate antigen. During the acute stages of *T. gondii*

infection, the fast-replicating tachyzoite form of the parasite will disseminate throughout the host where it will eventually infect and form cysts in the brain [5]. The pro-inflammatory response in the periphery promotes the expression of the second component that controls CNS passage; cell adhesion molecules [19]. The upregulation of VCAM-1 on endothelial cells at the blood brain barrier (BBB) allows for VLA-4-expressing CD8⁺ T cells to exit the vasculature through diapedesis [20, 21]. Antigen presenting cells that line the perivascular space will present antigen to CD8⁺ T cells to promote their retention. The generation of the last component needed for traversing the CNS, a chemokine gradient of CXCL10 secreted by neurons and glial cells, will promote the migration of CXCR3⁺CD8⁺ T cells into the brain parenchyma [22-24]. However, once within the infected brain parenchyma, it is unclear what tissue-specific signals drive CD8⁺ T cell maintenance, protection, and differentiation.

1.4 Figures & Legends

Figure 1.1.1 The Life Cycle of *Toxoplasma Gondii*. 1. Oocysts are shed from the felid definitive host. 2. Consumption of cysts by the intermediate host. 3. After cyst rupture in GI tract, parasites infect enterocytes where they can disseminate. 4. Parasites spontaneously form cysts due to immune pressures such as IFN γ . 5. Immunosuppression leads to parasite reactivation. 6. MRI highlighting ringed-lesions (red arrows) from an HIV/AIDS patient after parasite reactivation.



CHAPTER TWO

Toxoplasma Ex Vivo Recrudescence

2.1 Abstract

The recrudescence of the obligate intracellular parasite, *Toxoplasma gondii*, poses a significant health risk to immunocompromised patients, and precedes parasite dissemination. Attempts to study the recrudescence of tissue cysts have come up short as current *in vitro* models do not recapitulate many key features of the native stains found *in vivo*. Lab adaption in cell culture hinders the parasites capacity to form cysts both *in vitro* and *in vivo*. To overcome this issue, we pose a new *ex vivo* model of bradyzoite-initiated development that better preserves the key attributes of the intermediate life cycle. Here, we use excysted bradyzoites from the Type II ME49EW strain isolated from murine brain tissue to establish a dynamic developmental process involving two tachyzoite stages; a fast-growing RH-like stage that transitions into a slow-growing Pru-like stage from which bradyzoites spontaneously re-develop. Our model uses human foreskin fibroblast and neonatal astrocytes to demonstrate that the bradyzoite-to-tachyzoite stage conversion is host cell-independent, while the re-development of the bradyzoite is asynchronous, heterogenous, and strongly influenced by the cell type they infect. We also performed single cell RNA-sequencing on parasites that were isolated from infected astrocyte and fibroblast cultures over the course of recrudescence. In addition, the Type I (RH) and Type II (PruQHx) tachyzoite strains, and excysted bradyzoites (ME49EW) were used for comparative analysis. This reveals metabolically distinct gene signatures of these parasite populations and significant pluripotency of the non-adapted bradyzoite population. Furthermore, our data

uncover previously unknown complexity in the clinically important stage of the parasite and highlights important features of the *Toxoplasma* intermediate life cycle.

2.2 Introduction

Infection with *Toxoplasma gondii* (*T. gondii*) is first acquired by ingesting oocysts from environmental sources, or tissue cysts from undercooked infected meat. Once within the GI tract, proteases will release sporozoite and bradyzoite from oocysts and tissue cysts, respectively. The dissemination of *T. gondii* in infected mice is relatively quick, where parasites can be found in mesenteric lymph nodes 8h-post infection [25]. By 1-week post infection, tissue cysts can be detected in the central nervous system (CNS) [26]. The ability for the parasite to quickly establish itself within a host makes it nearly impossible to prevent infection. This has led to widespread distribution of this pathogen, where it is estimated that one third of the world's population is infected [27]. Immunocompetent individuals are at low risk for clinical complications from toxoplasmosis, however, parasite reactivation of chronically infected immunocompromised patients are most susceptible to life-threatening disease [28]. Prior to the introduction of HAART-therapy, *T. gondii* caused frequent life-threatening encephalitis in AIDS patients, with reactivating disease thought to be the most common cause [27]. Today, co-infection with *T. gondii* and HIV remain a significant clinical threat to large

populations that have limited access to HIV therapies. This will remain so until there is a cure for HIV and/or a therapy to eliminate the chronic tissue cyst stage.

The recrudescence of the bradyzoite tissue cyst is poorly understood. Studies of severely immunosuppressed mice indicate that *Toxoplasma* reactivation preferentially occurs in the frontal and parietal cortex of the brain [29]. Attempts to define the parasite developmental process associated with recrudescence in interferon- γ knockout mouse models and in AIDS patients that have succumbed to toxoplasmosis have uncovered heterologous parasite development in foci of reactivation [30, 31]. Vacuoles of varying sizes present in these lesions were filled with parasites expressing tachyzoite and/or bradyzoite markers. Consequently, the original ruptured cyst could not be identified nor could be sequenced for parasite developmental steps or host cell contributions [30, 31]. These few studies point to the challenges in studying *T. gondii* reactivation, which currently is limited to animal models. Moreover, the development for an *in vitro* model of bradyzoite reactivation is critically needed so we may understand these processes at the cellular and molecular level.

To overcome these issue, we pose a new *ex vivo* model of bradyzoite-initiated development that better preserves the competency of the intermediate life cycle. Here, we use excysted bradyzoites from a Type II ME49 strain isolated from murine brain tissue to infect human foreskin fibroblast and neonatal astrocytes.

Following infection, two growth phases emerged, a fast-growing RH-like phase that is host cell-independent, followed by a slow growing Pru-like phase that seems to be influenced by the host cell. Immunofluorescence assays demonstrate that recrudescing parasites from fibroblast have a linear bradyzoite-to-tachyzoite pathway. Although, the majority of recrudescing parasites replicating in astrocytes also have this trajectory, there is a subpopulation that retains and/or re-expresses bradyzoite antigen. Further studies revealed this BAG1⁺ parasites are producing tissue cysts. Single cell RNA-sequencing performed on parasites isolated from infected astrocyte and fibroblast cultures over the course of recrudescence uncovered previously unknown complexity in the clinically important stage of the parasite and highlights key features of the *Toxoplasma* intermediate life cycle. Overall, these results describe how this new *ex vivo* recrudescence model is able to illustrate the steps of bradyzoite recrudescence, and the developmental changes that occur during this process.

2.3 Materials and Methods

Parasite Strains and Host Cells: All laboratory-adapted strains were maintained in human foreskin fibroblasts (HFF) cells in high glucose DMEM with sodium bicarbonate (Sigma) supplemented with 5% heat-inactivated fetal bovine serum (FBS) and 1% penicillin-streptomycin in humidified incubators at 37°C with 5% CO₂ and ambient oxygen (21%). The Type II ME49EW strain was maintained in

mice as described below. Other HFF-adapted laboratory strains were used in this study: RH (Type I) [32], PruQ (Type II) [33].

Astrocyte purification: Neonatal C57Bl/6 mice born at 0-3 days were sacrificed via decapitation and brains (without cerebellum) dissected and placed in cold wash media (DMEM and 2% fetal bovine serum). Brains were pooled and homogenized through a sterile 40 micrometer cell strainer (Corning) using a 3 ml syringe plunger. Homogenate was washed twice with cold wash media and spun at 2,000 rpm for 10 minutes at 4°C. Homogenate was resuspended with 6 ml per brain of prewarmed complete media (DMEM [Corning]; 10% FBS; 1% Nonessential Amino Acids Mixture 100x, [Biowhittaker Reagents Lonza], 1% GlutaMAX supplement 100x [Thermo Fisher Scientific], 1% penicillin-streptomycin, [Genclone], 1% HEPES Buffer solution 1M [Thermo Fisher Scientific]. Resuspended cells were plated in non-vented T-25 cm² flasks with loose caps at 37°C, 5% CO₂. At days 3, 5, and 7 astrocyte media was replaced. To remove less adherent microglia and oligodendrocytes, astrocytes were shaken on day 8-10 at 260 rpm, 37°C for 1.5 hours. Media was replaced and cultures were shaken for an additional 24h at 100 rpm, 37°C. Astrocytes were lifted with 3ml of 0.25% Trypsin EDTA, counted, and plated at a density of 1x10⁶ cells per T-75cm² vented flask until confluent.

Animal Experiments: All animal research was conducted in accordance to the Animal Welfare Act. C57Bl/6, CBA/J, and SWR/J #689 mice obtained from

Jackson Laboratory (Jackson ImmunoResearch Laboratories, Inc., West Grove, PA, USA) were bred and maintained in a pathogen free vivarium under the Institutional Animal Care and Use Committee (IACUC) protocols established at the University of California, Riverside and the University of South Florida, Tampa.

The ME49EW strain was continually passed through 5 to 6 week old female mice by first infecting resistant strain SWR/J (Swiss Webster) with 10 cysts in 200 μ l of cortex homogenate by intraperitoneal (i.p.) injection (see Fig. S1 for details). Tissue cysts in brain homogenates from infected SWR/J mice were then used to infect CBA/J, sensitive mice (10 cysts in 200 μ l diluted brain homogenates, i.p.).

Brain homogenate preparation. At 14-60 days PI as indicated, infected SWR/J or CBA/J mice were euthanized, brain cortices dissected and placed in 3ml of cold PBS (cerebellum was discarded as it contained <5% of total brain tissue cysts). Tissue homogenization and tissue cyst yields were significantly improved (tissue cyst numbers >50% higher) by storing infected brain cortices overnight at 4°C in PBS. In direct comparisons, we determined tissue cysts held in brain tissues for up to 24h in cold PBS were viable, fully infectious, and yielded active excysted bradyzoites. After the 4°C overnight storage in 3ml of 1xPBS, cortexes were more easily serially homogenized by 3-4 serial passes through 18, 20 and finally, 22 gauge (blunt) sterile needles. Tissue cyst quality and enumeration was determined by a full examination of 30 μ l (x 3) of homogenate spread on a microscope slide. All tissue cyst mouse inoculum used in this study were diluted to 10 cysts in 200 μ l

in 1xPBS. In addition, the quantification of brain tissue cyst counts in mice infected with various parasite sources followed these protocols and were determined in triplicate.

Tissue Cyst Purification and Bradyzoite Excystation: Cysts were purified from mouse brain cortices infected with the indicated parasite numbers/cysts for 30-50 days. To purify tissue cysts, brain cortices were harvested and homogenates prepared as above (one cortex per 15 ml conical tube as combining cortices reduces cyst yields). Following cyst counts as above, homogenate volumes were brought up to 11ml with PBS, mixed by inversion, and then centrifuged at 500xg for 15 minutes. The supernatant was removed by aspiration and the homogenate pellet resuspended in 2.5ml of percoll-90 (90% percoll, 10% 1xPBS) followed by the addition of PBS to a final volume of 7.5ml (final percoll=30%). The tube was fully mixed by several inversions and then centrifuged at 1000xg for 15 minutes without a brake. Tissue cysts pelleted in this gradient protocol, while debris collects at the top of the gradient, therefore, the supernatant was carefully removed by aspiration. If multiple cortices are used, the pellets from the individual percoll gradients that contain tissue cysts were combined and the total volume raised to 10ml of PBS, followed by centrifugation at 30xg for 10 min and then removal of the supernatant by careful aspiration. A low speed 30g spin pellets medium to large tissue cysts (majority of bradyzoites) while >80% of red blood cells are retained in the supernatant. To obtain free bradyzoites, the tissue cysts were resuspended in

excystation solution (5mg/ml pepsin, 100mg/ml NaCl, 0.14N HCl), incubated for 90 seconds and then 10 ml of culture media containing 5% fetal bovine serum added. Bradyzoites counts were obtained using a hemocytometer.

Ex Vivo Bradyzoite Recrudescence Experiments: Preliminary investigations determined that native ME49EW parasites grew better in HFF cells under lower oxygen levels. Therefore, throughout this study we cultured ME49EW parasites in HFF or primary astrocyte monolayers that were placed in a hypoxic chamber and grown in the same media with the exception that astrocytes received a 1% GlutaMAX supplement. Confluent HFF or neonatal astrocyte monolayers were inoculated at various times with excysted bradyzoites, lab strains or recrudescing populations at a MOI 0.25. ME49EW parasites were passaged into new monolayers at indicated time points.

Visualization of Parasite Growth and Development: ME49EW bradyzoites and various recrudescing populations were inoculated onto 6 well glass coverslips of HFF or astrocyte cells at 0.25 MOI. All coverslips were cultured under low oxygen conditions. Infected coverslips were fixed with 4% PFA for 10min. Cells were permeabilized with either 100% acetone or 0.25% Triton-X for 10min. Cells were blocked with either 5% donkey serum or 1% BSA for 30min, followed by a 1h incubation of the following primary antibodies diluted in blocking buffer: biotinylated-dolichos biflorus agglutinin (DBA) [1:500] (Vector Laboratories),

rabbit-anti SRS9 [1:1000] and mouse-anti SAG1 [1:1000] (kindly provided by John Boothroyd, Stanford U.), rabbit-anti-Toxo [1:500] (Abcam), mouse-anti-CST-1 [1:1000] (kindly provided by Louis Weiss, Albert Einstein COM). Secondary antibody master mix were incubated for 1h: Goat-anti-rabbit-AF568 [1:1000], Goat-anti-mouse-AF488 [1:1000], streptavidin-AF647 [1:1000], DAPI (1mg/ml). All incubations were done at room temperature.

Single Cell RNA Sequencing: Single Cell RNA sequencing was performed on parasites from respective conditions using the 10X Genomics Chromium Next GEM Single Cell 3' Reagent Kits v3.1 as described by manufacture protocol. Sequencing depth was performed at 1 billion reads and generated at the UC San Diego IGM Genomics Center utilizing an Illumina NovaSeq 6000 that was purchased with funding from a National Institutes of Health SIG grant (#S10 OD026929). Sequencing reads were aligned to the ME49 *T. gondii* reference genome using 10X Genomics Cellranger (version 5.0.1). The Cellranger aggregation protocol was used to combine respective datasets for secondary analysis. All analysis was performed and visualized using the 10X Genomics Loupe Browser (version 6.1.0).

2.4 Results

2.4.1 ME49EW Bradyzoites in Mature Tissue Cysts are a Dormant and Diverse Population

A recurring question is the extent to which *in vivo* bradyzoites replicate in mature tissue cysts (>30 days PI). To test the homogeneous and unique nature of excysted bradyzoites, single parasites were captured using the 10x Chromium Single Cell Gel Bead kit and 3'-RNA-seq libraries constructed. To confirm the unique transcriptome of ME49EW tissue cysts from mice, transcriptomic data of ME49EW *ex vivo* bradyzoites (8,609 cells), and Type I RH (6,583 cells) and Type II PruQ (9,735 cells) tachyzoite datasets were aggregated using Uniform Manifold Approximation and Project (UMAP) plots. ME49EW bradyzoites were highly related and distinct from RH tachyzoites that do not spontaneously form cyst walls in cell culture, or PruQ tachyzoites which have the ability to form tissue cysts (**Fig. 2.4.1A**). Genes enriched in the excysted bradyzoite dataset included canonical bradyzoite markers BAG1, LDH2, enolase 1, SRS9 (SRS16B), and BRP1.

To assess the level of dormancy in excysted bradyzoites at the transcriptional level, *ex vivo* bradyzoite datasets were first aggregated with scRNA-seq datasets generated from parasites isolated from fibroblast- or astrocyte- infected cultures with the initial excysted bradyzoites at various time points. This was followed by a re-clustering on BAG1+ parasites (**Fig. 2.4.1B**). Although all parasites in this re-

clustering analysis exhibit bradyzoite character (via the expression of BAG1), the expression of the tachyzoite marker, SAG1, is not associated with excysted bradyzoites, suggesting dormant parasites (**Fig. 2.4.1B-C**). To further dissect the uniqueness of BAG1+ parasites, the dataset was broken up into Groups A-E. Comparative analysis of bradyzoite, merozoite, and tachyzoite gene expression revealed a continuum of bradyzoite maturity in groups A-C. BAG1+-Group B parasites expressed increased levels of canonical bradyzoite marker genes, and had the highest levels of key merozoite genes including AP2IV-3 and SRS22A, suggesting a more mature bradyzoite population (**Fig. 2.4.1C**). Conversely, BAG1+-Group C parasites lacked significant merozoite gene expression and expressed higher levels of early bradyzoite markers such as SRS9, suggesting a younger or less mature bradyzoite (**Fig. 2.4.1C**). The BAG1+-Group A mRNA expression patterns placed these parasites intermediate to Group B and C parasites, although with some overlap with genes expressed at higher levels in Group B and C parasites such as bradyzoite-specific cAMP dependent kinase and canonical marker BRP1 (**Fig. 2.4.1C**) [3]. Gene expression enriched in BAG1+-Group C parasites overlapped with Group D parasites where the Group D cluster was primarily comprised of recrudescing parasites from astrocytes (**Fig. 2.4.1C**). D2-Astro BAG1+ parasites distributed to SAG1- regions of Group D, while D7-Astro BAG1+ parasites spanned the Group D cluster and were SAG1+ or SAG1-. The small subpopulation of excysted bradyzoites that clustered with Group D parasites (i.e. Group E) were clearly expressing higher levels of critical growth

genes and were more consistently expressing growth-IMC genes than Group A-C parasites, suggesting a fraction of excysted bradyzoites are active or recrudescent (**Fig. 2.4.1B-C**). Taken altogether, this indicates that bradyzoites excysted from the ME49EW strain are primarily composed of dormant yet diverse parasites.

2.4.2 Bradyzoite-initiated recrudescence in fibroblast and astrocytes

To understand the developmental recrudescence process of ME49EW bradyzoites, we infected monolayers of fibroblast and astrocytes to investigate protein expression of two key surface antigens that are associated with specific forms of the parasite; SRS9 present on bradyzoites and the tachyzoite surface antigen SAG1. Between day 1 and 2 post-bradyzoite infection, SRS9+ expression begins to decline as SAG1 expression increases, where some vacuoles having equal expression of both of these antigens (**Fig. 2.4.2A**). The trend towards elevated SAG1 and low to absent SRS9 expression progressively became the major phenotype in Day-5 populations that form in either host cell type (**Fig. 2.4.2A-B**). Additionally, we quantified our results by flow cytometry. Analysis of excysted bradyzoites demonstrate that the majority of parasites express SRS9, confirming the bradyzoite phenotype that is observed in scRNAseq data (**Fig. 2.4.2C and 2.4.1**). Next, we followed the parasite's developmental state in both astrocyte and fibroblast infection at days 2, 3, 5, 7 (**Fig. 2.4.2C**). In day 2 astrocyte infection, a stage conversion of bradyzoite-to-tachyzoite is initiated as parasites begin to express SAG1 and turn off SRS9. By day 3, the intermediate

(SRS9+/SAG1+) population gradually declines, and the SRS9+ parasites are increased relative to day 2, suggesting either replicating bradyzoites, or a conversion of tachyzoites to bradyzoite development. Although by day 5 the dominant form of the parasite is the tachyzoite (SAG1+), a small SRS9-only population remains. However, from day 5 to 7, both the intermediate (SRS9+/SAG1+) and bradyzoite (SRS9+) populations are expanded suggesting a growth shift or a developmental switching of the parasite stage. Conversely, in fibroblasts, the main developmental pathway is bradyzoite-to-tachyzoite where the initial bradyzoite phenotype gradually converts to the dominant tachyzoite form for the duration of infection. Taken altogether, these data indicate that host cells can limit the developmental pathways the parasite can differentiate to.

2.4.3 Bradyzoite-to-Bradyzoite Development

The classical, and predicted, bradyzoite to tachyzoite differentiation was not the sole development process occurring during ME49EW bradyzoite recrudescence. In addition, we observed SRS9+/SAG1- bradyzoites replicating in astrocytes simultaneously to tachyzoite replication (SAG1+ only) in neighboring cells at days 2, 5, and 7 (**Fig. 2.4.3B**). Bradyzoite-to-bradyzoite replicating vacuoles were 15% of Day-2 populations in astrocytes. The SRS9+-only bradyzoites grew slower, progressing from an average vacuole size of 5.22 bradyzoites (SAG1+ tachyzoite vacuole=10) at day 2 to an average vacuole size of 12 bradyzoites by day 3 (SAG1+ tachyzoite vacuole=21) (**Fig. 2.4.3C**). Bradyzoite only replicating

vacuoles (SRS9+/SAG1-) were observed in Day 5-populations, although at lower frequencies (5%) (**Fig. 2.4.3C**). Neither HFF nor murine embryonic fibroblast cells supported bradyzoite-to-bradyzoite replication (**Fig. 2.4.3C** and data not shown). The rare SRS9+/SAG1-vacuoles present beyond day 1 in HFF cells contained single parasites indicating they were nonreplicating bradyzoites carried over during passage or growth arrested tachyzoites that re-expressed SRS9, while turning off SAG1. In astrocytes, but not HFF cells, parasite vacuoles containing SRS9+ only (SAG1-) parasites steadily increased after the Day-7 growth shift (**Fig. 2.4.3E-F**). Co-staining parasites in astrocytes with anti-SRS9 and anti-SAG1 antibodies and biotin-labeled *Dolichos biflorus* agglutinin (DBA) demonstrates spontaneous cyst wall assembly primarily in vacuoles undergoing bradyzoite-to-bradyzoite replication (SRS9+), whereas, spontaneous cyst wall formation occurred in <1% of the ME49EW vacuoles in HFF cells (**Fig. 2.4.3D-E**). Collectively, these data indicate that the bradyzoite-to-bradyzoite developmental pathway is host cell-dependent, and those parasites that exhibit bradyzoite character (i.e. SRS9+ only) have the ability to form cysts.

2.4.4 Resolving Parasite Development by Single Cell Transcriptomics

The analysis of SAG1 and SRS9 expressing parasites by immunofluorescence and flow cytometry revealed that bradyzoite recrudescence can lead to at least 2 developmentally distinct parasite populations (**Fig. 2.4.2 and 2.4.3**). To further elucidate the heterogeneity of bradyzoite recrudescence, scRNAseq datasets

were analyzed across the recrudescence growth period in both fibroblasts and astrocytes. Comparative analysis of AP2 transcription factors were used to determine parasite stage-specificity (**Fig. 2.4.4A**) [34-37]. Previous analysis of total RNA sequencing results from ME49EW *in vivo* tissue cyst populations compared to ME49B7 tachyzoites identified that AP2IX-9 (80 fold up) has the highest expressed AP2 factor, but AP2IV-5 was the fourth lowest (28 fold down) in tissue cysts. Furthermore, the merozoite AP2, AP2IV-3, [38] was also expressed at higher levels than AP2IV-5 in tissue cysts versus tachyzoites.

We used the distinctive AP2IX-9/AP2IV-3/AP2IV-5 profiles identified in total RNAseq data to investigate UMAP clusters in scRNAseq data from recrudescing parasites (**Fig. 2.4.4A**). The clusters of excysted ME49EW bradyzoites (D0) followed the pattern of the *in vivo* tissue cysts with AP2IX-9^{Hi}, AP2IV-5^{low} and AP2IV-3 intermediate (**Fig. 2.4.4A**). In contrast, this trio of AP2 factors in RH tachyzoites had an opposite relationships of AP2IV-5^{Hi}/AP2IX-9^{low} and AP2IV-3^{low} (**Fig. 2.4.4A**). As expected, ME49EW recrudescing parasites exhibited diverse AP2 expression patterns with the majority of parasites having the AP2IV-5^{Hi}/AP2IX-9^{low} tachyzoite pattern, which reflects the active bradyzoite to tachyzoite developmental pathway in these populations (**Fig. 2.4.4A**). Additionally, the AP2IX-9^{Hi}/AP2IV-5^{Low} bradyzoite profile was present in at least one cluster in each of the Day 2-7 astrocyte infections. Cluster 13 in Day-2 astrocytes (C13-D2), cluster 13 in Day-5 astrocytes (C13-D5), and cluster 11 in Day-7 astrocytes (C11-

D7) exhibited the bradyzoite profile (**Fig. 2.4.4A** circle and square paired markers) and these clusters accounted for nearly all parasites expressing high levels of the bradyzoite-specific heat shock protein, BAG1, [39] in ME49EW recrudescing scRNA-seq samples (**Fig. 2.4.4B**). The transcriptomes of C13-D2, C13-D5, and C11-D7 parasites had elevated expression of many other bradyzoite-specific genes. For example, the canonical bradyzoite genes lactate dehydrogenase (LDH2), enolase 1 (ENO1), and surface antigen SRS9 [40, 41] were all highly expressed in the D7-Astro C11 cluster but not in the other 20 clusters aggregated from D7-Astro transcriptome data (**Fig. 2.4.4C**). Gene lists ($P < 0.05$) from C13-D2 and C13-D5 were nearly all shared with C11-D7 gene expression results (**Fig. 2.4.4D**).

To deepen the analysis of bradyzoites in recrudescing populations, we focused on the parasites expressing high levels of BAG1 mRNA. A UMAP projection of BAG1+ parasites (**Fig. 2.4.4E**) revealed that most D0-bradyzoites were also SAG1- and distributed into three clusters (Group A-C) with the exception of a small group of parasites associated with Group D (a distinct group of 170 D0 parasites was designated as Group E). The large Group D parasites were primarily comprised of BAG1+ bradyzoites from day 2 and day 7 infected astrocytes (**Fig. 2.4.4E**) with many expressing SAG1+ mRNA along with parasites expressing low to undetectable SAG1 levels. A major difference between BAG1+ Groups A-C versus Group D was evidence of downregulation of mitochondrial gene expression

in dormant *in vivo* bradyzoites (**Fig. 2.4.4E**). By contrast, Group D parasites had upregulated these mitochondrial genes as well as mRNAs encoding surface antigens SRS25 and SRS20A, microneme proteins MIC3 and MIC10, and a nuclear transfer factor (ME49_233350) (**Fig. 2.4.4E**). The higher expression of mitochondrial genes in Group D indicated that many of these parasites were replicating, which was supported by other gene expression analysis. Collectively, transcriptomics demonstrates that astrocytes support a replicating bradyzoite-to-bradyzoite recrudescence pathway.

2.5 Discussion

The molecular basis for why some *Toxoplasma* strains produce thousands of tissue cysts in mouse brains, while other strains produce a couple of dozen is not known, but it has been a bottle neck in advancing our understanding of cyst biology. The native ME49EW and lab-adapted PruQ parasites studied here are largely equivalent in the alkaline-stressed *in vitro* model; both strains slow growth in pH8.2 media, and robustly assemble cyst walls in 48-72 h cell cultures. However, where it really counts in *Toxoplasma* infections these strains differ by two orders of magnitude in the ability to produce tissue cysts in mice. It is well known that repeated passage in HFF cells exacerbates the loss of developmental competency [42, 43], therefore, even if developmental competency is only partially affected after the initial HFF-adaptation, it is likely to be fully lost over time in HFF cell cultures. In tests of ME49EW tissue cyst production, we determined that in as

short as two weeks in either astrocyte or HFF cell culture ME49EW parasites permanently lose ~90% of their capacity to form tissue cysts in mice.

Native bradyzoites are the versatile, multifunctional stage of *Toxoplasma* life cycles. They initiate the definitive life cycle by converting to merozoites in feline epithelial cells or recrudescence into tachyzoites in a variety of host cells leading to reactivation of acute toxoplasmosis in immune-compromised hosts. Studies spanning 30 years support the concept that the cell cycle end point of tachyzoite to bradyzoite development is dormancy [44-46], which is substantiated by our study. ME49EW bradyzoites excysted from *in vivo* tissue cysts (>30 days post-infection) are deeply growth arrested. Sequencing the polyA⁺ mRNA content of >8,000 of these non-growing bradyzoites excysted from *in vivo* tissue cysts clearly demonstrated they are not a monolithic group. A group of bradyzoites expressed higher levels of mRNAs encoding early switching SRS antigens, such as SRS9, (Group C, Fig. S4), while another group possessed increased mRNA for surface antigens that are expressed in bradyzoites and merozoites, like SRS22A (Group B). Group B-bradyzoites with higher levels of SRS22A mRNA also expressed the highest levels of the bradyzoite/merozoite ApiAP2 factor, AP2IV-3 [34, 38]. All excysted bradyzoites exhibited incomplete growth factor gene expression, however, the Group B, cluster parasites had the lowest expression of these essential genes indicating these bradyzoites are likely the most mature of the excysted bradyzoite population. Like growth factor gene expression, transcript-

based GO analysis also indicated variations in the metabolic activity of excysted bradyzoites and potential new bradyzoite regulatory proteins were identified such as an uncharacterized cAMP dependent kinase uniquely expressed in Group A bradyzoites whose function will need to be investigated. Altogether, the transcript variations in the excysted bradyzoites may reflect the progression of younger to more mature bradyzoites or the priming of bradyzoites for specific developmental outcomes. Further studies will be needed to resolve these possibilities. The sporadic expression of IMC mRNAs that include the budding IMCs, IMC3 and IMC4, in non-replicating bradyzoites was unexpected, although similar to the recent reports that budding IMC proteins, IMC1 and 3, are localized to the mature cytoskeleton of bradyzoites [45, 47]. Here and in these previous reports, IMCs associated with daughter parasite formation in tachyzoites are being expressed in bradyzoites in the absence of budding. A major function of several IMC proteins is to strengthen the parasite cell shape [47], and therefore, it is unlikely these genes can be completely turned off. The demonstration that IMC proteins, like IMC4, are recycled to build new daughter parasites established that there are mechanisms of disassembly and reassembly of the IMC operating in *Toxoplasma* parasites [48]. Bradyzoites *in vivo* have much longer lifespans than the short lived replicating tachyzoite (there is no natural growth arrested state for the tachyzoite stage) and this may require periodic repair of the inner membrane complex to maintain the long term health of bradyzoites in tissue cysts. The hit and miss nature of IMC mRNA expression in the non-replicating excysted bradyzoites of this study could

be this renewal process in action maintaining parasite integrity and readiness for replication.

Once awakened by cyst disruption and host cell invasion, the development initiated by ME49EW bradyzoites follows a similar pathway that we previously described for sporozoite infections [49, 50]. ME49EW bradyzoites sequentially develop into two types of replicating parasites; a fast-growing parasite that switches in days to a slow-growing parasite. ME49EW bradyzoites occupy single parasite SRS9+SAG1- vacuoles for ~24 h and it takes ~5 days to fully transition to majority SAG1+ tachyzoites. The switch from non-growing bradyzoite to fast-growing tachyzoite required reactivation of the mitochondria, which is a bradyzoite vs. tachyzoite difference others have noted [51], and fast-growth was transient suggesting there may be a finite resource limiting this developmental transition. The amylopectin content of *in vivo* bradyzoites that tachyzoites lack is a prime candidate to investigate as has been suggested [52]. The rapid differentiation of ME49EW bradyzoites into a fast-growing tachyzoite tracked with the same timeframe in both fibroblasts and astrocytes as did the shift to slower growth at 6-7 days indicating these growth changes are host cell-independent and pre-programmed. The fast-growing ME49EW tachyzoites that can only be obtained from *ex vivo* ME49EW bradyzoite infections *in vitro* are an important new resource for producing transgenic, *in vivo* tissue cysts.

The new *ex vivo* model of bradyzoite recrudescence confirmed that an alternative bradyzoite-bradyzoite replication pathway exists in the intermediate life cycle that had been inferred by other research [53, 54]. Bradyzoites that invaded primary astrocytes exhibit two forms of replication simultaneously that follow the 24 h reawakening period: bradyzoite to tachyzoite conversion and replication (~85% vacuoles) and bradyzoite to bradyzoite replication (~15% vacuoles). Our results revealed astrocytes are permissive for bradyzoite to bradyzoite replication while fibroblasts are resistant as evaluated in two mammalian sources of this cell type. The scRNA-seq of recrudescing parasites in astrocytes confirmed the persistence of bradyzoites through the 7 day period we sampled recrudescing populations. To identify bradyzoites in UMAP clusters of the Day 2-7 RNA samples, we initially used ApiAP2 factor profiles. We had previously determined that AP2IX-9 and AP2IV-3 had roles in bradyzoite development [34, 36] and the bulk RNA-seq analysis of ME49EW *in vivo* tissue cysts identified AP2IV-5 as one of the most downregulated AP2 factor and AP2IX-9 as the most upregulated. The pattern of AP2IX-9^{Hi} and AP2IV-5^{Low} and its inverse were predictive of parasite clusters enriched for bradyzoites or tachyzoites in all recrudescing parasite RNA samples indicating that the expression relationship of these two AP2 genes is a key feature of bradyzoite to tachyzoite developmental switching and the reverse. Based on high quality results (P values <0.05), only three clusters from Day 2, 5, and 7 parasites had high levels of AP2IX-9 mRNA and lower levels of AP2IV-5 and these clusters were also the parasites expressing BAG1 and other canonical bradyzoite

genes. This raises renewed interest in how these AP2 factors function in bradyzoite development, which is now possible with the new genetic models based on the *ex vivo* recrudescence model presented here. The recently identified myb protein (BFD1) that is required for tissue cyst formation in mice [55] was constitutively expressed at very low mRNA levels in all recrudescing parasites, whereas, in mature ME49EW tissue cysts, BFD1 mRNA is expressed at 27 fold higher levels than tachyzoites (RNAseq data, Database S1). It is possible BFD1 functions to promote tissue cyst maturity *in vivo*, which is a mechanism that needs to be investigated further. The deeper analysis of Day-2-7 bradyzoites (BAG1+ aggregation) demonstrated these parasites are closely related as they cluster in one group in BAG1+ UMAP neighbor constructions. These bradyzoites show mixed expression of SAG1, elevated expression of mitochondria genes, and are the only BAG1+ bradyzoites we sequenced that express high levels of all the IMC mRNAs as well as other critical growth factors. Collectively, the cell biology and scRNAseq data indicates this group of BAG1+ parasites is composed of replicating bradyzoites as well as some level of spontaneous conversion of tachyzoites back to the bradyzoite stage after the growth shift at Day 7.

For close to 100 years, studies of the *Toxoplasma* tachyzoite have been conducted using *in vitro* cultured fibroblasts, indeed the ease of this culture system facilitated the study of *Toxoplasma* tachyzoites as a model for apicomplexan biology. In contrast, our new *ex vivo* model of bradyzoite recrudescence captures two distinct

pathways, one host cell dependent and the other independent. Host cell dependency rather than immune-stress induction has been the key feature of *Toxoplasma* development since the discovery of spontaneous cyst development occurring in neurons and myocytes [56]. Yet the heterogeneity achieved in astrocyte cultures of tachyzoite and bradyzoite replication is new and suggests a major portion of the life cycle that has been overlooked. *Toxoplasma* encounters many cell types during its lifecycle some of which induce cyst production and some that facilitate dissemination. Recrudescence most commonly occurs at three different sites i) in the gut following ingestion of tissue cysts where parasites encounter gut epithelial cells followed by innate immune cells ii) in peripheral organs such as the muscle and liver and iii) in the brain/CNS containing neurons, astrocytes, microglia and, during infection, peripheral immune cells. Determining what characteristics of the astrocyte support bradyzoite-bradyzoite replication and whether such characteristics exist in other cell types the parasite encounters will have important implications for managing the amplification of bradyzoites and the development of cysts. Of note we have documented bradyzoite replication in astrocytes in a culture dish devoid of IFN γ . This cytokine is critical for protection against toxoplasmic encephalitis (TE) in part by limiting parasite replication in astrocytes [57, 58] indeed in the absence of IFN γ signaling, cyst formation is observed in astrocytes [5, 58]. Our *ex vivo* model by no means solves the question of what prompts a cyst to reactivate, however, in the context of TE (absence of IFN γ) and during initial infection the developmental pathway uncovered by this *ex*

vivo model suggests the parasite is pre-programmed to undertake two important functions: 1. Amplify parasite burden to maximize dissemination and 2. Seed tissues with cysts that will continue transmission. These functions occur not sequentially driven by immune responses but are pre-programmed hence cyst formation even in the absence of IFN γ . Recrudescence is therefore a point in the lifecycle in which *Toxoplasma* has the potential to go from a homogeneous to a heterogeneous population composed of both replicating bradyzoites and tachyzoites in the same environment. We propose that this heterogeneity is functional. Bradyzoite to bradyzoite replication allows for the growth and maintenance of the cyst population either in neurons resulting in larger cysts and 'twin cysts' or via astrocytes as an energy-rich vessel facilitating optimal brady-brady replication and local cyst dissemination. Although significant progress has been made using genetically modified lab-strains to understand transcriptional regulation, cyst location, number and kinetics *in vivo*, in the absence of the complete recrudescence pathway (quickly lost *in vitro*), these studies are likely testing the initial seeding of cysts in the brain. Our results show that the complete bradyzoite to tachyzoite recrudescence pathway that unfolds over one week following purified bradyzoite infections is required for robust expansion, dissemination, and establishing tissue cysts in brain tissue. This window of opportunity is consistent with a recent study showing maximum tissue cyst formation in pig muscle is reached seven days after oral infection with tissue cysts from mice tissues [59]. Infections with the 3 growth forms of the excysted ME49EW

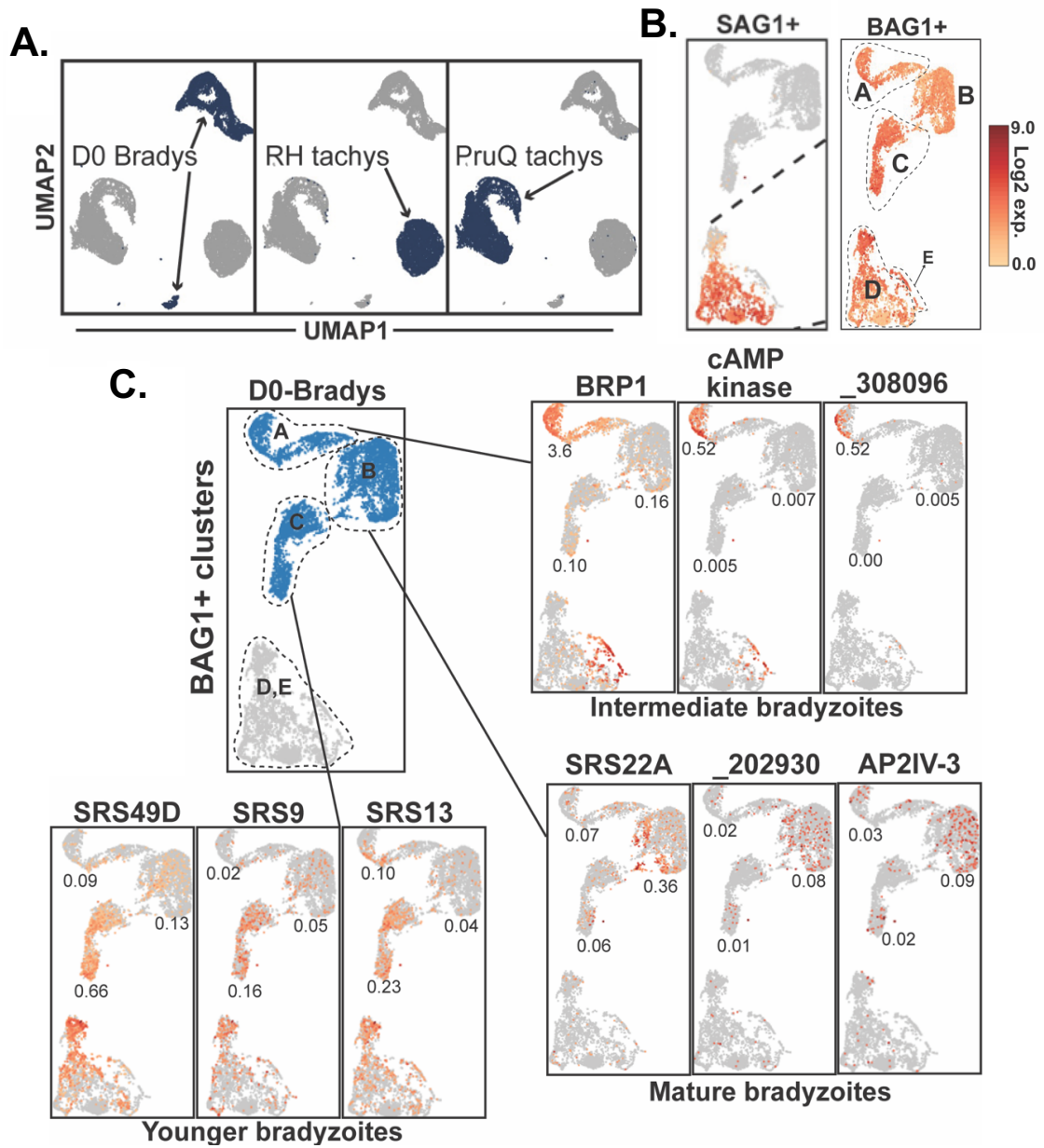
bradyzoite paints a picture of recrudescence following tissue cyst infection. Efficient bradyzoite infection of cells followed by a rapidly dividing phase after 24 h leading to almost 40% of cells infected by day 5 and a measurable number of extracellular parasites disseminating in the blood and migration to tissues with the lung showing early signs of infection. For the next four days fast-growing tachyzoites are seeding tissue especially the brain at which point they will encounter neurons encouraging cyst formation. By this time high systemic IFN γ activates host cells to limit parasite replication and clear this lytic form of infection. The pre-programmed switch to a slower-growing tachyzoite stage by day 7-9 enhances both the immune clearance of the acute infection and promotes conversion to the bradyzoite stage. This timing is supported by our data showing that drug treatment after day 9 is ineffective at limiting cyst burden confirming the slowing of parasite growth effectively ends dissemination. If the complete pathway is not intact and the fast-growing tachyzoite phase is skipped, as is the case when we infect with slow-growing tachyzoites, then cysts in the brain are >50-fold lower than infection with purified bradyzoites. The viability of these cysts is intact demonstrating that the parasites are cyst-competent. Instead it is the slow growth and poor dissemination of this slow-growing stage of the recrudescence pathway supported by fewer infected cells and a delay and reduction in the magnitude of the host response that likely accounts for low cyst numbers. We postulate that many of the lab-adapted strains that remain cyst-competent are stuck in this slow-growth phase of replication. In contrast, purified bradyzoites that remain single

undivided parasites for 24h result in a greater cyst burden in the brain over the rapidly dividing tachyzoites. Of note, the bradyzoite infections exceed the fast-growth tachyzoite in almost every parameter except the number of cells recruited to the site of infection. This could suggest a 'stealth-like' component of the excysted bradyzoite stage that would be missed in the rapidly dividing and lytic (immune-amplifying) fast-growth tachyzoite infections or an enhanced capacity to manipulate host cell migration thereby increasing dissemination as has been documented for tachyzoites [60].

In summary, the dormant bradyzoite in ME49EW tissue cysts possesses remarkable developmental flexibility and ability to tailor the parasite-encoded developmental program to the type of host cell infected (definitive or intermediate host), which is fully captured by the application of cell biology and scRNA-seq in a new *ex vivo* astrocyte recrudescence model. In the right host cell, ME49EW parasites can choose to replicate as bradyzoites or fully convert to the tachyzoite stage in order to disseminate. Native bradyzoites, like the sporozoite stage, develop into the tachyzoite stage using a two-step pathway that permits rapid biomass expansion but is also self-limiting. These versatile tachyzoites also have the ability to re-develop into the dormant bradyzoite at any time within a host cell environment that is permissive for tissue cyst development. Adapting native strains to HFF cell culture disrupts these pathways and may cause transcriptional confusion as recent single parasite RNA-seq studies have suggested [61].

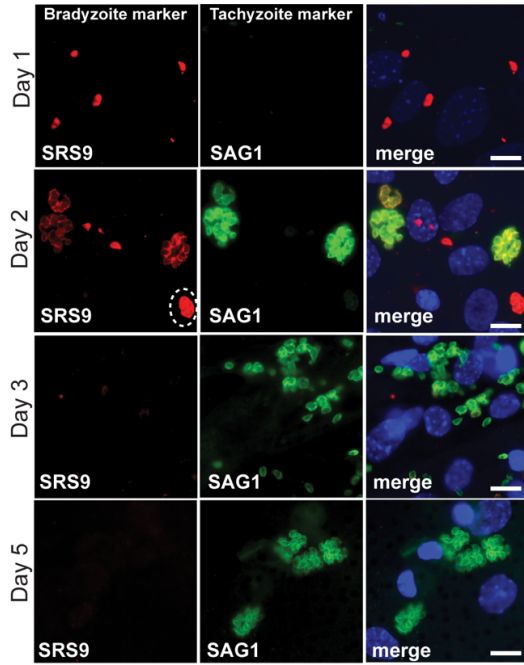
2.6 Figures & Legends

Figure 2.4.1 ME49EW Bradyzoites in Mature Tissue Cysts are a Dormant and Diverse Population. **[A.]** ME49EW bradyzoites compared to laboratory strain tachyzoites (Type II PruQ or Type I RH) subjected to single cell RNA-sequencing (scRNA-seq) visualized by uniform manifold approximation and projection (UMAP). **[B.]** UMAPs depicting the expression (Log2 Fold Change) of SAG1 or BAG1 in reclustered BAG1+ parasite. The population is comprised of five distinct clusters, Groups A-E. **[C.]** UMAP projection of BAG1+-bradyzoites showing three groups of dormant D0-bradyzoites (A-C, not including Group E). Replicating BAG1+ parasites in Groups D/E are not shaded. Three examples of gene expression enriched in the A- C clusters are shown. Shading shows the relative gene expression of individual parasites, while the indicated A-C expression values are average group expression for each gene. Gene IDs: Group A rhoptry kinases; BRP1 (TgME49_314250), cAMP kinase (TgME49_209985), ROP32 family (TgME49_308096). Group B; SRS22A (TgME49_238440), AP2IV-3 (TgME49_318610). Group C; SRS49D (TgME49_207160), SRS9 (TgME49_320190), SRS13 (TgME49_222370). Note, the three genes shown for Group B are expressed in merozoites of the feline definitive life cycle. Parasite numbers: Group A=1280, B=2642, C=1623, D=2994, E=170



2.4.2 Bradyzoite-Initiated Recrudescence in Fibroblast and Astrocytes. [A.] Representative images of parasite staining patterns Day-1 and -2 (1st monolayer) and Day-5 (2nd monolayer) from the original ME49EW bradyzoite infection of astrocytes. Infected astrocytes were fixed and co-stained for SAG1 (tachyzoite marker, green) and SRS9 (bradyzoite marker, red) with DAPI staining included as a reference (DNA, blue). Note parasites appear rounder in astrocytes than HFF cells due the thicker monolayer. The dashed circle in the Day 2-image is a SRS9^{Hi}/SAG1^{low} vacuole, while the other three replicating vacuoles in this microscope field are SRS9^{low}/SAG1^{Hi}. Day-5 parasites are primarily SAG1+. Scale bars=10 μ m. **[B.]** Quantification of the SAG1+ and SRS9+ expression of parasites in (A) and fibroblast data. **[C.]** Flow cytometry plots depicting SRS9 or SAG1 expression of parasites isolated from astrocyte or fibroblast (HFF) infection at indicated timepoints. *Ex vivo* bradyzoites corresponds to the initial excysted parasites prior to monolayer infection. Numbers indicate a percentage from a representative flow plot.

A. Developmental antigen expression



B. Bradyzoite-to-tachyzoite recrudescence

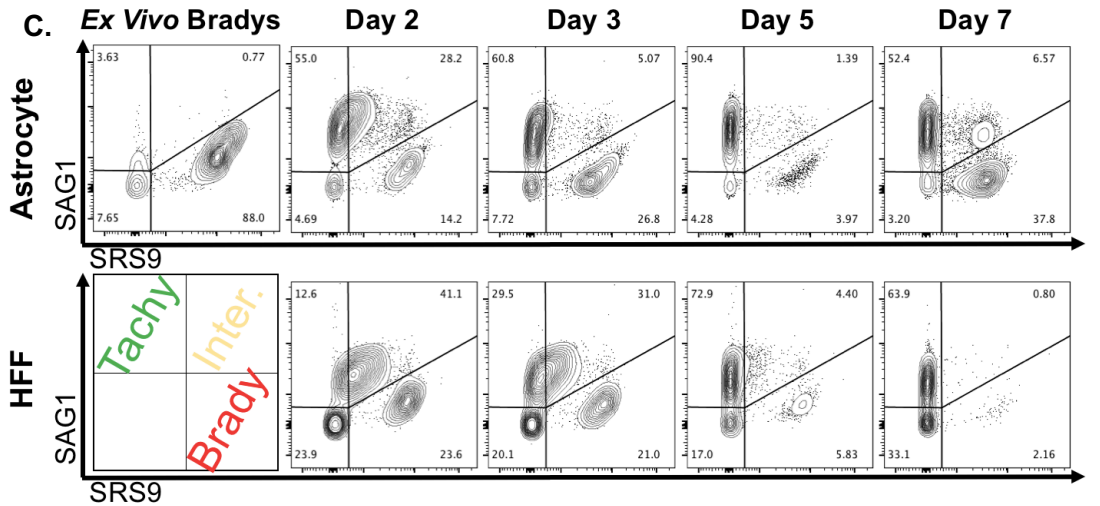
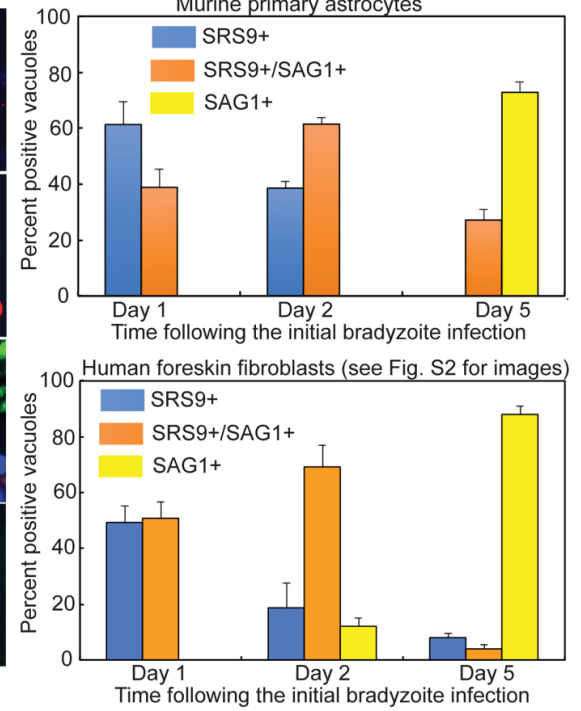


Figure 2.4.3 Bradyzoite-to-Bradyzoite Development. [A.] Diagram of bradyzoite-to-bradyzoite replication. [B.] Top two panels: representative images of parasite vacuoles from Day-2 and -5 infected astrocytes. Parasites were co-stained with antibodies against SRS9 (red) and SAG1(green) and with biotin-labeled *Dolichos biflorus* agglutinin (DBA) to identify vacuoles possessing cyst walls. Bottom panel: Day- 7 post-bradyzoite infection of astrocytes was co-stained for SRS9 (red), SAG1 (green) and DAPI (blue, DNA). Host nuclei in merged image are prominent. Size bars (10 μm) are indicated and the dashed circles indicate the vacuole containing SAG1+ parasites. [C.] Growth of SRS9+ only vacuoles over three days in HFF and mouse fibroblasts (MEF) versus primary astrocyte host cells. Vacuoles sizes were determined in randomly selected microscopic fields. Note that in HFF and MEF host cells vacuoles containing SRS9+ parasites showed minimal replication, while SRS9+ parasites were undergoing active replication in astrocytes. [D.] Quantitation of tissue cyst wall formation (DBA+) as compared to surface antigen expression (SRS9 vs SAG1). Note: no vacuole containing SAG1+ only parasites showed evidence of cyst wall formation and only a minor fraction of vacuoles with parasites expressing both SRS9 and SAG1 were found to have cyst walls. [E and F.] Representative images of tissue cysts in ME49EW infected astrocytes at Day-3 (first growth period) and Day-14 (fourth growth period) from the original ME49EW bradyzoite infection. CST1 staining (cyst wall, green), anti-*Toxoplasma* (red), and Dapi (DNA, blue). Scale bars=10 μm . Note the Day-3 image shows a single cyst along side two large vacuoles of rapidly growing tachyzoites. The cluster of cysts in the Day-14 image highlights the focal nature of some cyst formation in these cultures. Graph: quantitation of the average percent of vacuoles containing a tissue cyst wall at various times from the original bradyzoite infection. Growth/monolayer periods: Day 0-3, Day 3-5, Day 5-7, Day 9-14.

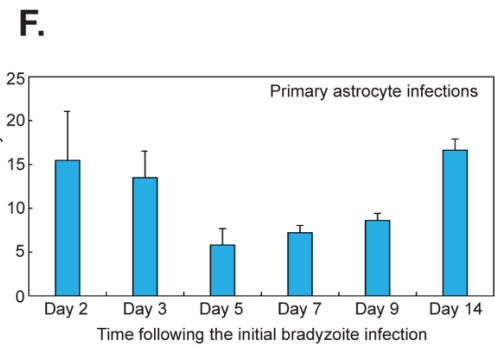
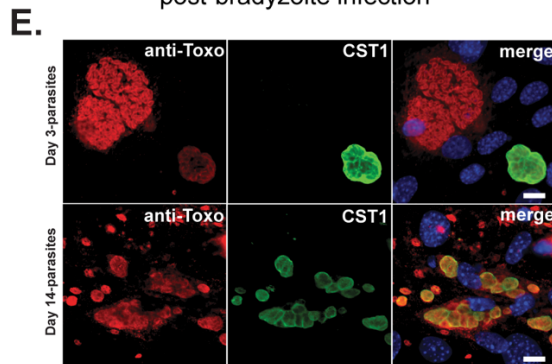
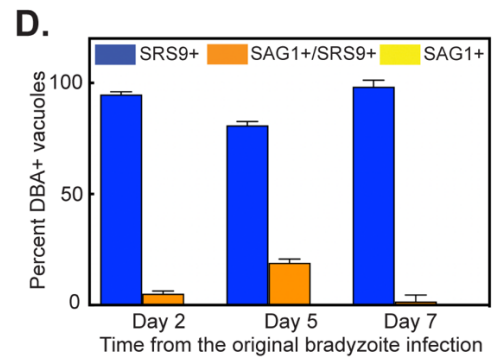
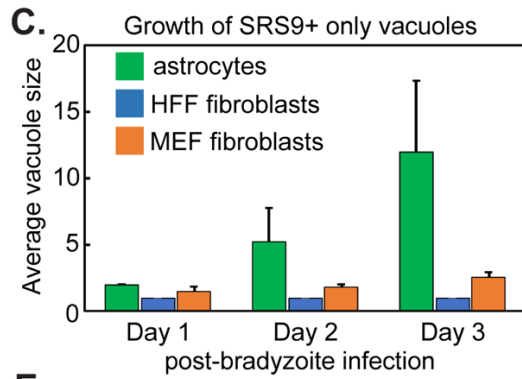
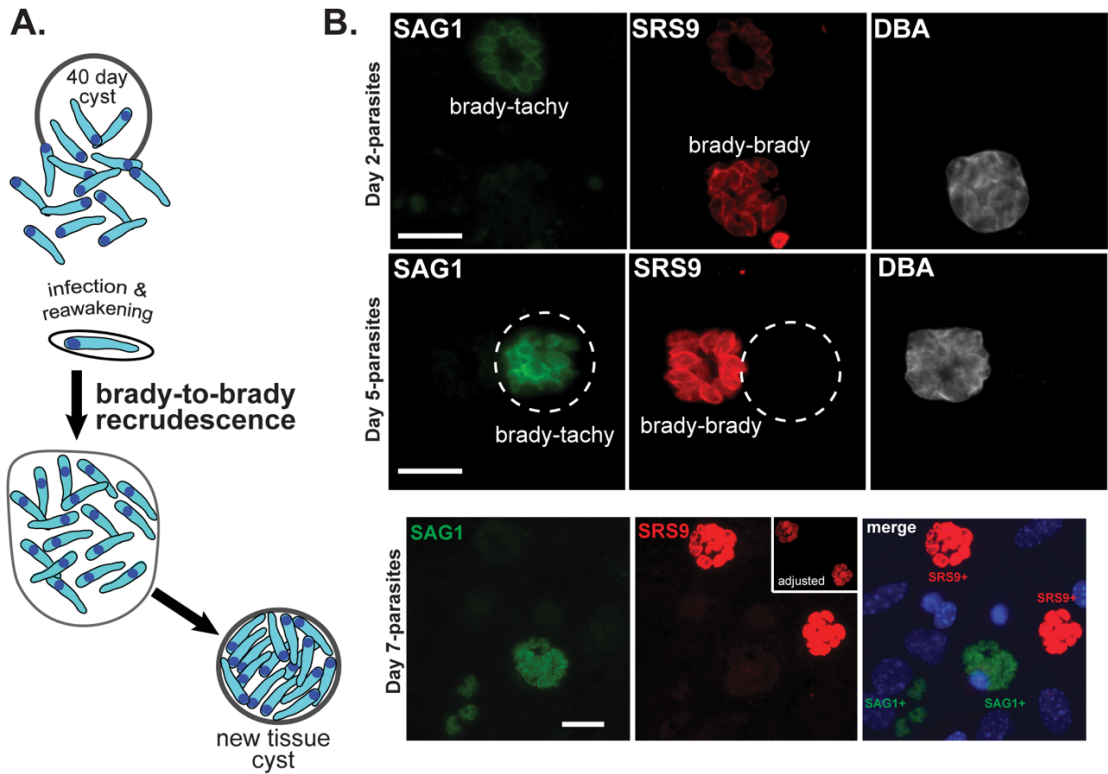
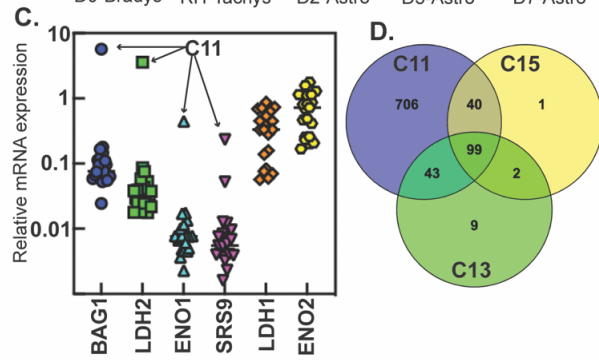
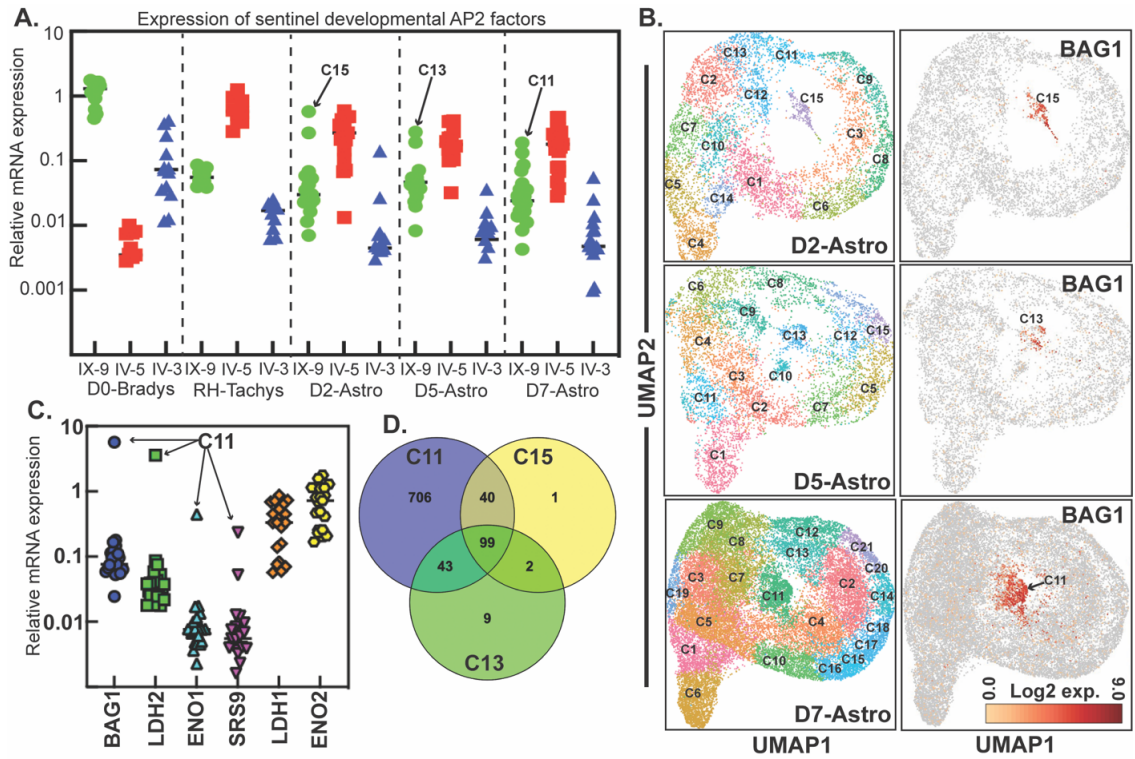
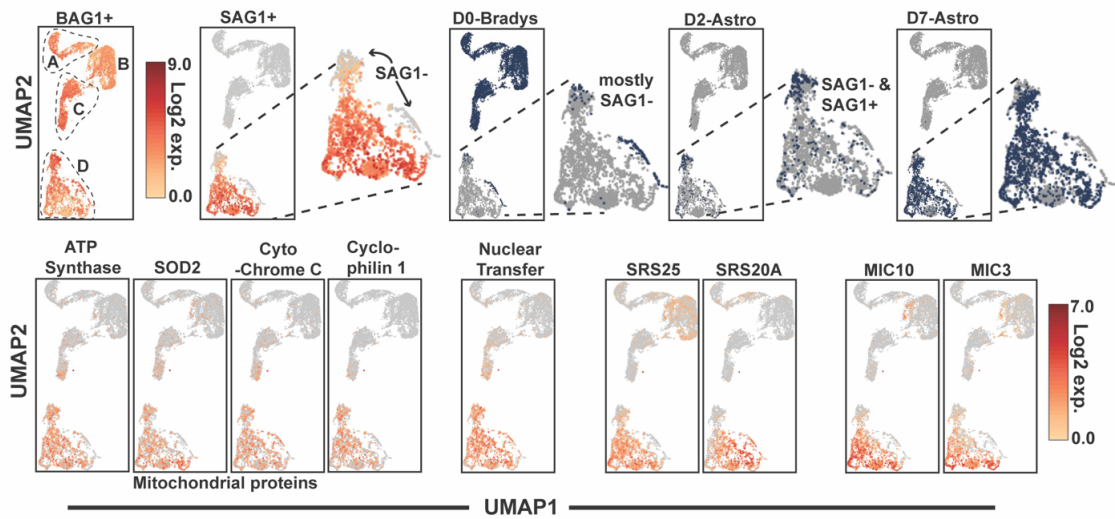


Figure 2.4.4 Resolving Parasite Development by Single Cell Transcriptomics.

[A.] Relative expression of AP2IX-9 (green dots), AP2IV-5 (red squares), and AP2IV-3 (blue triangles) within UMAP clusters (aggregated scRNA-seq data) from D0 excysted bradyzoites, RH tachyzoites, and Day-2, Day-5, and Day-7 parasites from astrocyte infections. High quality AP2IX-9 expression ($P < 0.05$) in single clusters C15, C13, and C11 are indicated. **[B.]** UMAP projection of parasite clusters from Day-2, Day-5 and Day-7 infected astrocyte samples (left images). Shading for BAG1 expression in UMAP projections shows clusters C15 (Day-2), C13 (Day-5), and C11 (Day-7) from astrocyte infections accounts for the majority of BAG1+ parasites. **[C.]** Relative expression of canonical bradyzoite genes (as well as tachyzoite LDH1 and ENO2 genes) in the 21 parasite clusters from Day-7 astrocyte infections. Levels of BAG1, LDH1, ENO2, and SRS9 expression in cluster 11 are indicated. **[D.]** High quality gene expression ($P < 0.05$) from cluster C15, C13, and C11 were identified and compared. **[E.]** Clustering of total BAG1+ parasites from all samples are visualized by UMAP projection (A-D clusters are indicated). Shading of BAG1+ parasite clusters A-D by SAG1 expression. BAG1+ parasites from D0-bradyzoite and Day-2 and Day-7 astrocyte infections are individually overlaid on the total BAG1+ UMAP. Selected gene expression is shaded on the total BAG1+ parasite UMAP.



E. Re-clustering of BAG1+ parasites



CHAPTER THREE

*Group 1 Metabotropic Glutamate Receptor Expression on CD8 T Cells Define a
Memory Subset in the Toxoplasma-Infected Brain*

3.1 Abstract:

Within the brain, a pro-inflammatory response is essential to prevent clinical disease due to *Toxoplasma gondii* reactivation. Infection in the immunocompromised leads to lethal Toxoplasmic encephalitis while in the immunocompetent, there is persistent low-grade inflammation which is devoid of clinical symptoms. This signifies that there is a tightly regulated inflammatory response to *T. gondii* in the brain. T cells are the dominant immune cell that prevent clinical disease, and this is mediated through the secretion of effector molecules such as perforins and IFN γ . The presence of cognate antigen, the expression of survival cytokines, and the alteration of the epigenetic landscape drive the development of memory T cells. However, other extrinsic signals that promote the formation and maintenance of memory T cells within tissue are poorly understood. During chronic infection, there is an increase in extracellular glutamate that, due to its function as an excitatory neurotransmitter, is normally tightly controlled in the brain. Thus, we hypothesize that glutamate is an important environmental signal of inflammation that promotes T cell function within the CNS. Our data demonstrate that CD8⁺ T cells from the *T. gondii*-infected brain are enriched for metabotropic glutamate receptors (mGluR's) compared to secondary lymphoid-derived cells. Characterization studies determined that brain mGluR⁺ T cells are a distinct population at the transcriptional and protein level relative to their mGluR⁻ counterparts. Furthermore, these studies determined that mGluR expression on CD8⁺ T cells defines a memory population in the infected brain. Finally, functional

studies revealed that mGluR signaling optimizes CD8⁺ T cell production of the effector cytokine IFN γ . Therefore, understanding glutamate's influence on T cells in the brain can provide insights into the mechanisms that govern protective immunity against CNS-infiltrating pathogens and neuroinflammation.

3.2. Introduction:

It is commonly known that the central nervous system (CNS) is an immune-privileged site [62]. In order for T cells to traverse the blood brain barrier (BBB) during an inflammatory insult, a concert of antigen presentation, the production of proinflammatory mediators, and the generation of chemokine gradients is orchestrated [63, 64]. In addition to this, a combination of survival cytokines such as IL-7 and IL-15, and the remodeling of the epigenetic landscape in activated CD8 T cells in the periphery promote the formation of memory precursors [65-70]. Molecules such as TGF β that are present in inflamed compartments have been shown to promote the formation of tissue resident memory T cells (T_{RM}), the presence of these cells alone, suggests that environmental cues in the tissue are important for T cell maintenance and differentiation [71].

T. gondii remains in a relatively dormant cyst-state in neurons, conferring life-long chronic infection within the brain [5]. A T cell-mediated pro-inflammatory response is essential to control parasite burden and prevent clinical disease. This is in contrast to many inflammatory events in the brain which are associated with severe

clinical pathology and suggests a well-balanced inflammatory response in the CNS. Contributions to this response include ILC recruitment [72], T cell expression of the chemokine receptors CXCR3 and CCR7 [73-75], inhibition of T cell inflammatory responses via Treg induction and exhaustion [21, 76, 77] and potential signals derived from extracellular matrix remodeling [78]. The T cell population in the *T. gondii*-infected brain is a heterogeneous mixture of effector & memory CD4⁺ & CD8⁺ T cells, including a significant proportion of a CD8⁺CD103⁺ T_{RM} population that are an important source of the protective cytokine IFN γ [79]. The tissue-specific signals that drive and maintain memory cells within the brain during *Toxoplasma* infection are unknown.

One aspect of the environment in the brain that differs from other tissues is the tight regulation of glutamate at this site. Under homeostatic conditions, the role of glutamate in the brain is as the primary excitatory neurotransmitter. Increases in extracellular glutamate concentrations can lead to enhanced neuronal firing, excitability, neurotoxicity and cell death. Extracellular glutamate is tightly regulated in the CNS by astrocytic glutamate transporter-1 (GLT-1). Dysregulation of GLT-1 leads to increased glutamate concentrations, spontaneous seizures and significant neuronal pathology due to excitotoxicity [80, 81]. During *Toxoplasma* infection, GLT-1 is downregulated and EC concentrations are pathological. Thus, a major component of the infected brain environment is the easy availability of glutamate [82-84]. High EC glutamate concentrations are not exclusive to *T. gondii* infection

and occur during multiple inflammatory CNS pathologies such as multiple sclerosis (MS), traumatic brain injury, and epilepsy [83-85]. All of these are situations in which significant inflammation occurs and recruitment of T cells is a feature [83-85]. There is therefore a clinical demand to find effective glutamate-lowering drugs to protect against neuronal loss; however, the role of glutamate in mediating protective and critical immunity during infection remains unknown [82].

Glutamate is found throughout the body and, as well as a neurotransmitter, acts as a basic amino acid for cells. In addition to this, the uptake of exogenous glutamine into T cells can be converted to glutamate, where it will be shuttled to the citric acid cycle or will be secreted out of the cell by the cystine/glutamate antiporter (Xc-) [86, 87]. Although the import of cystine is used as a precursor for glutathione synthesis, the export of glutamate by T cells has an undefined function [88]. Glutamate concentration in the blood can range from 10-100 μ M, whereas concentrations in the brain exceeding 1 μ M can lead to clinical pathology [83]. The ability for immune cells to interact with neurotransmitters such as glutamate, has been an active field of research. It is known that Jurkat and human peripheral T cells express metabotropic (mGluR's) and ionotropic glutamate (iGluR's) receptors, where stimulation of these receptors can lead to Ca²⁺ mobilization [84, 89-93]. However, most studies dissecting the molecular mechanism of group 1 mGluR (receptor 1&5) signaling have been in the context of signaling in neurons where it plays an important role in promoting synaptic plasticity, regulating long

term potentiation, and memory formation [94, 95]. In contrast, group 1 mGluR's expressed on anti-CD3-activated human peripheral T cells promote their proliferation, and inhibit activation induced cell death [89, 96]. However, knowledge of mGluR's role within a tissue environment in the context of inflammation or infection is lacking.

Here we demonstrate that in the *T. gondii*-infected brain, a CD8⁺ T cell population that has the potential to sense glutamate and expresses the G protein-coupled metabotropic glutamate receptors, mGluR1 and mGluR5. This expression is enriched in CD8⁺ T cells recruited to the brain compared to secondary lymphoid-derived cells. Furthermore, we utilized single cell RNA-sequencing (scRNA-seq) and multianalyte flow cytometry analysis to examine T cell ontology and heterogeneity. This revealed the mGluR expressing cells are a replicating population that exhibit a memory phenotype. Furthermore, the production of the protective cytokine IFN- γ is enhanced through mGluR signaling. Our findings reveal an important tissue-specific context for the regulation of T cells in the inflamed brain and could lead to potential therapies targeting mGluR signaling.

3.3. Materials and Methods:

Mice and Parasites: The Type II ME49 strain of parasites were maintained in female CBA mice for at least 3 weeks post infection (wpi). Brains were harvested from chronically infected mice and were serial homogenized through 18, 20 and

22 gauge blunt needles in 3ml of 1xPBS. After counting, cysts were diluted in 1xPBS to infect 6-8 week old female C57Bl/6 mice intraperitoneally at 10 cysts per mouse in a 200 μ L volume. Female C57Bl/6 and CBA mice were obtained from the Jackson Laboratory (Jackson ImmunoResearch Laboratories, Inc., West Grove, PA, USA). Mice were maintained in a pathogen-free environment under IACUC established protocols at the University of California, Riverside. Mice were given free access to water and food at all times.

Cell Preparation: Mice were euthanized in accordance to the Animal Welfare Act and brains, spleens, and cervical lymph nodes were harvested for downstream applications at respective timepoints. *Brain Mononuclear Cell (BMNCs) Preparation:* prior to harvesting organs, mice were intracardially perfused with 20mL ice-cold 1xPBS. Mononuclear cells were isolated from the brain by homogenization passage through an 18-gauge needle in complete RPMI (cRPMI) (86% RPMI, 10% FBS, 1% penicillin/ streptomycin, 1% L-glutamine, 1% NEAA, 1% sodium pyruvate, <0.01% β -mercaptoethanol). The homogenate was incubated for 1h at 37°C/ 5%CO₂ with 3mg DNase and 100 μ g collagenase/dispase. After incubation, the suspension was passed through a 70 μ m strainer, washed once, and spun at 1200 RPM, 10 minutes, 4°C. The homogenate was resuspended in a 30% Percoll density gradient diluted in cRPMI, followed by a spin at 2,000 RPM for 25 min with no brakes at room temperature. Brain mononuclear cells (BMNCs) were isolated from the gradient and washed

once with cRPMI and counted. *Splenocytes Preparation:* spleens were homogenized through a 40µm strainer using the blunt end of a 5mL syringe. The homogenate was washed with cRPMI, and 5ml of cold ACK buffer (Lonza) was added for 5min to lyse red blood cells. Splenocytes were then washed with cRPMI and counted. All spins were performed at: 1200 RPM, 10 minutes, 4°C. *Cervical Lymph Nodes Preparation:* lymph nodes were homogenized through a 40µm strainer using the blunt end of a 5mL syringe. The homogenate was washed once with cRPMI and counted. All spins were performed at: 1200 RPM, 10 minutes, 4°C.

Sample Preparation for Flow Cytometry: After isolation, cells were washed once with FACS Buffer (1L 1xPBS, 4g bovine serum albumin, 50mg EDTA), blocked for 10 min with Fc block (BD Biosciences), and incubated with a panel of antibodies (*see list of antibodies below*) for 30 min protected from light at 4°C. Samples were washed twice with FACS Buffer, fixed and permeabilized with Cytofix/Cytoperm (BD) for 10min at 4°C and washed with BD Wash Perm Buffer (BD). For detection of intracellular proteins, samples were incubated with a second panel of intracellular antibodies (*see list of antibodies below*) for 30 min protected from light at 4°C. Samples were washed twice with BD Wash Perm Buffer followed by resuspension in FACS Buffer. All spins were performed at: 1500 RPM, 3 minutes, 4°C. All samples were analyzed on either the FACS Canto (BD Biosciences) or the Novocyte Advanteon Flow Cytometer (Agilent). Flow cytometry analyses were

performed using FlowJo 10.7.2, and statistical analyses were performed using GraphPad Prism 7.

The following flow cytometry antibodies were purchased from BD Biosciences: anti-CCR7 ([1:100]; clone 4B12); anti-T-bet ([1:100]; clone O4-46); anti-ID3 ([1:50]; S30-778); The following antibodies were purchased from ThermoFisher Scientific: anti-CD8a ([1:100]; clone 53-6.7); anti-CD3e ([1:100]; clone 145-2C11); anti-CD103 ([1:50]; clone 2E7); anti-KLRG1 ([1:100]; clone 2F1); anti-CXCR3 ([1:100]; clone CXCR3-173); anti-CD127 (1:100 dilution; clone A7R34); anti-CD45 ([1:100]; 30-F11) anti-EOMES ([1:50]; clone Dan11mag); anti-CD25 ([1:100]; clone PC61); anti-CD212 ([1:100]; clone 114); anti-CD69 ([1:100]; clone H1.2F3); anti-Ki67 ([1:100]; clone SolA15; anti-IFN- γ ([1:50]; dilution; clone XMG1.2); anti-IL-2 (1:50 dilution; clone JES6-5H4); anti-perforin ([1:50]; eBio0MAK-D); The following flow cytometry antibodies were purchased from BLOSS: anti-mGluR1a ([1:100]; clone bs-12011R); anti-mGluR5 ([1:100]; clone bs-1247R); The following flow cytometry antibodies were purchased from Novus: TCF1 ([1:100]; clone 812145)

Cell Sorting and Single Cell RNA Sequencing Analysis: Cells were isolated and prepared for flow cytometry as described above. Cells were diluted to 20E6cells/ml and the MoFlo Astrios Cell Sorter (Beckman Coulter) was used to sort on CD3⁺CD8⁺mGluR1⁺mGluR5⁺ and CD3⁺CD8⁺mGluR1⁻mGluR5⁻ T cells. Single Cell RNA sequencing was performed on sorted cells using the 10X Genomics

Chromium Next GEM Single Cell 3' Reagent Kits v3.1 as described by the manufacture protocol. Sequencing depth was performed at 800 million reads and generated at the UC San Diego IGM Genomics Center utilizing an Illumina NovaSeq 6000 that was purchased with funding from a National Institutes of Health SIG grant (#S10 OD026929). Sequencing reads were aligned to the GRCm38-mm10 reference genome using 10X Genomics Cellranger (version 5.0.1). The Cellranger aggregation protocol was used to combine indicated datasets for secondary analysis. All analyses were performed and visualized using the 10X Genomics Loupe Browser (version 6.1.0). Gene ontology and KEGG pathway analysis was performed using the Database for Annotation, Visualization and Integrated Discovery (DAVID) on genes with a Log₂ fold change of 1 and greater. Genes used for this analysis as well as individual mGluR- and mGluR+ replicates can be found in "Supplemental Table 1_ScRNA seq Database_Figure 2." Expression profiles examining effector and memory gene signatures can be found "Supplemental Table 2_ScRNA seq Database_Figure 3." Genes to identify cell cycle stages were generated using supplemental datasets from [97], and the addition of known gene families to be important for G0/G1, S, and M phase. The full set of genes used for this analysis can be found in "Supplemental Table 3_ScRNA seq Database_Figure 4". All scRNA-seq datasets have been uploaded to GEO (accession number [GSE211727](https://www.ncbi.nlm.nih.gov/geo/query/acc.cgi?acc=GSE211727))

Restimulation Assay: Brain mononuclear cells and splenocytes were collected from mice at 3 wpi and incubated for 6h (flow cytometry) or 24h (ELISA) with respective stimulations diluted in complete T cell media (86% RPMI, 10% FBS, 1% penicillin/streptomycin, 1% L-glutamine, 1% NEAA, 1% sodium pyruvate, <0.01% β -mercaptoethanol). Cells were untreated (-control) or activated with 5 μ g/mL α CD3 and 2 μ g/mL α CD28 (BD Biosciences) antibody (+control), and treated with glutamate [100 μ M] (DHPG;Tocris), or [100 μ M] dihydroxyphenylglycol (DHPG;Tocris), or 100 μ M 2-chloro-5-hydroxyphenylglycine (CHPG; Tocris), or [100 μ M] (RS)-1-Aminoindan-1,5-dicarboxylic acid (AIDA; Tocris), [1mM] 3-((2-Methyl-1,3-thiazol-4-yl)ethynyl) pyridine hydrochloride (MTEP; Tocris), [1mM] (RS)- α -Methyl-4-carboxyphenylglycine (MCPG; Tocris). Supernatant was collected at 24h post-stimulation for IFN- γ ELISA. For flow cytometry studies, cells were treated with BD Golgi Plug 3h post-stimulation and harvested for an IL-2, IFN- γ , and perforin intracellular cytokine stain. IFN- γ was measured in supernatants by ELISA following 24h stimulation. IFN- γ capture antibody [1:1000] (clone: AN-18 ebioscience, 14-7313-81) was incubated overnight at 4°C on high binding plates (Corning Cat: 3590). Recombinant IFN- γ (ebioscience, 14-8311-63) was used to create the standard. Standard and supernatant samples were diluted in diluent buffer (1XPBS, 0.1% BSA, 0.05% Tween-20) and incubated at 37°C for 2h. Biotin conjugated anti-mouse IFN- γ [1:1000] (clone: R4-6A2 ebioscience, 13-7312-85) was diluted in diluent buffer and incubated at 37°C for 1h. Peroxidase conjugated streptavidin [1:2000] (Jackson ImmunoResearch, 016-030-084) was

diluted in diluent buffer and incubated for 30min at 37°C. TMB substrate (Thermo, N301) was used for the colorimetric reaction, and an equal part of 0.16M sulfuric acid was used to stop the reaction. Absorbances were measured on a spectrophotometer at 450nm. Analysis was conducted in GraphPad Prism (version 7).

Statistics and reproducibility: Graphs were generated using Prism v.7 (GraphPad Software) and statistical significance was determined using a one or two way-ANOVA with multiple comparisons where * $p < 0.05$, ** $p < 0.01$, *** $p < 0.001$, **** $p < 0.0001$ was considered statistically significant. Total n refers to the number of biologically independent samples in each respective group. All graphs show the mean \pm SD (Standard Deviation).

3.4 Results

3.4.1 Expression of Group 1 Metabotropic Glutamate Receptors are Enriched on CD8⁺ T Cells in the Toxoplasma-Infected Brain

In contrast to the homeostatic healthy brain where extracellular glutamate concentrations are kept magnitudes lower than the blood, a glutamate-rich environment is generated in the brain during *T. gondii* infection due to a downregulation of the astrocytic glutamate transporter, GLT-1 [82, 98]. To determine if glutamate could potentially be an important microenvironmental cue

for CD8⁺ T cells which are critical for the control of parasite burden and reactivation, flow cytometry was performed on brain mononuclear cells (BMNCs) and peripheral organs (spleen & cervical lymph nodes) from *T. gondii*-infected mice during the late acute, early chronic, chronic, and late chronic time points (2, 3, 6, and 12 weeks post-infection (wpi), respectively) to test for the expression of group 1 mGluR's. Splenic and cervical lymph node derived CD8⁺ T cells express both mGluR1 and mGluR5, however, they do not make up the majority of the peripheral T cell repertoire (**Fig. 3.4.1 a-c, left and middle panels**). In contrast, a significant proportion of CD8⁺ T cells recruited to the infected brain during the early stages of infection (2 & 3wpi) express group 1 mGluR's (84±3% & 69±6%, respectively). This is reflected in the absolute numbers of mGluR⁺ cells in the brain which are a log fold more than the mGluR⁻ population (**Fig. 3.4.1 a-c, right panel**). However, this mGluR1⁺mGluR5⁺ population in the brain declines significantly to less than 20% of the total CD8 population during late chronic stages of infection (6weeks, 19±6% and 12 weeks, 5±2%), although there remains a steady population expressing only mGluR1 (~40%). Together these data indicate that there is a glutamate-sensing CD8⁺ T cell population that has the capacity to interact with glutamate via mGluR's in both the CNS and periphery following *Toxoplasma* infection.

3.4.2 Glutamate Receptor Expression Identifies a Transcriptionally Distinct Population of CD8⁺ T cells in the Brain

Although a significant population of CD8⁺ T cells express group 1 mGluR's in the infected brain, it is unclear if mGluR expression defines a unique population. To test if mGluR⁺ CD8⁺ T cells are transcriptionally distinct from their mGluR⁻ counterparts, scRNA-seq (10X Genomics) was performed on cell-sorted BMNC's 3wpi, to enrich for the mGluR⁻ and mGluR⁺ CD8⁺ T cell fractions. Uniform Manifold Approximation and Projection (UMAP) dimensional reduction plots of the aggregated transcriptional datasets demonstrate that the mGluR⁻ (blue) and the mGluR⁺ (orange) populations cluster markedly away from each other suggesting transcriptionally distinct subsets (**Fig. 3.4.2a**). In addition, there were 3998 differentially expressed genes (DEG) found in the mGluR⁺ and 3586 DEG found in the mGluR⁻ fraction (**Fig. 3.4.2b**). Any overlapping genes between the two populations were mainly associated with T cell-related ontology. To identify significantly enriched pathways and gene ontology (GO) terms in the brain mGluR⁺ CD8⁺ T cells, DEG with a Log₂ fold change (FC) greater than or equal to 1 were placed into DAVID (Database for Annotation, Visualization and Integrated Discovery) (**Fig. 3.4.2c-d**) [99, 100]. Enrichment analysis revealed that the mGluR⁺ fraction is enriched for GO Terms such as cell migration, ion transport, cell differentiation, and cell development (**Fig. 3.4.2c**). KEGG Pathway enrichment analysis demonstrated that adhesion molecules, extracellular-receptor interactions, and calcium signaling were all enriched pathways in the mGluR⁺CD8⁺

T cells (**Fig. 3.4.2d**). Although the “glutamatergic synapse” term is typically associated with neurons, the upregulation of both metabotropic (encoded by *Grms*) and ionotropic glutamate receptor (encoded by *Grins* & *Grias*) transcripts in the mGluR⁺CD8⁺ T cells promote the enrichment for this KEGG Pathway (**Fig. 3.4.2 c,e-f**). These data suggest that glutamate regulation of the mGluR⁺ subset of T cells is multifaceted.

Although group 1 mGluR signaling uses a Gαq pathway in neurons, there has been confounding data as to which signaling cascade T cells use [101]. To determine if Gq signaling mediators are upregulated in mGluR⁺CD8⁺ T cells, downstream molecules of the Gq signaling cascade was investigated. When testing for the expression of *Gnaq* (encodes Gαq subunit), there is an upregulation (Log₂FC=1.6) in the mGluR⁺ fraction relative to the mGluR⁻ T cells (**Fig. 3.4.2g**). To further test if a Gq signaling pathway is implicated, other genes including *Plcb2* (encodes Phospholipase C) and *Prkca* (encodes Protein Kinase C) were also assessed. Both genes were slightly upregulated compared to the mGluR⁻ fraction. Collectively, these data suggest that brain mGluR⁺CD8⁺ T cells have a distinct transcriptional profile relative to their mGluR⁻ counterparts, and multiple glutamate receptor expression and signaling are one of the defining features of this population which supports a Gαq mechanism.

The expression of surface proteins to define a population may miss the dynamic nature of many G-protein coupled receptors. To help determine the origin of mGluR⁺ cells and rule out a continuous turnover of the receptor, trajectory analysis (Monocle v3) was performed on the aggregated CNS mGluR⁻ and mGluR⁺ CD8⁺ T cell datasets to determine the number of lineages and direction of the population. This type of modeling revealed 14 related lineages amongst the combined datasets, where only lineage 3 promoted the formation of the mGluR⁺ subset (**Fig. 3.4.2h, left panel**). Pseudotime analysis was used to predict the direction of the CNS CD8⁺ T cell population, where the earliest inferred pseudotime is represented as purple, and the latest inferred pseudotime is yellow. Data suggests that the mGluR⁺ subset is derived from the mGluR⁻ fraction, rather than the mGluR⁺ subset differentiating into mGluR⁻ CD8⁺ T cell (**Fig. 3.4.2h, right panel**). Taken all together, these data continue to support the mGluR⁺ population being a unique and defined subset of CD8⁺ T cells, and that the mGluR⁺ subset is generated from one lineage that originates from the mGluR⁻ CD8⁺ T cell population.

3.4.3 mGluR⁺CD8⁺ T cells Exhibit a Memory Phenotype

Classically, surface receptors have been used to define the memory status of a T cell. Emerging data suggest that memory T cells are more plastic than previously thought, and this is in part due to a core set of transcription factors that are in common with stem cells [102-104]. These shared genes define a 'stem cell-likeness' which promotes the capacity of memory T cells to remain long-lived, self-

renew, and proliferate [105]. To determine if the mGluR⁺ CD8⁺ T cell fraction in the infected brain exhibit memory potential, genes that are indicative of a memory signature (both receptors and transcription factors) were examined (**Fig. 3.4.3A, red genes**). In comparison to mGluR⁻CD8⁺ T cells, mGluR⁺ CD8 T cells exhibit elevated levels of gene transcription associated with memory precursors such as *Id3*, *CCR7*, *Bcl6*, *Sell*, *Bach2*, *Foxo1*, and *TCF7*. For comparison, genes that are associated with an effector signature were also included in the analysis (**Fig. 3.4.3a, blue genes**). The upregulation of genes implicating a terminally differentiated status such as *KLRG1*, *Id2*, *Stat4*, and *Baft* were observed to be associated with the mGluR⁻ population indicating that the mGluR⁺CD8⁺ fraction has more memory potential relative to their mGluR⁻ CD8⁺ counterparts in the infected brain (**Figure 3a**).

To validate our scRNA-seq findings at the protein level, a multi-parameter flow cytometry panel was performed on BMNC's at 2, 3, 6, and 12 wpi to test for the expression of molecules that define a memory (CD127, EOMES, *Id3*, CD69, CD103) or terminally differentiated effector status (*KLRG1*, Tbet) in the mGluR⁺CD8⁺ T cell population. Concatenation of brain CD8⁺ T cells from early chronic time points (2-3wpi) reveal two populations that are enriched for mGluR1 (**Fig. 3.4.3b**). The two defined clusters may suggest that there is a stable population of mGluR⁺CD8⁺ T cells, and an mGluR⁺ population that is in the process of transitioning, supporting what is observed in our scRNA-seq UMAP plots (**Fig.**

3.4.2a, 3b). The lack of KLGR1 expression on mGluR⁺CD8⁺ T cells for the duration of the study suggests they are not a terminally differentiated effector population (**Fig. 3.4.3b**) while the survival cytokine receptor, CD127, which is typically expressed by naïve and memory T cells, is found on the mGluR⁺ fraction suggesting they are long-lived memory cells [106] (**Fig. 3.4.3b**). The transcription factor T-bet is important for promoting effector function of T cells, whereas the transcription factor, EOMES, has been shown to have an opposing role to T-bet which promotes the formation of memory CD8⁺ T cell [107, 108]. The decreased ratio of T-bet/EOMES signifies the establishment of a memory population in the mGluR⁺ CD8⁺ T cells (**Fig. 3.4.3b**). Coupled with the fact that no naïve T cells are found in the infected brain, these data suggest that the mGluR⁺ population display a memory signature [109].

A significant population of memory cells in the *T. gondii*-infected brain are CD8⁺ tissue resident memory cells expressing CD69 and CD103 [79, 110]. To address if mGluR-expressing T cells resemble a T_{RM} cell phenotype, the expression of CD69 and CD103 was evaluated. CD103 protein was not defined by mGluR expression and remains low in mGluR⁺CD8⁺ T cells for the duration of infection (**Supp. Fig. 3.4.3a**). In contrast, although CD69 protein levels are equally expressed on both CD8⁺ T cell populations during early chronic infection, the expression of CD69 is retained predominantly by the mGluR⁺ T cell during late chronic infection (**Supp. Fig. 3.4.3a**).

DNA-binding inhibitors consist of four proteins (Id1-4) which regulate the binding activity of E-protein transcription factors [111]. Id2 and Id3 family members have both been implicated in lymphocyte development [112, 113]. In the context of viral infection, high Id2 expression skewed CD8⁺ T cells to a short-lived effector lineage, whereas high Id3 expression in virus-specific CD8⁺ T cells correlates with a transition to a memory status, [114]. Additionally, Id3 transcript levels associated with high Id3 expression during late chronic infection suggesting a 'progenitor-like' population has formed. Taken altogether, these data demonstrate that the brain-infiltrating CD8⁺ T cell that express mGluR's exhibit a memory phenotype, and may be CD69⁺ T_{RM} cells. are also upregulated in CD8⁺ T cell memory precursors during chronic viral infection [104, 115]. As *Id3* is among the top 'stem-like' transcripts enriched in the mGluR⁺ fraction, *Id3* protein levels were examined during the course of infection (**Fig. 3.4.3a and 3c**). Although neither CD8⁺ T cell fraction have significant *Id3* protein levels during early chronic infection, the mGluR⁺CD8⁺ T cells are strongly

3.4.4 mGluR⁺CD8⁺ T cells Recruited to the T. gondii-Infected Brain are a Proliferating Population

The effect of glutamate stimulation on mGluR expressing T cells in the brain is unknown. To test whether proliferation of T cells is a possible downstream function of mGluR expression or if mGluR expression defines a replicating population,

unbiased cluster analysis was performed on aggregated scRNA-seq datasets from 3 independent cell sort experiments from purified mGluR⁺CD8⁺ T cell populations. UMAP analysis revealed 3 unique clusters with a ring-like formation which is characteristic of replicating cells (**Fig. 3.4.4a**). Differential expression analysis of genes with a $\text{Log}_2\text{FC} \geq 1$ and a significance of ≤ 0.05 demonstrate that there are 559, 1897, and 1662 DEGs in Clusters 1-3, respectively (**Fig. 3.4.4b**). Using DAVID to perform pathway and GO Term enrichment analysis, terms such as “cell division”, “mitotic nuclear division”, and “cell cycle” were found in cluster 1 (**Fig. 3.4.4c, top**) and KEGG pathways such as pyrimidine metabolism and DNA replication are enriched in cluster 2 (**Fig. 3.4.4c, middle**). Taken together, clusters 1 and 2 terms suggest an actively replicating population. GO Terms found in cluster 3 such as “cell migration” and “cell adhesion,” imply that a portion of this subgroup are not replicating, but rather are involved in biological processes critical for the T cell response to *T. gondii*. However other terms found in cluster 3 such as “regulation of transcription” and “DNA-template” indicate a fraction of cells may be in the transition to replicate (**Fig. 3.4.4c, bottom**). Given that there are several cell cycle phases, genes that are associated with G0/G1, S, and M stages of cell replication and division were assessed. Histone deacetylases (HDACs) are a class of enzymes that remove acetyl groups from lysine residues on histones [116]. This in turn will condense the chromatin structure affecting access of transcriptional and replication machinery, and thus promote a state of quiescence [116, 117]. Genes that encode various HDAC family members are most enriched in cluster 3,

however are most downregulated in cluster 2 suggesting that cells in cluster 3 are more likely to be in G0 phase than those in cluster 2, and to an extent, cluster 1 (**Fig. 3.4.4d**). Next, the expression of genes associated with DNA replication were assessed to identify cells in S phase of the cell cycle. Families of genes such as minichromosome maintenance complex components (*Mcms*), DNA polymerases, and histone subunits were all predominantly upregulated in cluster 2 [118] (**Fig. 3.4.4d**). In addition, replication factor C (*Rfc3-4*), a complex crucial for rapid DNA-synthesis, is among the top S phase genes in cluster 2 [119, 120]. GIN family members are important for the initiation of DNA replication and are upregulated in Cluster's 2 and 3, but not 1 (**Fig. 3.4.4d**) [121]. Although a subset of DNA polymerase genes are shared between clusters 1 and 3, the lack of GIN expression in cluster 1 implies that cluster 1 is in late S phase or beyond, but a subset of cluster 3 are in the early stages of replication. Overall, these findings indicate that the majority of cells in cluster 2 are in S phase.

M phase is the shortest stage of the cell cycle and is also when the cell is actively dividing. To determine if any clusters are in M phase, genes associated with mitosis were assessed. NIMA-related kinases (NEKs) are a family of proteins that regulate mitotic spindle formation and mitotic progression [122, 123]. In addition, Ki-67 (encoded by *Mki67*) it is indicative of proliferation and has been shown to be upregulated in a graded fashion where expression is absent in G0/G1 phase, but is peaked during M phase [124, 125]. The upregulation of *NEKs* 1, 3, 4, 8, 9, and

Mki67 in cluster 1 suggest that this subgroup is in M phase (**Fig. 3.4.4d**). Taken altogether, data presented here suggests that cells in Clusters 1 and 3 are likely to be in G0/G1 phase, the majority of Cluster 2 is in S phase, a fraction of Cluster 1 is in M phase, and suggest a recently replicated population.

Trajectory analysis was performed on the aggregated CNS mGluR⁺ CD8⁺ T cell datasets to determine the number of lineages that can stem from this one population. Unlike the trajectory inferences that revealed 14 related lineages in Figure 2h, only one lineage was identified in the mGluR⁺ fraction where cluster's 1 and 3 are most related, and a small subset of cluster 1 is associated with cluster 2, supporting the observations made from cell cycle analysis (**Fig. 3.4.4d-e**). Furthermore, pseudotime analysis suggests that the mGluR⁺ lineage derives from cluster's 1 and 3, and differentiates into cluster 2 (**Fig. 3.4.4e, right panel**). Collectively, these data indicate a homogenous mGluR⁺ population that generates one lineage.

As a further test of proliferative history and/or capacity, protein levels of Ki67 were assessed over the course of infection on both mGluR⁺ and mGluR-deficient CD8⁺ T cells. Data indicates that although Ki67 positivity is observed in mGluR⁻CD8⁺ T cells, there was a significantly higher percentage of mGluR⁺ cells that express Ki67, ~40% during late chronic infection (6-12wpi) (**Fig. 3.4.4f**). These data taken together with the scRNA-seq analysis suggests that mGluR⁺ cells are a recently

proliferated population. Although, it is unclear if replication is taking place in the periphery, perivascular space, or within the brain parenchyma.

A further indication of the ability to proliferate is the expression of the IL-2 receptor, CD25. Analysis of CD25 demonstrate that almost all (~98%) mGluR-expressing CD8⁺ T cells uniformly express CD25 during early chronic infection (**Fig. 3.4.4g**). Furthermore, mGluR⁺CD8⁺ T cells express significantly more CD25 (MFI) for the duration of infection than those T cells that were deficient in mGluR's suggesting a more responsive T cell to the proliferation cytokine, IL-2 (**Fig. 3.4.4g**). Additionally, Pearson correlation analysis performed on CD25 and respective group 1 mGluR MFI expression levels determined there is a significant associated between these receptors expressed on mGluR⁺ CD8⁺ T cells (**Fig. 3.4.4h**).

As CD8⁺ T cells are a dominant source of IL-2 and can signal in an autocrine and paracrine fashion to promote proliferation, BMNC cultures isolated from mice 3wpi were re-stimulated with α CD3/ α CD28 in the presence of mGluR modulators for 24h and intracellular flow cytometry for IL-2 was conducted. Data demonstrates that although ~40% of the mGluR⁺ fraction make up the IL-2 producing CD8⁺ T cells, the major source of IL-2 is derived from the mGluR⁻ population (**Supp. Fig. 3.4.4**).

3.4.5 Production of IFN- γ is Partially Dependent on mGluR⁺ Stimulation

IFN γ is a critical effector cytokine produced by T cells that enables parasite killing and prevents clinical pathology due to parasite reactivation in the CNS [11]. To determine if mGluR signaling on T cells promotes IFN- γ production, IFN- γ concentrations were measured from BMNC culture supernatants that were activated with α CD3/ α CD28 and treated with or without respective mGluR agonist or antagonist for 24h (**Fig. 3.4.5a-b**). T cells isolated from the infected brain (no T cells are in the naïve brain) are often already producing IFN- γ , however non-specific TCR stimulation enhances this production by ~10-fold. Treatment with additional glutamate or specific stimulation of the mGluR receptors via mGluR5 (CHPG) or the combined mGluR1/5 agonist, DHPG, significantly enhances IFN- γ production indicating mGluR signaling enhances IFN- γ production (**Fig. 3.4.5a**). Furthermore, inhibition of mGluR signaling in activated T cells with mGluR1 (AIDA), mGluR5 (MTEP), or mGluR1/5 (MCPH) antagonist significantly reduced ($p < 0.05, 0.01, 0.01$, respectively) IFN- γ levels further demonstrating mGluR's role in IFN- γ regulation (**Fig. 3.4.5b**). mGluR agonist or antagonist treatment alone or in the presence of only α CD28 produced IFN- γ levels similar to that of media control suggesting that T cells need to be activated for mGluR-mediated IFN- γ production.

To determine if the mGluR⁺CD8⁺ T cells are the main contributors of the IFN γ -producing population, T cells from BMNC cultures were activated with

α CD3/ α CD28, and in the presence of group 1 mGluR agonist (glutamate, DHPG) or antagonist (MCPG) for 6h and analyzed by flow cytometry to determine the cellular source of IFN- γ . These data reflected the findings observed by ELISA where glutamate receptor stimulation on activated CD8⁺ T cells enhanced the overall proportion of IFN γ -producing cells, whereas inhibition of the receptors significantly reduced this population (**Fig. 3.4.5c**). Group 1 mGluR expression was analyzed on IFN γ ⁺CD8⁺ T cells to determine the cellular source of IFN γ (**Fig. 3.4.5d-e**). Data revealed that CD8⁺ T cells that are secreting IFN γ are overwhelmingly mGluR⁺ making up approximately 70% of the overall IFN γ ⁺CD8⁺ T cell repertoire (**Fig. 3.4.5d-e**). To validate these findings, the CD8⁺ T cell population that is not producing IFN γ was also assessed (**Fig. 3.4.5d,f**). Although there are mGluR⁺CD8⁺ T cells that are not producing IFN γ , the main contributor to the IFN γ -deficient population is the mGluR⁻CD8⁺T cells (**Fig. 3.4.5d,f**). Taken altogether, the main cellular source of IFN γ are mGluR⁺CD8⁺ T cells, and mGluR stimulation on activated CD8⁺ T cells enhances IFN γ production.

In addition to determining the cellular source of IFN γ producing cells, perforin was also assessed as described above. Although IFN γ is critical to prevent uncontrolled parasite replication, perforin is another CD8⁺ T cell-derived effector molecule important for the control of tissue cyst burden [126, 127]. Data suggest that over 60% of the mGluR⁺ fraction makes up the perforin⁺CD8⁺ T cells, whereas those CD8⁺ T cells that are not producing perforin are mGluR-deficient (**Supp. Fig.**

3.4.5). Taken altogether, mGluR expression and stimulation on activated CD8⁺ T cells is associated with enhanced effector function.

3.5. Discussion:

In these studies we demonstrate that following infection with a common neurotropic pathogen, a population of T cells express mGluRs and this expression defines a T cell subset that have upregulated almost 4000 transcripts over their mGluR negative counterparts. This T cell subset most resembles a CD69⁺CD25⁺ memory population and their primary function, IFN- γ production, is dependent on metabotropic glutamate receptor signaling.

Historically, mGluR expression and function has focused on neuronal synaptic plasticity where its Gq signaling promotes cognitive function [94, 95, 128]. However, our work is supported by two previous studies demonstrating the expression of mGluR's on human PBMCs including T cells and dendritic cells [89, 96]. Our studies have expanded our knowledge of T cell expression of mGluR's using an infection model that requires a continuous T cell presence in the brain allowing us to demonstrate that both naïve and activated CD8⁺ T cells express mGluR's in their spleen and cervical lymph nodes in the periphery, and that a significant proportion of activated CD8⁺ T cells in the infected brain are expressing both mGluR1 and mGluR5 (**Fig. 3.4.1 & Supp. Fig. 3.4.1a**). Although, significant expansion of the mGluR⁺ T cells occurs following infection, the presence of these

cells in naïve mice also implies that mGluR expression does not depend on an inflammatory event but may serve a more fundamental role in T cell regulation.

T. gondii represents one of the few examples of a well-balanced inflammatory event in the brain with sufficient activation and recruitment of peripheral and CNS resident cells to combat parasite proliferation without causing inflammation-induced pathology. Within this context, our previous studies have demonstrated a population of brain resident T cells (T_{RM}) that are a significant source of IFN- γ [79]. Microenvironmental cues that define tissue for the migrating T cell and what stimulates their functional immunological memory are important mechanisms to understand if we are to regulate inflammation and immunity within the CNS. A characteristic feature of brain tissue compared to other locations in the body is the tight control of extracellular glutamate. Due to glutamate's additional function as a neurotransmitter, mechanisms are required to preserve a greatly reduced extracellular concentration and minimize neuronal toxicity [82]. Thus, a T cell migrating from the blood into the brain can experience up to a 1000 fold drop in EC glutamate concentrations [129]. The mechanisms that maintain the EC glutamate blood-brain gradient include the transporter GLT1 present on CNS resident astrocytes. GLT1 removes glutamate from the synapse following neuronal firing and converts and releases it as glutamine, reducing its neuronal toxicity. A decrease in GLT1 and subsequent increase in EC glutamate is observed during chronic *T. gondii* infection [82] as well as many other neuroinflammatory diseases

[83-85]. Increased EC glutamate is therefore a defining feature of the brain during inflammation. Significant increases in EC glutamate occur only at 4 weeks post infection and continue to rise as infection progresses [96]. Thus, a decrease in the proportion and number of mGluR⁺ cells is observed at a time when parasite burden, inflammation and EC glutamate is increasing in the B6 mouse [130] (**Fig. 3.4.1**).

Expression of mGluRs, could be transitory, reflecting a cycling of expression common to GPCR proteins [131, 132]. However, transcriptional scRNAseq analysis demonstrates that T cells expressing mGluR1 and 5 are also enriched for many other metabotropic glutamatergic and ionotropic receptors with pathway analysis picking out 'Glutamatergic Synapse' and 'Ion Transport' underlining the dominance of this signaling in this subset of cells. This, along with almost 4000 uniquely upregulated genes defines this as a T cell subpopulation rather than cells that are a snapshot of the membrane recycling process. Furthermore, lineage and pseudotime analysis supports mGluR⁺ cells as a separate population and most likely derived from their mGluR⁻ cells. The initial priming of CD8⁺ T cells in response to a pathogen promotes asymmetric cell division, where the majority will commit to short-lived terminally differentiated effector T cells (defined by KLRG1 expression), while a minority are pre-programmed to diverge to a long-lived memory lineage [133, 134]. During acute infection with pathogens that can be cleared, the KLRG1⁺ terminally differentiated effector population will undergo

clonal contraction where ~5-10% will differentiate into memory T cells capable of an efficient recall response upon secondary exposure [135]. Phenotypic analysis of mGluR⁺ T cells define these cells as a memory population. The commitment to differentiate into specific memory T cell subsets is context-dependent, and is shaped by the microenvironment, and the expression of specific receptors and transcription factors. In the context of chronic *T. gondii* infection, persistent antigen presentation prevents T cell contraction, and the KLRG1⁺ effector population is maintained by memory CXCR3⁺KLRG1⁻ and intermediate CXCR3⁺KLRG1⁺ CD8⁺ T cells in the periphery [136], while during LCMV infection, CXCR3 expression orchestrates rapid memory recall in T_{CM} [137, 138]. CXCR3 protein expression is highly expressed by mGluR⁺CD8⁺ T cells (**Supp. Fig. 3.4.3b**). This coupled with the expression of CD127, and the inverse relationship between the transcription factors T-bet and EOMES in the mGluR⁺ fraction (**Fig. 3.4.3a-b**), further supports the mGluR⁺ cells as a memory population. More specifically, the original hypothesis that EC glutamate concentrations could be a signal for tissue residency is supported by the expression of CD69. Although CD103 does not map to mGluR expression, it is likely that there are both CD103 positive and negative tissue resident memory cells in the CNS. In addition, the transcription factor ID3, recently reported to regulate T_{RM} in the gut [114] is particularly expressed on the mGluR⁺ population further supporting a tissue resident memory phenotype.

Of note, mGluR expression strongly correlates with the expression of the IL-2 receptor, CD25. Recent T cell activation induces CD25 upregulation, where the IL-2/CD25/STAT5/Akt signaling axis is important for mediating T cell proliferation and survival during infection [139, 140]. However, IL-2 signaling is also implicated in fate-determination of activated T cells including during LCMV infection [141-143] and characterization of human memory CD8⁺ T cells [144]. Here, we demonstrated there is persistently high CD25 surface expression on CD8⁺ T cells for the duration of CNS-*T. gondii* infection. Moreover, cells that are particularly high for CD25 are also those that express higher levels of mGluRs suggesting that either these molecules directly regulate each other or are driven by a master regulator (**Fig. 3.4.4g-h**). It is worth noting that T cells also produce glutamate and therefore, like IL-2, could act to stimulate mGluR signaling in an autocrine manner. Inevitably, the implication is that this CD25⁺ population is primed and ready to be responsive to IL-2. In line with this, scRNA-seq and Ki-67 expression analysis points towards the mGluR⁺CD8⁺ T cells being a replicating population. In addition, the downregulation of transcripts associated HDACs, and the upregulation of genes that encode histones, DNA polymerases, CDKs, and NEK's, all things necessary for DNA replication, support a proliferating population. Moreover, trajectory analysis indicates that mGluR⁺ T cells are a homogenous lineage, differentiating into one cell type.

The production of IFN γ is critical to protect against *T. gondii* at all stages of infection including within the brain where it mediates the clearance of the cell lytic tachyzoite form of the parasite during reactivation [11]. Previous published work has suggested that mGluR signaling can enhance cytokine production [145]. Here we establish that *ex vivo* restimulation of T cells from the infected brain with mGluR agonist not only promotes the production of IFN γ , but significantly increase the proportion of CNS-derived IFN γ -producing CD8⁺ T cells (**Fig. 3.4.5 a-c**). In contrast, inhibition of mGluR signaling significantly decreased this production of IFN γ . Finally, ~70% of the IFN γ ⁺CD8⁺ T cell population are from the mGluR⁺ population. This pattern is mirrored when analyzing perforin production, suggesting that mGluR signaling on T cells is ultimately required for optimal effector function in the brain (**Fig. 3.4.5 d-e**). The fact that mGluR stimulation alone does not lead to IFN γ production suggests that T cells need to be activated. When comparing downstream mediators between TCR and group 1 mGluR activation, PLC, PKC, and increased intracellular calcium are all molecules that overlap in their signaling cascades. This may suggest the mGluR signaling on activated T cells acts as an amplification signal. Recent work using a Nur77 reporter determined that memory formation is independent of secondary T cell receptor (TCR) engagement of *T. gondii*-specific CD8⁺ T cells, implying that fate-commitment occurs during the initial effector response [110] and indeed supporting an antigen-independent stimulus for memory function. For a T cell migrating from the glutamate rich environment of the blood across the blood brain barrier into the

brain, the sudden reduction in EC glutamate may be a significant signal that indicates it has entered a new environment and one that requires careful control of inflammation. Withdrawal of mGluR signaling in glutamate low conditions may encourage tissue residency and minimize cytokine production. Upon inflammation, in the case of parasite reactivation or damage, increasing EC glutamate and subsequent mGluR signaling will promote effector function on a T cell population that is primed and ready to respond.

In conclusion, these data shed light into understanding the effects the microenvironment has on protective immunity during infection in the brain. Our study has identified a population of brain-infiltrating CD8⁺ T cells that have the capacity to interact with glutamate through the expression of mGluR's. Furthermore, these studies determined that mGluR positivity on T cells defines a memory population in the infected brain in which effector function is dependent on mGluR signaling. Future studies focused on how glutamate regulates T cell function and signaling through metabotropic glutamate receptor modulation could set the foundations for generating prospective therapeutic targets for manipulating T cells where glutamate agonism enhances an exhausted T cell response to cancer or a chronic CNS pathogen. Alternatively, the drive for glutamate inhibition during neurological disease may not only limit excitotoxicity of neurons but also limit pathological inflammatory responses.

3.6 Figures & Legends

Figure 3.4.1 Expression of Group 1 Metabotropic Glutamate Receptors are Enriched on CD8⁺ T Cells in the *Toxoplasma*-Infected Brain. Immune cells were isolated from the spleen, cervical lymph nodes (cLN), and brain from *T. gondii*-infected mice at designated time points. **(a)** Flow cytometry plots of each organ illustrate the expression of group 1 mGluR's (receptor 1/5) for cells gated on live CD3⁺CD8⁺ cells at 2wpi. Numbers indicate the proportion of mGluR1⁻mGluR5⁻ and GluR1⁺mGluR5⁺ CD8 T cells. Percentage **(b)** and the absolute cell numbers **(c)** of CD8 T cells that are mGluR⁻ (**blue**) and mGluR⁺ (**orange**) during infection at indicated time points. Numbers indicate mean percentage \pm SEM of $n = 4$ biological replicates. A two way-ANOVA with multiple comparisons was used to test for significance. * $p < 0.05$, ** $p < 0.01$, *** $p < 0.001$, **** $p < 0.0001$. Data are representative of two independent experiments with similar results.

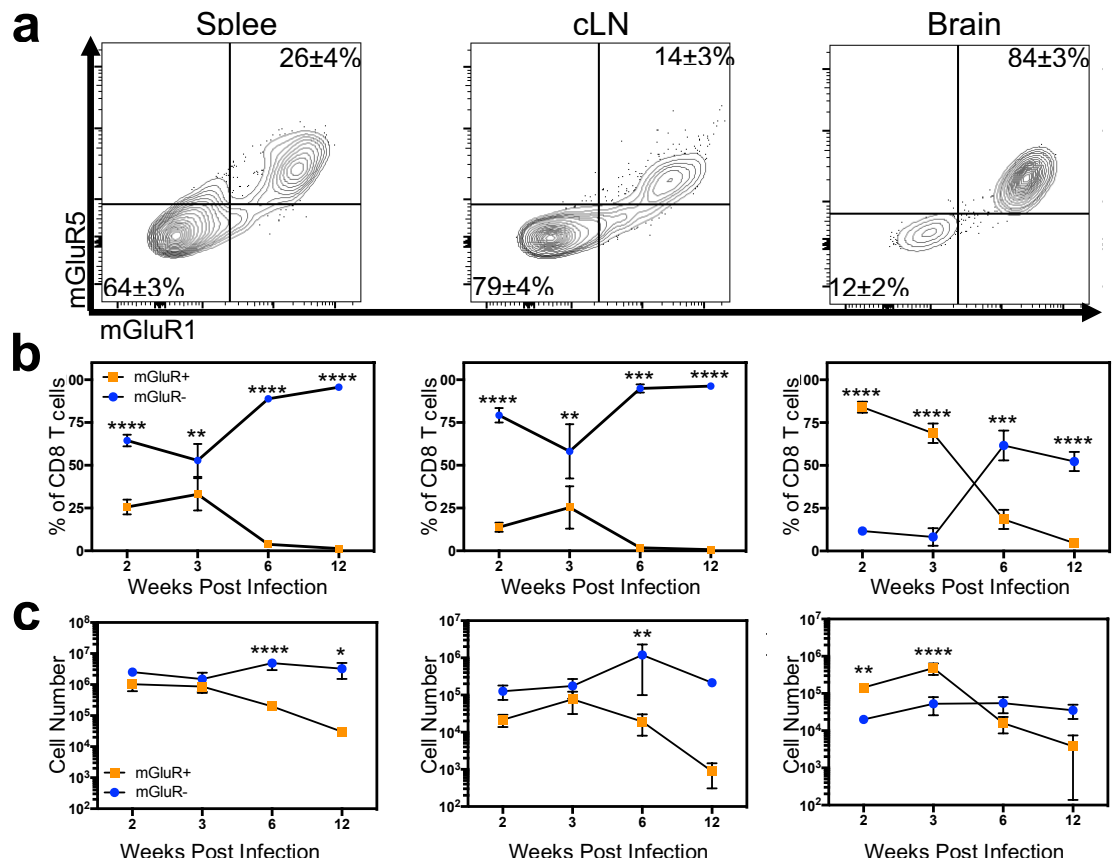


Figure 3.4.2 Glutamate Receptor Expression Identifies a Transcriptionally Distinct Population of CD8⁺ T cells in the Brain. Pooled brain mononuclear cells from *Toxoplasma*-infected mice (n=10) were cell sorted according to live CD3⁺CD8⁺mGluR1⁻mGluR5⁻ and CD3⁺CD8⁺mGluR1⁺mGluR5⁺ expression. Sorted cells were utilized for single cell RNA-sequencing. **(a)** UMAP plots were used to visualize aggregated mGluR⁻ (**blue**) and mGluR⁺ (**orange**) scRNA-seq datasets. **(b)** Venn diagram of differentially expressed genes (DEGs) between mGluR⁻ and mGluR⁺ datasets. DAVID was used to identify enriched KEGG Pathways **(c)** and GO Process terms **(d)** from DEGs in the mGluR⁺ datasets. Heatmap of genes under the categories: metabotropic glutamate receptors **(e)**; ionotropic glutamate receptors **(f)**; Gq Signaling **(g)**. Upregulated Genes (red); downregulated genes (blue). Two additional cell sorts were performed only on mGluR⁺ CD8 T cells. **(h)** UMAP plots depict pseudotime analysis (monocle v3) of aggregated brain CD8⁺ T cell scRNA-seq datasets. The plot on left shows location of cell type and numbers denote lineages. The plot on the right indicates direction of the population where the population begins at purple (1), and ends towards yellow.

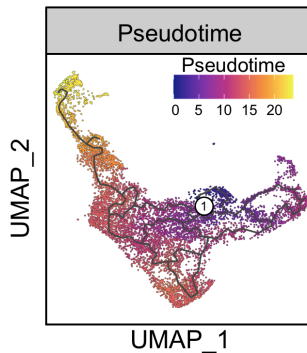
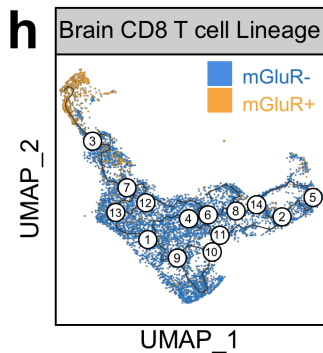
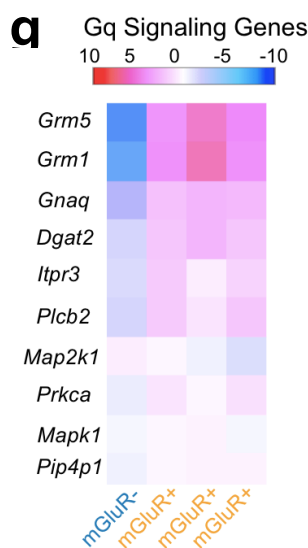
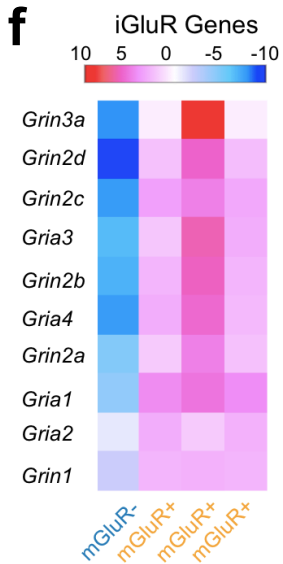
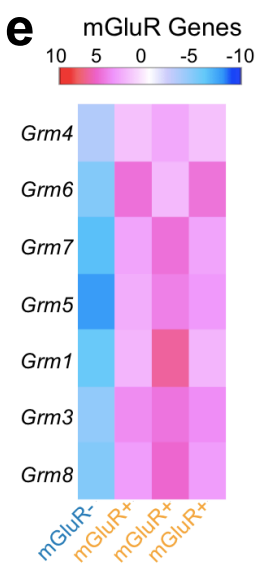
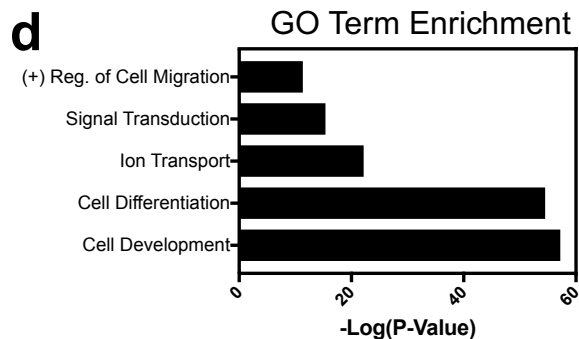
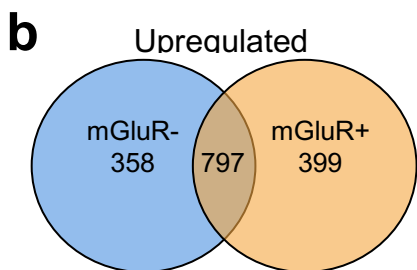
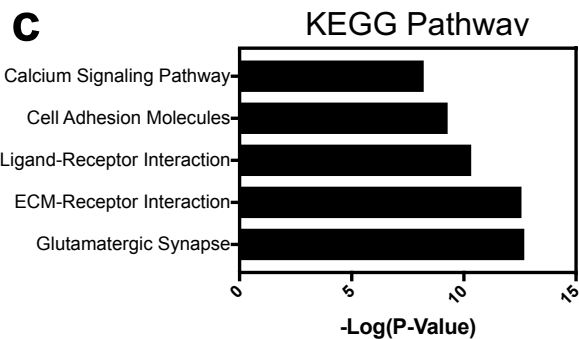
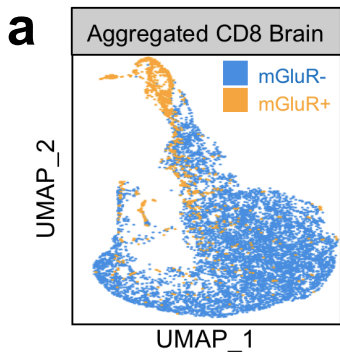


Figure 3.4.3 mGluR⁺CD8⁺ T cells Exhibit a Memory Phenotype. Pooled brain mononuclear cells from *T. gondii*-infected mice (n=10) were cell sorted according to live CD3+CD8+mGluR1–mGluR5– and CD3+CD8+mGluR1+mGluR5+ expression. Sorted cells were utilized for single-Cell RNA-sequencing. **(a)** Heatmap of genes associated with memory and terminally differentiated status. Upregulated Genes (red); downregulated genes (blue). Two additional cell sorts were performed only on mGluR⁺ CD8 T cells. **(b)** BMNC's were isolated from *T. gondii*-infected mice (n=5) at designated time points. Flow cytometry TSNE plots shows the relative expression level of indicated surface receptors (mGluR1, KLRG1, CD127) and transcription factors (T-bet, EOMES) on CD3+CD8+ T cells during early chronic infection (2 & 3wpi). Histograms and line graphs depict the expression of indicated molecules for CD3+CD8+mGluR1–mGluR5– (blue) and CD3+CD8+mGluR1+mGluR5+ (orange) cells for the duration of infection. **(c)** Flow cytometry TSNE plots shows the relative expression level of mGluR1 and ID3 on CD3+CD8+ T cells during late chronic infection (6 & 12wpi). Histograms and line graphs depict the expression of ID3 for CD3+CD8+mGluR1–mGluR5– (blue) and CD3+CD8+mGluR1+mGluR5+ (orange) cells for the duration of infection. A two way-ANOVA with multiple comparisons was used to test for significance between mGluR- and mGluR⁺ CD8 T cells for each respective molecule at indicated timepoint. *p<0.05, **p<0.01, ***p<0.001, ****p<0.0001.

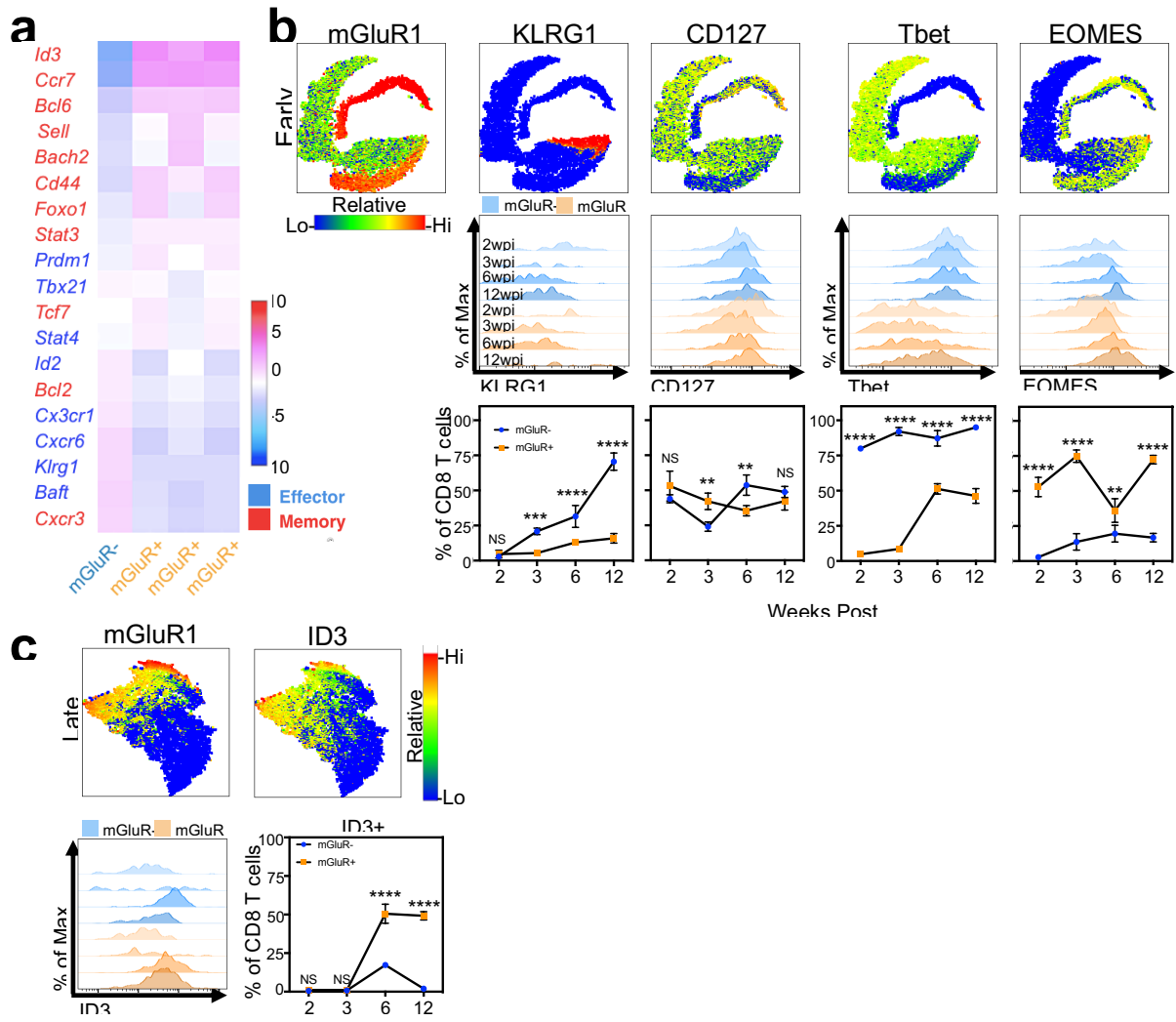
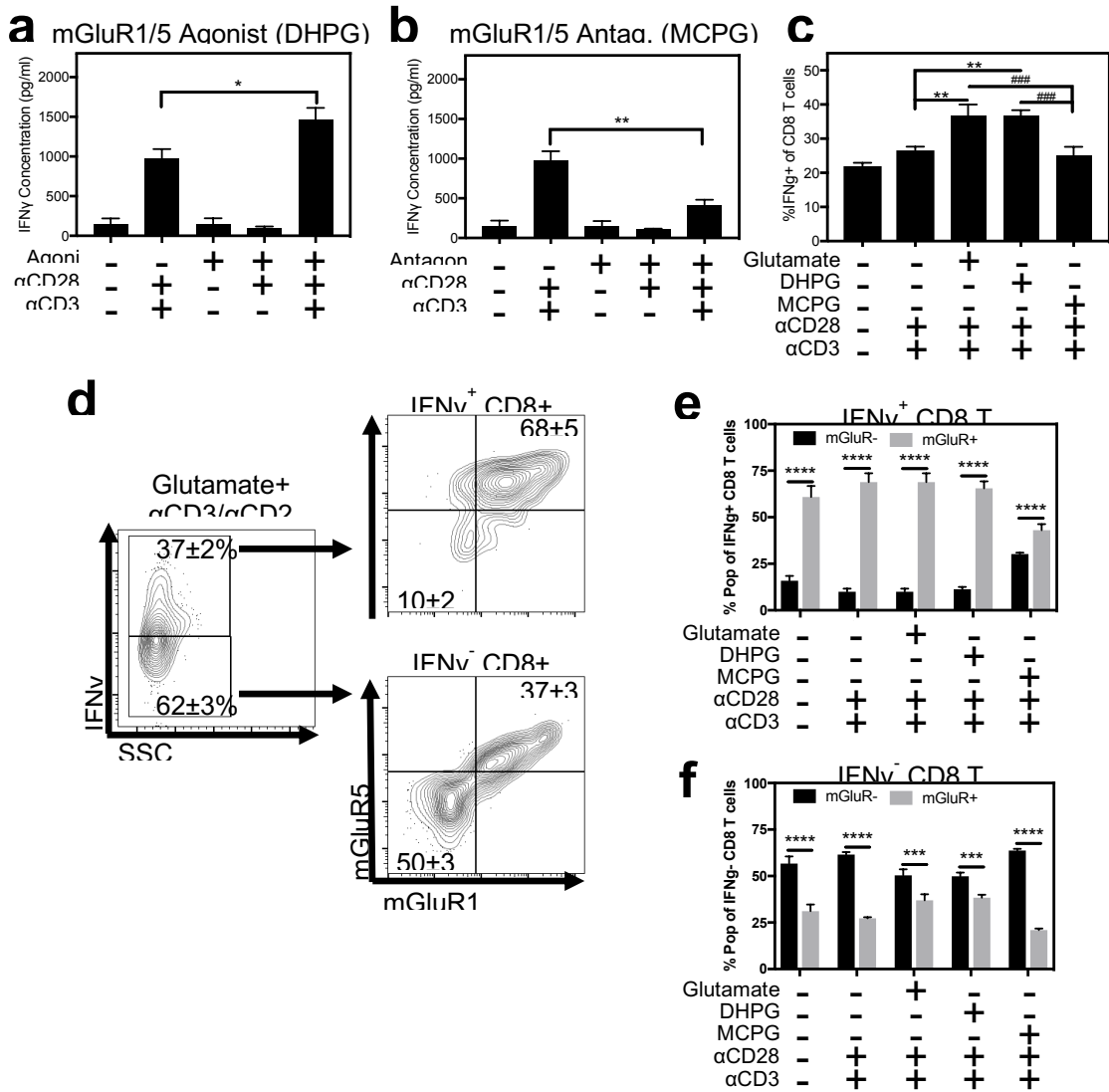
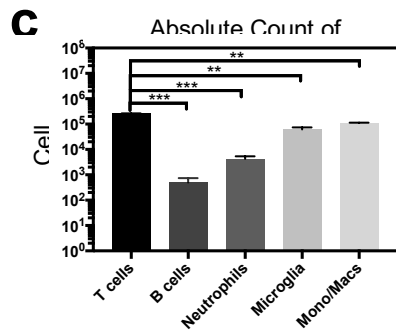
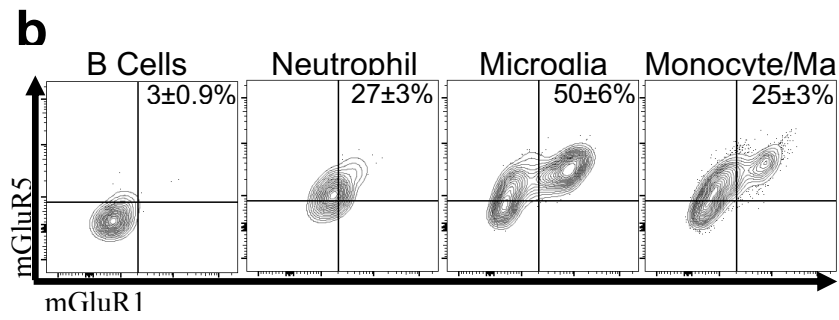
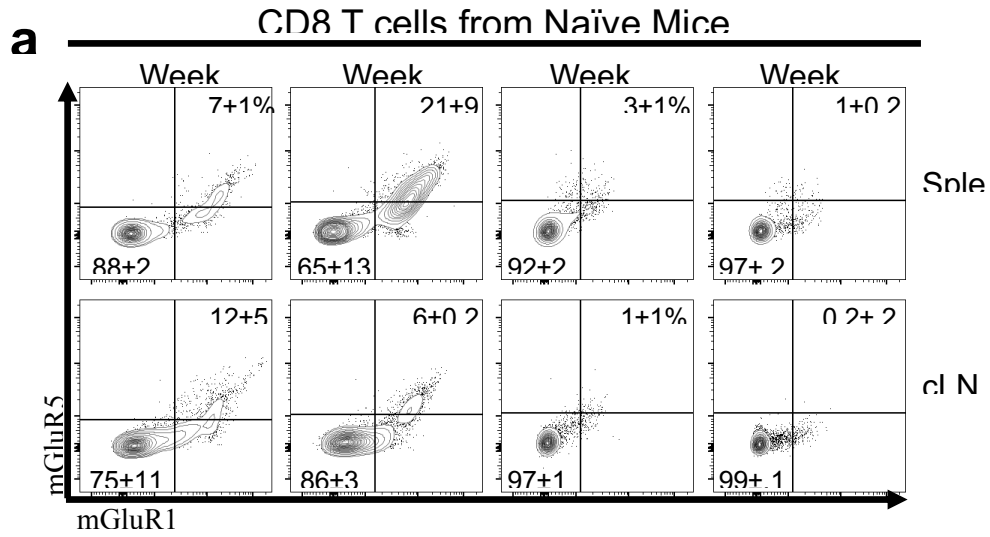


Figure 3.4.4: mGluR⁺CD8⁺ T cells Recruited to the *T. gondii*-Infected Brain are a Proliferating Population. Pooled brain mononuclear cells from *T. gondii*-infected mice (n=10) were cell sorted according to live CD3⁺CD8⁺mGluR1⁺mGluR5⁺ expression. Sorted cells were utilized for single cell RNA-sequencing. **(a)** UMAP plot was used to visualize aggregated mGluR⁺CD8⁺ T cell scRNA-seq datasets from three independent experiments. A total of 3 clusters were identified and color-coded. **(b)** Venn diagram of differentially expressed genes (DEGs) between the three identified clusters. **(c)** DEGs identified from respective clusters were placed into DAVID to identify enriched KEGG Pathways (**black bars**) and GO Process terms (**grey bars**). **(d)** Heatmap of genes that are associated with G0/G1, S, or M phase of the cell cycle. Upregulated Genes (red); downregulated genes (blue). **(e)** UMAP plots depict pseudotime analysis (monocle v3) of aggregated mGluR⁺CD8⁺ T cell scRNA-seq datasets. Plots on left show location of cluster and number lineages, and plot on the right indicates direction of the population where the population begins at purple, and ends towards yellow. **(f-g)** BMNC's were isolated from *T. gondii*-infected mice (n=5) at designated time points. Histograms and line graphs depict the protein expression of Ki67 **(f)** or CD25 **(g)** for CD3⁺CD8⁺mGluR1⁻mGluR5⁻ (blue) and CD3⁺CD8⁺mGluR1⁺mGluR5⁺ (orange) cells for the duration of infection. A two way-ANOVA with multiple comparisons was used to test for significance between mGluR⁻ and mGluR⁺ CD8 T cells for each respective molecule at indicated timepoint. *p<0.05, **p<0.01, ***p<0.001, ****p<0.0001 **(h)** Graphs depict MFI expression levels of CD25 and mGluR1 or mGluR5 on CD3⁺CD8⁺mGluR1⁺mGluR5⁺ T cells from the duration of infection (2-12wpi). R, R-squared, and P-values were determined by Pearson two-tailed correlation analysis. Solid line represents the best fit line, and dashed lines represent the confidence interval range.

Figure 3.4.5 Production of IFN- γ is Partially Dependent on mGluR⁺ Stimulation. Brain mononuclear cells (BMNC) were harvested from *T. gondii*-infected mice (3wpi) followed by treatment with α CD3/ α CD28 antibodies and glutamate receptor modulators. IFN γ ELISA was performed on supernatants from cells stimulated for 24h. (a) Graphs depict IFN γ ELISA data from agonist (a) or antagonist (b) treatments. Agonist used (receptor target): Glutamate (mGluR1/5); CHPG (mGluR5); DHPG(mGluR1/5); Antagonist used (Receptor target): AIDA (mGluR1); MTEP (mGluR5); MCPH (mGluR1/5). In parallel stimulations, cells were harvested 6 hours post-stimulation, and intracellular cytokine staining was performed. Data were gated on live CD3⁺ CD8⁺ T cells and then the proportion (%) of IFN γ producing cells was analyzed (c). CD8⁺ T cells were split into IFN γ ⁺ and IFN γ ⁻ subsets for subsequent expression analysis for group 1 mGluR's (d). Data depicts the proportion of mGluR⁻ (black bar) or mGluR⁺ (grey bar) CD8 T cells that are IFN γ ⁺ (e) or IFN γ ⁻(f). Numbers indicate mean percentage \pm SEM of $n = 4$ biological replicates. A one way-ANOVA with multiple comparisons was used to test for significance. * $p < 0.05$, ** $p < 0.01$, *** $p < 0.001$, **** $p < 0.0001$.

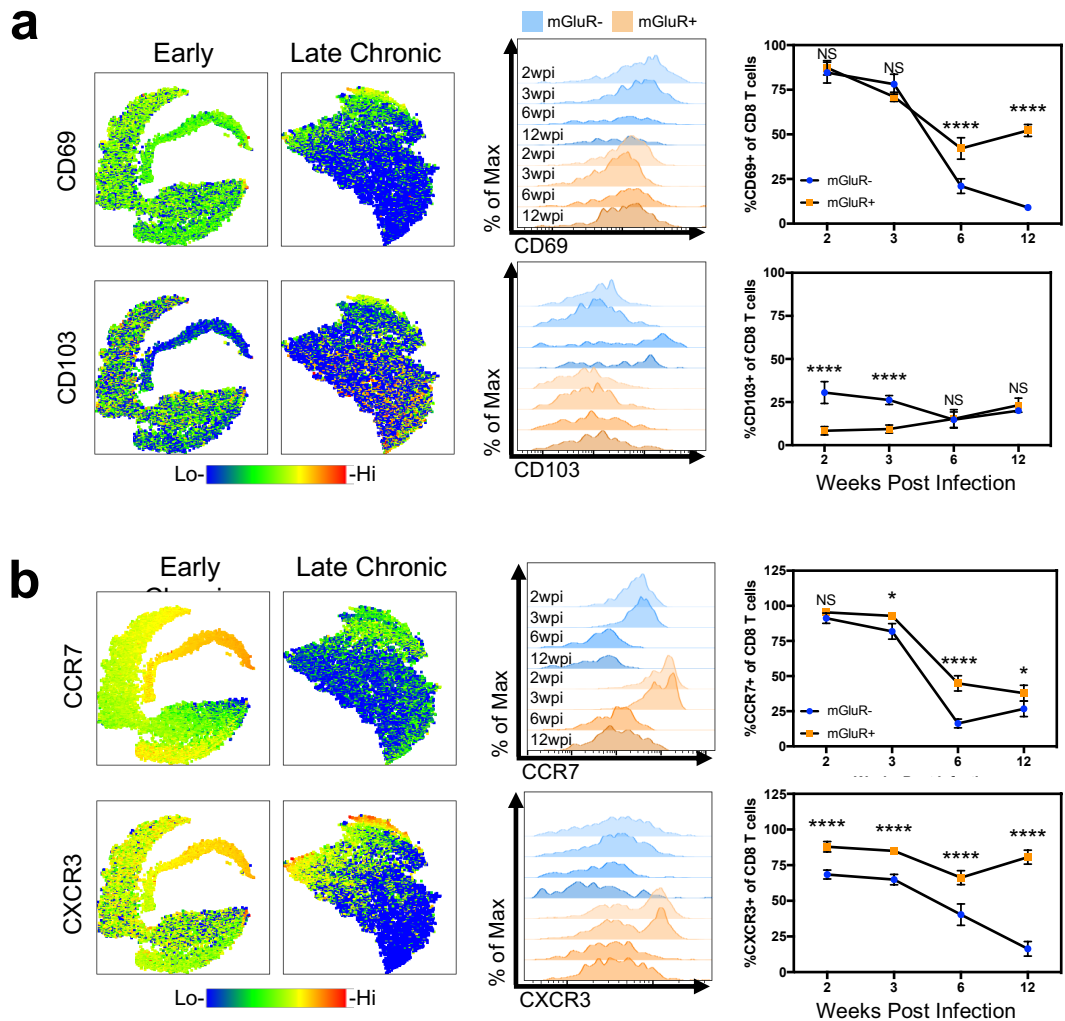


SUPPLEMENTAL FIGURE 3.4.1: Expression of Group 1 Metabotropic Glutamate Receptors are Expressed by Immune cells in *Toxoplasma*-Infected Brain. Immune cells were isolated from the spleen and cervical lymph nodes (cLN) of naïve mice. **(a)** Flow cytometry plots of each peripheral organ illustrate the expression of group 1 mGluR's (receptor 1/5) for cells gated on live CD3+CD8+ cells. **(b)** Immune cells were isolated from the brain 3wpi. Flow cytometry of B cells (**CD45+B220+CD19+**), Neutrophils (**CD45+CD11b+Ly6G+**), Microglia (**CD45LoCD11b+**), and Monocytes/ Macrophages (**CD11b+CD45Hi**) illustrate the expression of group 1 mGluR's (receptor 1/5). **(c)** Bar graph depicts the absolute cell counts of each respective immune cell that is mGluR+. Numbers indicate mean percentage \pm SD of $n = 4$ biological replicates of mGluR1-mGluR5- and GluR1+mGluR5+ CD8 T cells. A two way-ANOVA with multiple comparisons was used to test for significance. * $p < 0.05$, ** $p < 0.01$, *** $p < 0.001$, **** $p < 0.0001$. Data are representative of two independent experiments with similar results.

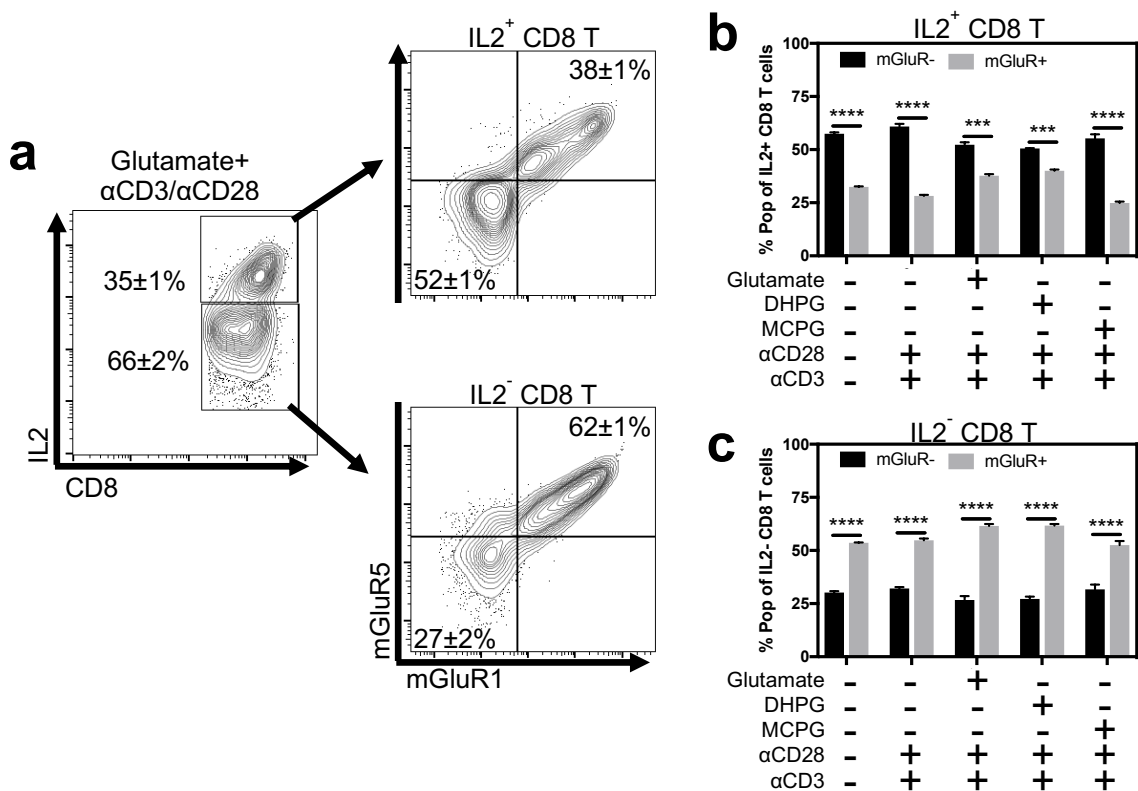


SUPPLEMENTAL FIGURE 3.4.2: Expression of Integrins and Chemokine Receptors on mGluR- and mGluR+ CD8+ T cells from the Infected Brain.

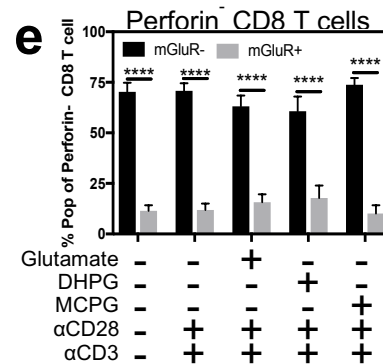
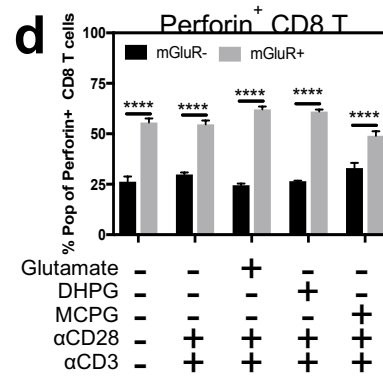
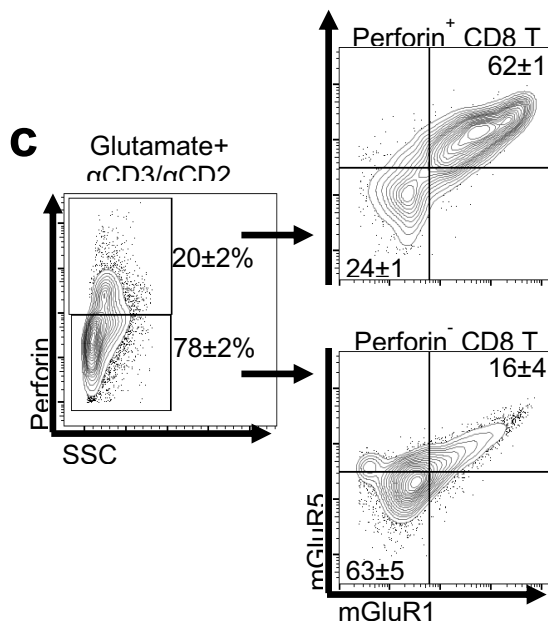
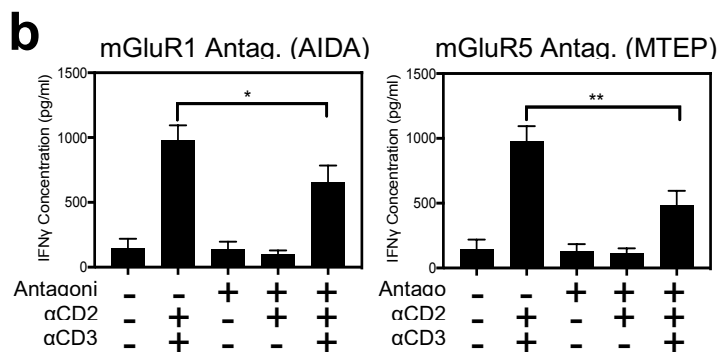
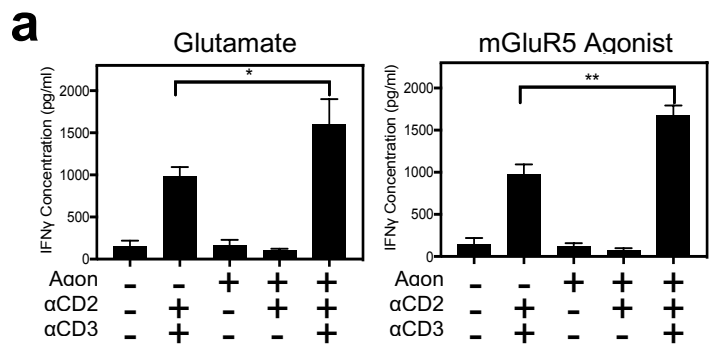
Brain mononuclear cells (BMNC) were harvested from *T. gondii*-infected mice (n=5) at designed timepoints. Flow cytometry TSNE plots show the relative expression level of indicated integrins (CD69, CD103) (a) or chemokine receptors (CCR7, CXCR3) (b) on CD3+CD8+ T cells during early (2, 3wpi) and late (6, 12wpi) chronic infection. Histograms and line graphs depict the expression of indicated molecules for CD3+CD8+mGluR1-mGluR5- (blue) and CD3+CD8+mGluR1+mGluR5+ (orange) cells for the duration of infection. A two way-ANOVA with multiple comparisons was used to test for significance between mGluR- and mGluR+ CD8 T cells for each respective molecule at indicated timepoint. *p<0.05, **p<0.01, ***p<0.001, ****p<0.0001.



SUPPLEMENTAL FIGURE 3.4.3: IL-2 Production in Activated mGluR⁺CD8⁺ T Cells From the Infected Brain. Brain mononuclear cells were harvested from *T. gondii*-infected mice (3wpi) followed by treatment with α CD3/ α CD28 antibodies and glutamate receptor modulators. Cells were harvested 6 hours post-stimulation, and intracellular cytokine staining was performed. **(a)** Data were gated on live CD3⁺CD8⁺ T cells and then the proportion (%) of IL-2 producing cells was analyzed. CD8⁺ T cells were split into IL-2⁺ and IL-2⁻ subsets for subsequent expression analysis for group 1 mGluR's. Data depicts the proportion of mGluR⁻ (black bar) or mGluR⁺ (grey bar) CD8 T cells that are IL-2⁺ **(b)** or IL-2⁻ **(c)**. Agonist used (receptor target): Glutamate (mGluR1/5); DHPG(mGluR1/5); Antagonist used (receptor target): MCPH (mGluR1/5). Numbers indicate mean percentage \pm SEM of $n = 4$ biological replicates. A one way-ANOVA with multiple comparisons was used to test for significance. * $p < 0.05$, ** $p < 0.01$, *** $p < 0.001$, **** $p < 0.0001$.



SUPPLEMENTAL FIGURE 3.4.5: Perforin Levels are Enhanced in Activated mGluR⁺CD8⁺ T Cells from the Infected Brain. Brain mononuclear cells were harvested from *T. gondii*-infected mice (3wpi) followed by α CD3/ α CD28 antibody treatment and glutamate receptor modulators. Cells were harvested 6 hours post-stimulation, and intracellular cytokine staining was performed. **(a)** Data were gated on live CD3⁺CD8⁺ T cells and then the proportion (%) of perforin producing cells was analyzed. CD8⁺ T cells were split into perforin⁺ and perforin⁻ subsets for subsequent expression analysis for group 1 mGluR's. Data depicts the proportion of mGluR⁻ (black bar) or mGluR⁺ (grey bar) CD8 T cells that are perforin⁺ **(b)** or perforin⁻**(c)**. Agonist used (receptor target): Glutamate (mGluR1/5); DHPG(mGluR1/5); Antagonist used (receptor target): MCPH (mGluR1/5). Numbers indicate mean percentage \pm SEM of $n = 4$ biological replicates. A one way-ANOVA with multiple comparisons was used to test for significance. * $p < 0.05$, ** $p < 0.01$, *** $p < 0.001$, **** $p < 0.0001$.



CHAPTER FOUR

Strain-Specific Effects of T. gondii on GLT-1 Expression in Primary Cultured

Astrocytes

4.1 Abstract

Toxoplasma gondii (*T. gondii*) is the most effective transmissible apicomplexan in the world where one-third of the human population is infected. Encystment of the parasite in neuronal tissue in the brain results in a lifelong chronic infection. Astrocytes are a supportive cell for neurons in the brain. The key function of astrocytes is to keep a homeostatic low concentration of extracellular (EC) glutamate in the brain. To do this, astrocytes import exogenous glutamate by expression of glutamate transporter-1 (GLT-1). The import of glutamate is converted to glutamine via glutamine synthetase, which can be recycled back for neuronal usage. Unregulated EC glutamate concentrations can clinically manifest into epilepsy, seizures, or neurodegenerative diseases. Our lab has shown that in a *T. gondii*-infected brain, there is an increase in EC glutamate due to a downregulation of GLT-1. However, the mechanism of GLT-1 downregulation remains to be elucidated.

Although this is a work in progress, here we demonstrate that direct invasion of primary astrocyte cultures with a high multiplicity of *T. gondii* infection leads to graded downregulation of GLT-1 which was dependent on the parasite strain used. Additional studies suggest that the downregulation mechanism is mediated by a degradative pathway. Further studies need to probe if this is regulated by GRA or ROP secretory proteins, and if GLT-1 downregulation is observed in recently infected astrocytes *in vivo*. What we learn here can expand on the unknown

mechanisms that govern GLT-1 downregulation during *T. gondii* infection in mice, and potentially find an effective therapeutic to restore disrupted neuronal networks and changed behavior *in vivo*.

4.2 Introduction

The obligate intracellular pathogen *Toxoplasma gondii* (*T. gondii*) is an apicomplexan and the world's most proliferative parasite infecting 30% of people. Cats are the definitive host for *T. gondii*, where the parasite can replicate in its sexual form, the sporozoite, which will develop oocyst. However, in the intermediate host *T. gondii* can only differentiate into its asexual tachyzoite or bradyzoite form [46, 52]. Transmission is most common through the consumption of tissue cyst from undercooked infected meat, or by ingesting contaminated food or water with oocytes that originate from infected cat fecal matter. While *Toxoplasma* has the capacity to infect any nucleated cell, encystment of the parasite in neuronal brain tissue results in a lifelong chronic infection [5]. Pathology from infection is rarely seen, and is only apparent in patients with compromised immune systems due to a requirement of a pro-inflammatory cytokine milieu to keep this apicomplexan in a dormant state.

Astrocytes are the most abundant glial cell in the brain where its primary function is to act as a caretaker for neurons. One way astrocytes provide support is by maintaining homeostatically low concentration of extracellular (EC) glutamate in

the brain. This is mediated by expression of glutamate transporter-1 (GLT-1). Unregulated EC glutamate concentrations can clinically lead to spontaneous seizures, and neurodegeneration due to excitotoxicity. Previous work in our lab has demonstrated that astrocyte foot swelling during chronic *T. gondii* infection is significant relative to uninfected mice suggesting a molecular change [82]. Upon further investigation, it was determined that there were increased levels of EC glutamate due to a downregulated of astrocytic GLT-1. However, the reason and mechanism of GLT-1 downregulation remains to be elucidated.

Upon invasion, parasite attaches themselves to a host cell using their micronemes which recognize glycoconjugates on host cell surfaces. This is followed by the secretion of RON-proteins from the neck portion the parasite to form an anchor point. The rhoptry bulbs secrete ROP-proteins into the host cytosol and lumen of the protective parasitophorous vacuole (PV). The combination of micronemes and motor-complex proteins work in concert to promote a gliding motion that leads to host-cell entry. Once the parasite has fully invaded and the PV is fully formed, dense gradual proteins (GRAs) are secreted into the PV, where subtypes will help maintain optimal conditions for parasite growth, as well as provide anchorage within the infected host cells. This newly formed parasite home does not fuse with endosomes or lysosomes, thus shielding it from degradation. The barrier prevents contact with the host cell endomembrane and the cytosol, allowing for the

maintenance of a neutral pH. In addition, PV membranes become permeable to small metabolites to allow for passive nutrients to nourish the parasite.

T. gondii is classified as Types I-III, where the former is most virulent and the latter is avirulent. Although Type's I and II are most associated with immune suppressed patients and congenital infection, Type III is mainly observed in cats and wild animals [27, 146]. A defining feature between the different types is Type I, such as the RH strain, lacks the ability to form cysts, whereas Type's II and III will spontaneously form cysts. In addition to this, each have evolved mechanisms to evade the immune system.

One of these manipulation tactics is by inhibiting the nuclear localization of the p65 subunit of NF- κ B via the pseudokinase, ROP18. In immune cells, NF- κ B is a transcription factor that induces pro-inflammatory cytokines to defend against invading pathogens. However, in astrocytes, NF- κ B contributes to GLT-1 expression by NF- κ B submits attaching to three distinct binding sites upstream of GLT-1 Exon 1. We hypothesize that signaling mechanisms involved in GLT-1 expression may be interrupted due to parasitic-specific secretory proteins.

4.3 Materials and Methods

Maintenance of Cell Lines- *Human Foreskin Fibroblast cell cultures*: Human Foreskin Fibroblast (HFF) Cells (obtained from ATCC, Manassas, VA) were cultured using DMEM (1x with 4.5 g/L glucose, L-glutamine, & sodium pyruvate. Corning, cat#: 10-013-CM) as a base containing 10% Fetal Bovine Serum (Seradigm, cat#: 1300-050), 1% penicillin-streptomycin (10,000 units penicillin + 10,000 µg streptomycin / 1mL saline. Genclone Cat#: 25-512), 2% L-glutamine (29.2 mg/mL. Genclone, cat#: 25-509), and 1 mL/L gentamicin (50 mg/mL. Quality Biological, cat#: 120-098-661). Cell cultures were grown using a VWR Water Jacketed CO₂ Incubator (cat#: 10810-744) with parameters set at 37°C, 5% CO₂.

Astrocyte Harvesting and Passage: All animal research has been done in accordance to the Animal Welfare Act. C57Bl/6 mice obtained from Jackson Laboratory (Jackson ImmunoResearch Laboratories, Inc., West Grove, PA, USA) were bred and maintained in a pathogen free vivarium under the Institutional Animal Care and Use Committee (IACUC) protocols established at the University of California, Riverside. Neonatal C57Bl/6 mice born at 0-3 days were sacrificed via cervical dislocation and brains (without cerebellum) were dissected and placed in cold wash media (Dulbecco's Modified Eagle Medium with 2% Fetal Bovine Serum). Once dissected, each brain was pushed and homogenized through a sterile 40 micrometer cell strainer (Corning, cat#: 431750) using a 3 mL syringe plunger (Henke Sass Wolf, cat#: 53548-003). Samples were then washed twice

with 5-10 mL of the above mentioned wash media and spun at 2000 RPMS for 10 minutes at 4°C. Homogenate was resuspended in 6mL of prewarmed Astrocyte Media (DMEM (4.5 g/L glucose, L-glutamine, & sodium pyruvate. Corning, cat#: 10-013-CM) supplemented with 10% FBS, 1% Nonessential Amino Acids Mixture 100x, 1% GlutaMAX, 1% penicillin-streptomycin, 1% HEPES) per brain sample, and seeded onto vented T-25 cm² flasks and grown at 37°C, 5% CO₂. Media was replaced at days 3, 5, and 7. Once cultures reached confluency (~Day 8-10), flasks were placed in an Amerex Instruments Inc. Incubator Shaker with the following parameters: 260 RPM, 37°C for 1.5 hours. Media was then replaced and placed in the incubator shaker for an additional 24h at 100 RPM at 37°C.

Parasite culture: Type's I, II, and III (RH, PruQHX, and CTG, respectively) strains of the tachyzoite form of *T. gondii* were maintained and serially passaged *in vitro* using confluent HFF monolayers grown on T25cm² and T175cm². Parasite-specific media (DMEM, 5% FBS, 1% penicillin-streptomycin, 1% L-glutamine, and 1 mL/L gentamicin) was used during HFF infection.

In vitro infections and western blot analysis: Astrocyte cultures were infected with RH, PruQHX, or CTG at a multiplicity of infection of 1 and 10. After 24 or 48 hours of infection, infected astrocytes were lysed with RIPA buffer and protein concentrations were determined using a Pierce™ BCA Protein Assay Kit - Reducing Agent Compatible (Thermo Scientific, cat#: 23250).

Cell lysate was loaded at a 10ug per lane, and mixed with Laemmli Sample Buffer 4x (Bio-Rad, cat#: 161-0747) and 2-mercaptoethanol (Sigma, cat#: 5HBF0646V). Samples were then denatured at 60 or 80°C for 5 minutes. After placing samples on ice for 30 seconds and centrifuging at 4°C, at max RPM for 1 minute, samples are then loaded into premade gel casts and ran at 110 Volts in running buffer. The gel was transferred to a nitrocellulose membrane using 150 volts and 400 microamps for 70 minutes. The membrane was then blocked with a solution containing 0.1% PBST and 5% Nonfat Dry Milk Blotting Grade Buffer (Bio-Rad, cat#: 170-6404) at room temperature for 1 hour. The blot was washed with 0.1% PBST and incubated with primary antibodies (Rabbit polyclonal antibody to EAAT2, abcam at 1mg/mL, cat#: ab41621) of a 1:1000 concentration within a 0.1% PBST and 5% Bovine Serum Albumin (Gemini Bio-Products, cat#: 700-100P) solution overnight at 4°C. The membrane was washed in 0.1% PBST and incubated in secondary antibodies (Goat-anti-rabbit HRP) of a 1:10,000 concentration in 0.1% PBST and 5% Nonfat Dry Milk Blotting Grade Buffer for 1h at room temperature. Membrane is washed again in 0.1% PBST and developed with Pierce ECL Western Blotting substrate (Thermo Scientific, cat#: 32106), which is then exposed to Blu-Lite UHC Western blotting film (MTC Bio, cat#: A8813). PageRule Plus Prestained Protein Ladder (Thermo Scientific, 26619) was used as a ladder and Beta-Actin (Rabbit Beta-Actin. Cell Signaling Technologies, cat#: 49675) was used as a loading control.

4.4 Results:

4.4.1 Direct Parasite Invasion of Astrocytes Downregulates GLT-1

The principle glutamate transporter in the brain, GLT-1, is significantly downregulated during chronic *T. gondii* infection *in vivo* [82]. Mechanisms which lead to this downregulation are currently unknown. To assess the possibility of direct parasite invasion contributing to GLT-1 dysregulation, primary cultured astrocytes were infected with *T. gondii*, and GLT-1 protein expression was assessed via western blot analysis. It is important to note that primary cultured astrocytes typically express little to no GLT-1 protein (**Fig. 4.4.1A Lanes 1-3**). To overcome this, dexamethasone, a corticosteroid, was added to cell cultures for 72 hours prior to infection [147]. This leads to prolonged expression of GLT-1 as seen in **Fig. 4.4.1A, lanes 4-6**. Parasites were subsequently added to astrocyte cultures at a multiplicity of infection (MOI) 10 for 24 hours. GLT-1 induced cultures that were infected show a significant decrease in GLT-1 protein expression relative to mock-treated cells suggesting that *T. gondii* has the ability to alter GLT-1 expression (**Fig. 4.4.1A, lanes 7-9 & 1B**).

T. gondii injects secretory proteins during the invasion of cells that manipulate host cell signaling pathways. One of these mechanisms is the inhibition of NF- κ B translocation into the nucleus via ROP18 [148]. Upstream of the NF- κ B pathway are pathogen recognition receptors that initiate the pro-inflammatory response. To

determine if parasite invasion is sufficient to induce downregulation, astrocytes were treated with Type II-specific antigen (**Fig. 4.4.1C, lanes 6-8**) or Type II-heat inactivated (HI) parasites (**Fig. 4.4.1C, lanes 9-11**) for 24 hours. Uninfected astrocytes that are untreated (**Fig. 4.4.1C, lanes 1-2**) or treated (**Fig. 4.4.1C, lanes 3-5**) with dexamethasone, are used as negative and positive controls for GLT-1 expression, respectively. In addition to this, Type I and III heat inactivated antigen was also assessed at 5, 50, or 500 $\mu\text{g/ml}$ for 48 hours (**Supp. Fig. 4.4.1-3**). Western blot analysis determined there is no significant differences between the antigen or heat-inactivated treatment conditions, compared to the dexamethasone-treated mock control group, suggesting the presence of *T. gondii* is not sufficient enough to induce GLT-1 downregulation, but rather direct invasion is required.

Finally, to determine if GLT-1 downregulation is dependent on parasite concentration, primary cultured astrocytes were infected with an MOI of 1 (**Fig. 4.4.1E, lanes 6-8**) and 10 (**Fig. 4.4.1E, lanes 9-11**). Although there is a trend of reduced GLT-1 expression in cells infected with an MOI 1 relative to the mock treated control group, there is significant downregulation in astrocytes infected with an MOI 10. Taken altogether, these data suggest that GLT-1 downregulation is not mediated through pathogen recognition receptors and that direct invasion of astrocytes is required to downregulate GLT-1 expression.

4.4.2 *Toxoplasma* Virulence Factors Contribute to GLT-1 Downregulation

Type I-III strains of *T. gondii* are in decreasing order of virulence, where Type I is the most virulent, and Type III is considered avirulent. To test if virulence contributes to GLT-1 downregulation, astrocytes were infected with each of the three respective types of *T. gondii* at an MOI 10 (**Fig. 4.4.2 A & 2B**). Protein analysis for GLT-1 demonstrates that all three types have the ability to decrease GLT-1 protein expression, however the degree of downregulation may be type-dependent. This suggests that virulence factors may be implicated in leading to GLT-1 downregulation.

To test if there is a difference in the number of parasites that have replicated at the end of the 24 hour infection, parasite protein levels were probed via western blotting. Protein analysis for the *T. gondii* indicates there is significantly more Type I parasites for both MOI 1 and 10, relative to Type II and III (**Fig. 4.4.2 D-2G**). Additionally, increased parasite burden in astrocytes led to four distinct *T. gondii* bands during RH infection, and three in Type's II-III, suggesting that virulence factors may be implicated.

4.4.3 Downregulation of GLT-1 in Primary Cultured Astrocytes is Mediated by a Degradative Pathway

As *T. gondii* has the ability to alter NF- κ B signaling [148], GLT-1 mRNA transcript levels were assessed to determine if GLT-1 downregulation is due to a

transcriptional modification after astrocyte infection with Type's I-III infection. To test this, GLT-1-induced astrocyte cultures were infected with Type's I-III strains of *T. gondii* at an MOI of 1 or 10 for 24 hours. Cultures were harvested and RNA was isolated from respective conditions. Mock treated cells with or without dexamethasone were used as controls. All data was first normalized to the housekeeping gene GAPDH, followed by normalization to the GLT-1 induced mock treated control. In all three types of *T. gondii* infection, there is no significant difference for GLT-1 mRNA levels between control groups and infected groups, suggesting that astrocytes a base level of GLT-1 transcripts. This also indicates that GLT-1 downregulation is not due to a transcriptional modification. (**Fig. 4.4.3A-3C**).

Heat Shock Protein 90 (HSP90) plays an important role in protein stabilization, folding, and protein degradation [149]. HSP90 β is upregulated in reactive astrocytes during post-status epilepticus *in vivo*, and negatively regulates GLT-1 protein levels by binding to and forming a complex with a proteasome to degrade the transporter [149, 150]. To test if HSP90 β is implicated in our *in vitro* infection model, GLT-1 expressing primary cultured astrocytes were infected with a Type I strain of *T. gondii*, and subsequently treated with increasing concentrations [10, 100, 1000nM] of the HSP90 β inhibitor, 17-allylamino-17-demethoxygeldanamycin (17AAG) (**Fig. 4.4.3 D& 3E**). Western blot protein analysis indicates that 17AAG

has no effect on GLT-1 expression during infection suggesting that HSP90 is not involved in the GLT-1 downregulation mechanism.

To test if GLT-1 downregulation is dependent on proteasomal degradation, infected astrocytes that express GLT-1 were treated with the potent proteasome inhibitor, MG132, at increasing concentration [1, 10, 100 μ M] (**Fig. 4.4.3 F & G**). Relative to infected astrocytes that were untreated with MG132, the proteasome inhibitor increased GLT-1 protein levels in a dose-dependent manner during Type I infection of astrocytes. This phenomenon is recapitulated in MG132-treated cultures that were infected with Type II and III infection (**Supp. Fig. 4.4.3A-3D**). To verify that MG132 alone does not induce GLT-1, uninfected astrocytes were treated with or without MG132 in the presence or absence of dexamethasone (**Supp. Fig. 4.4.3 E-F**). There are no observable differences in GLT-1 protein levels between cells treated with MG132 alone and cells treated with only media. There is also no distinction between dexamethasone treated astrocytes that are in the presence or absence of MG132. The rescue of GLT-1 expression with MG132 suggests that GLT-1 downregulation is mediated by a degradative pathway.

4.5 Conclusions and Future Direction

We have demonstrated that there is significant GLT-1 downregulation during direct infection with Type's I and II at a high MOI, and a subtle downregulation in Type

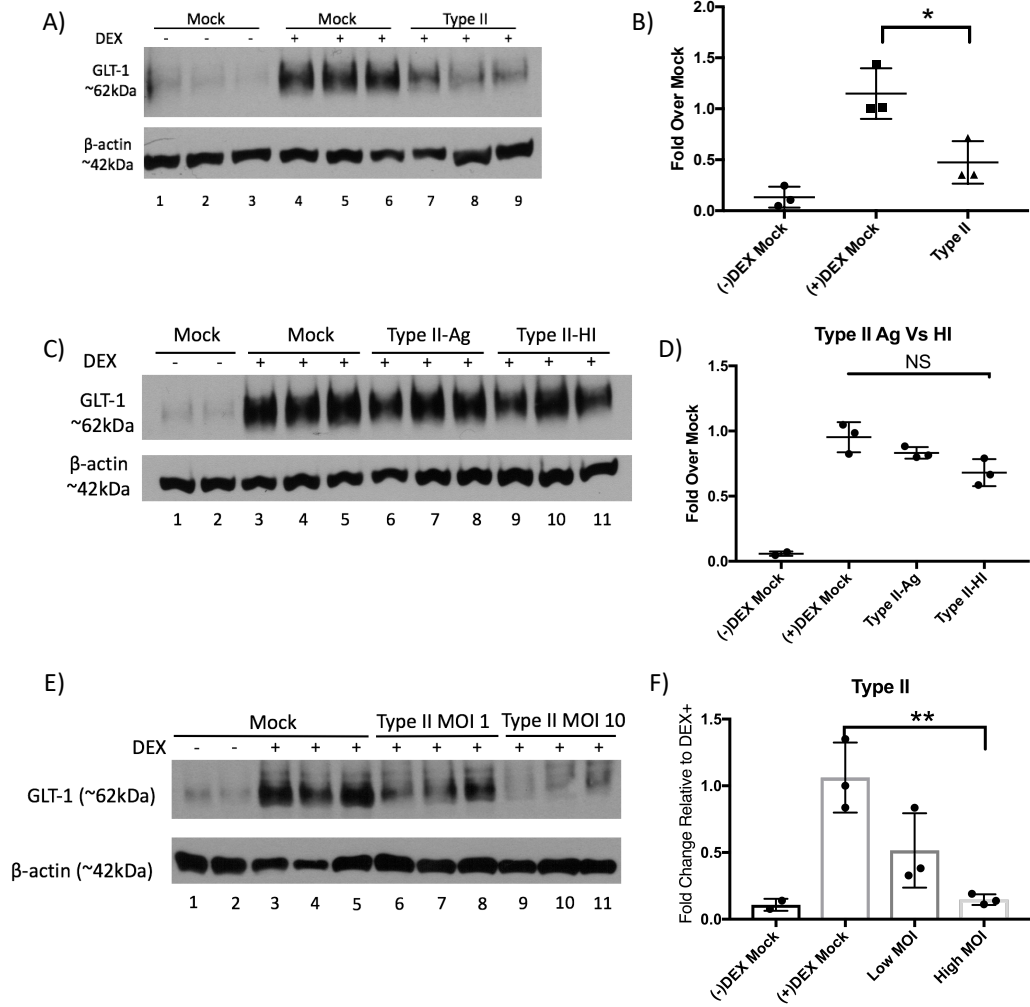
III. Additionally, *T. gondii* antigen or heat-inactivated parasites are not sufficient to induce GLT-1 downregulation in primary cultured astrocytes, suggesting that direct invasion is required for GLT-1 downregulation. These data also suggest that there is type-dependency which further infers that parasite-specific secretory proteins may be implicated in this downregulation mechanism. We also demonstrated that there are no significant changes of GLT-1 mRNA levels in infected astrocytes relative to uninfected suggesting a post-transcriptional mechanism may be leading to GLT-1 downregulation. Finally, we showed that the proteasome inhibitor MG132 and the deubiquitinase inhibitor NEM rescues GLT-1 protein levels in a dose-dependent manner during Type I infection of astrocytes, suggesting that infect is somehow leading to post-translational modifications that marks the transporter for degradation.

The fact that GLT-1 downregulation is a focal and not a global phenomenon throughout the infected brain, and that there is not a requirement for cysts to be localized to sites of reduced GLT-1 expression suggest that there is an internal component that is leading to GLT-1 downregulation. Our future studies will investigate if NF- κ B signaling is involved in GLT-1 regulation in our model. We will accomplish this by looking at phosphorylated and unphosphorylated subunits of NF- κ B during Type's I-III infection. In addition, we will utilize GRA and ROP inhibitors to determine if either of these secretory families are implicated in the GLT-1 downregulation mechanism. We will do this by pre-treatment with

respective inhibitors prior to infection, followed by harvesting cell lysates 24 hours post-infection to perform GLT-1 protein analysis.

4.6 Figures & Legends

Figure 4.4.1 Direct Parasite Invasion of Astrocytes Downregulates GLT-1. Dexamethasone (DEX) treatment was used to induce GLT-1 expression in primary cultured astrocytes. DEX treated astrocytes were subsequently infected with a type II strain of *T. gondii*. **A)** Cells were harvested with RIPA buffer and 10ug of total protein was used per lane of a western blot. GLT-1 (~62kDa) expression was assessed for untreated astrocytes (Lanes 1-3), DEX-treated astrocytes (Lanes 4-6), and infected DEX-treated astrocytes (Lanes 7-9). B-actin (~42kDa) is used as a positive loading control. **B)** Quantification of fig 1A where data is normalized to uninfected DEX treated astrocytes. **C)** Astrocytes were treated with Type II antigen (Ag) [50ug/ml] or Type II heat inactivated (HI) parasite. GLT-1 expression levels were assessed. **D)** Quantitation of GLT-1 levels from 1C where data is normalized to uninfected DEX treated astrocytes. **(E)** Astrocytes were infected with Type II *T. gondii* at an MOI of 1 (low) or 10 (high). Uninfected (mock) astrocytes with (+) or without (-) dexamethasone (DEX) were used as controls. All cells were harvested at 24 hours post-infection. GLT-1 (~62kDa); Beta-actin (~42kDa) is a positive loading control; (+) indicates cells were treated with DEX 72h pre-infection and the duration of infection. **F)** Quantitation of GLT-1 western blot data of DEX treatment astrocytes infected with a low or high MOI of Type II parasite.



Supplementary Figure 4.4.1 Antigen Titration for Types I-III. Astrocytes were treated with 5, 50, or 500ug/ml of strain-specific antigen of **(A)** Type I, **(B)** Type II, or **(C)** Type III *T. gondii*. Uninfected (mock) astrocytes with dexamethasone (DEX) were used as controls. Cells were harvested at 48 hours post-treatment. GLT-1 (~62kDa); Beta-actin (~42kDa) is a positive loading control; (+) indicates cells were treated with DEX 72h pre-infection and the duration of infection.

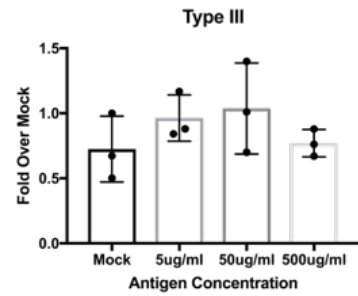
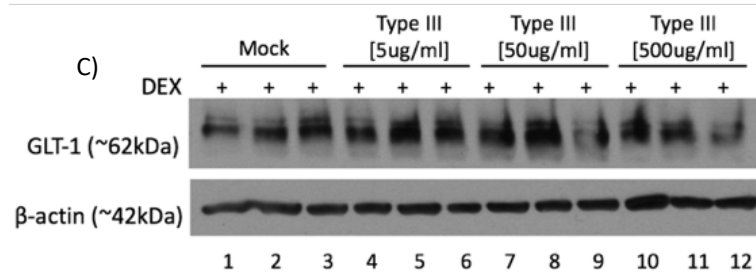
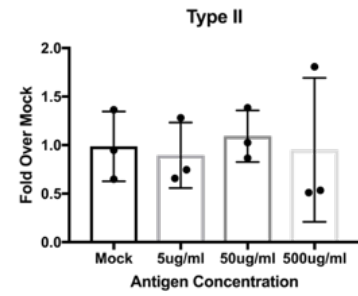
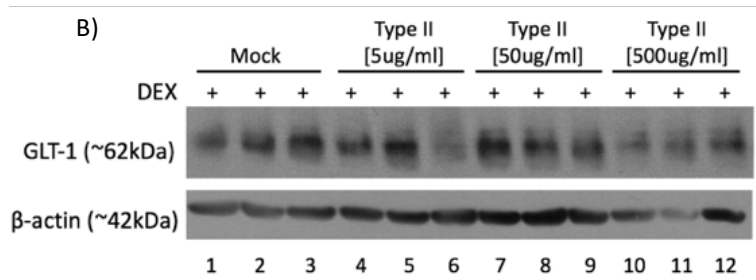
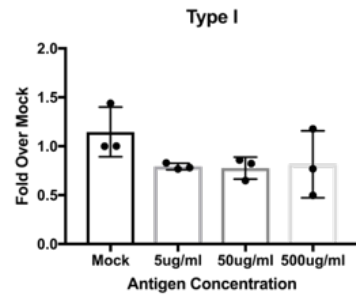
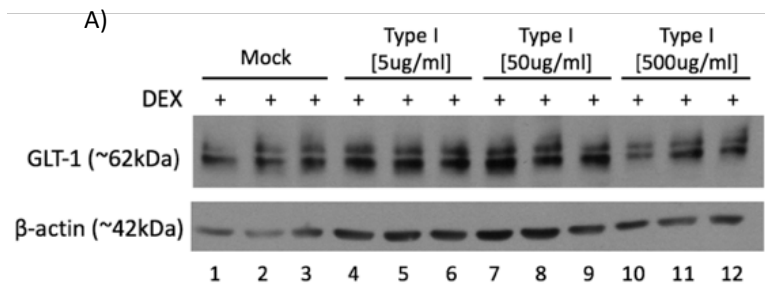


Figure 4.4.2: Toxoplasma Virulence Factors Contribute to GLT-1 Downregulation. (A/B) Astrocytes were infected with Type's I-III *T. gondii* at a multiplicity of infection (MOI) of 10. Uninfected (mock) astrocytes with (+) or without (-) dexamethasone (DEX) were used as controls. All cells were harvested at 24 hours post-infection. GLT-1 (~62kDa); Beta-actin (~42kDa) is a positive loading control; (+) indicates cells were treated with DEX 72h pre-infection and the duration of infection. Astrocytes were infected with Type's I-III *T. gondii* at an MOI 1 (C/D) or MOI 10 (E/F). Toxoplasma expression levels were assessed 24 hours post-infection. (H) H&E stain of astrocytes with no infection (mock) or infected with Type's I-III strain at an MOI 1 or 10.

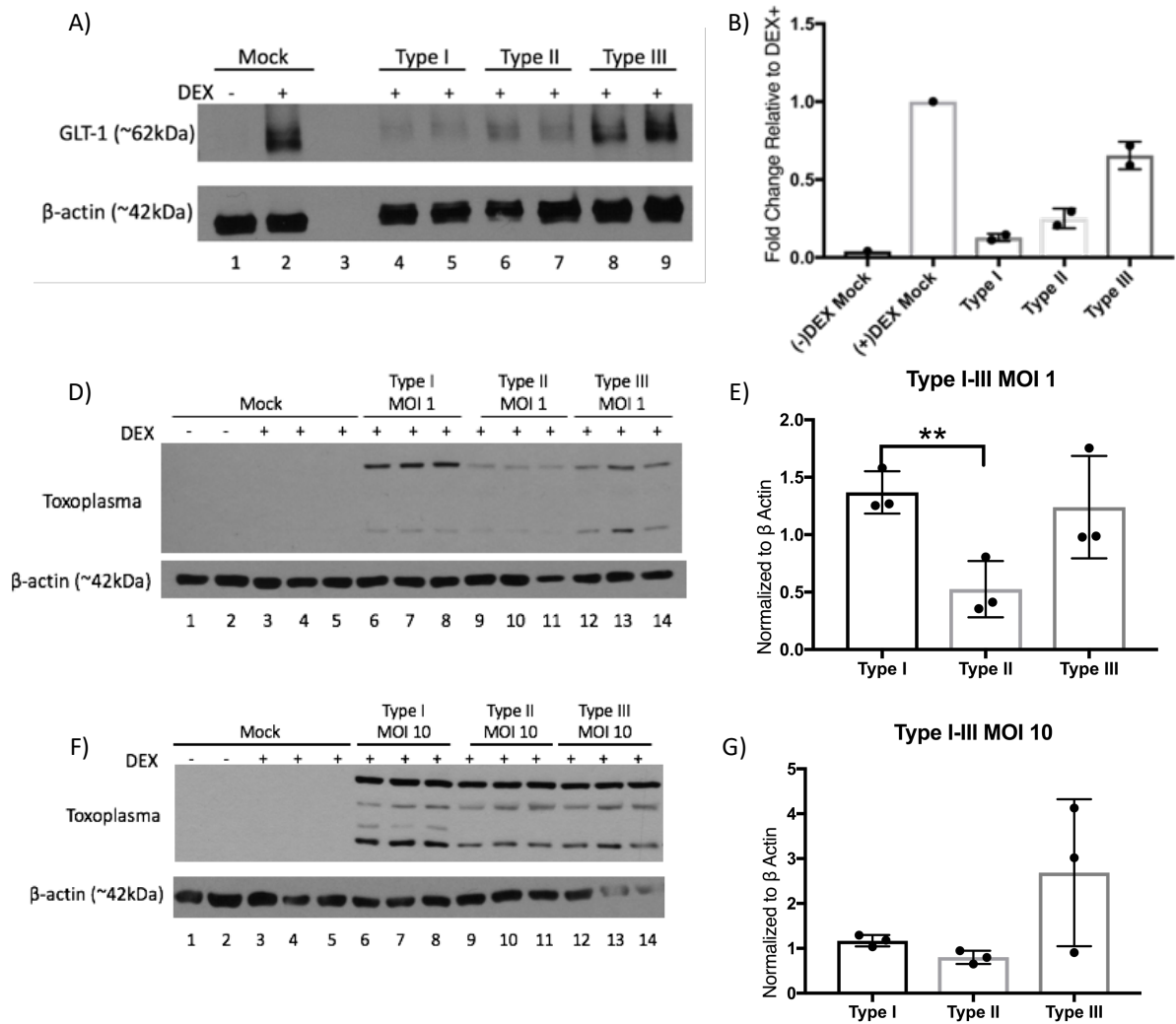
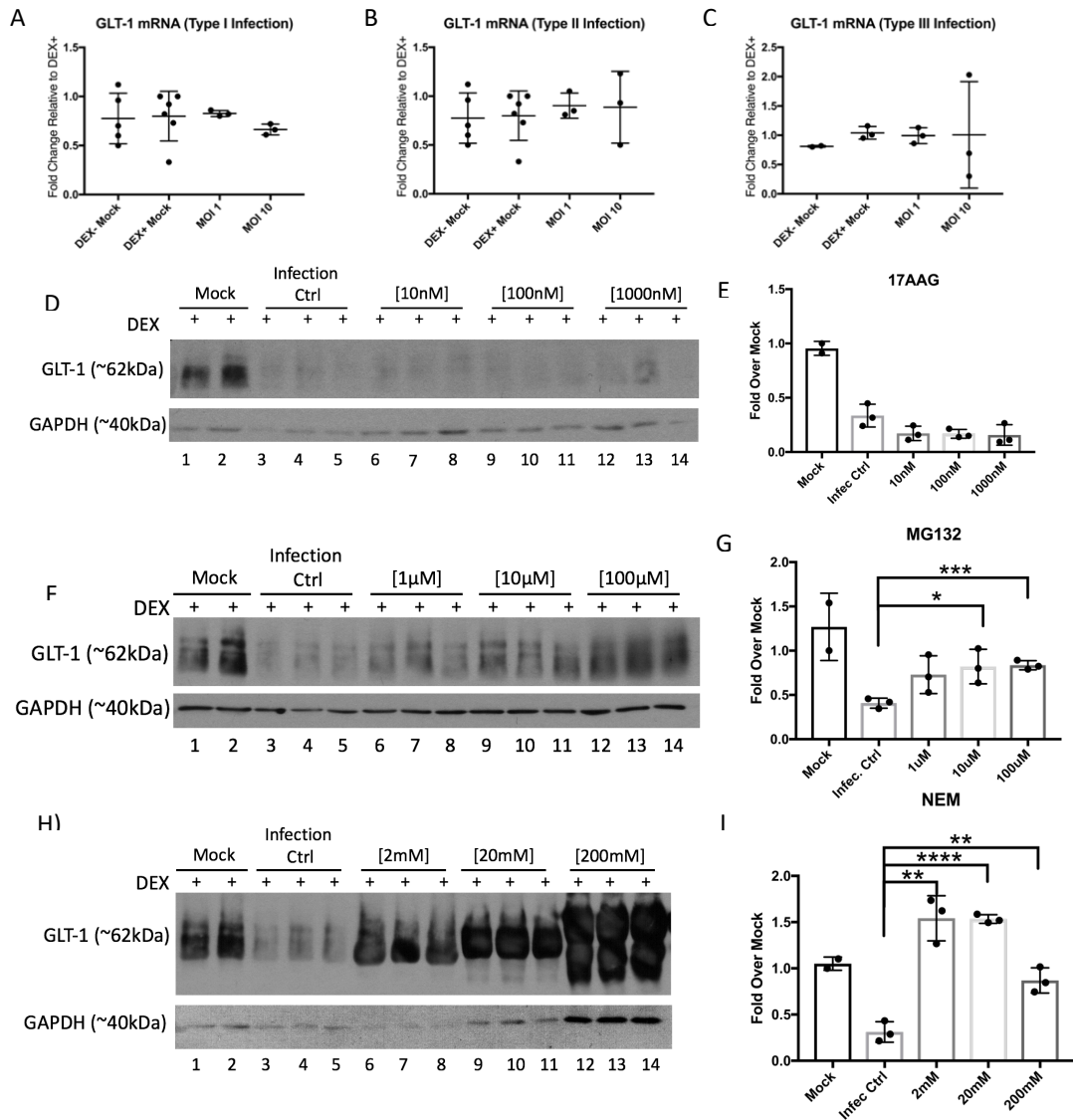
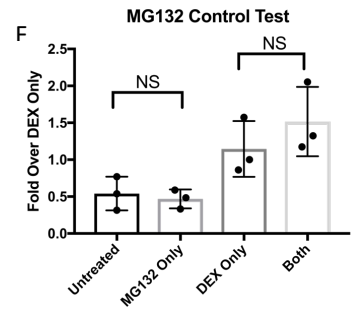
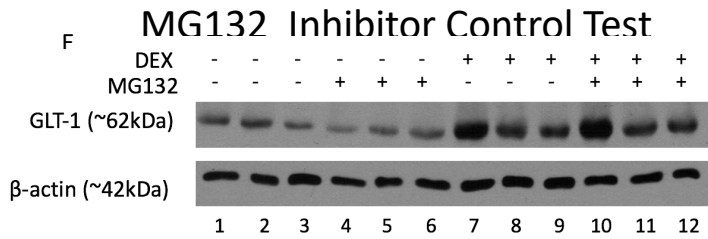
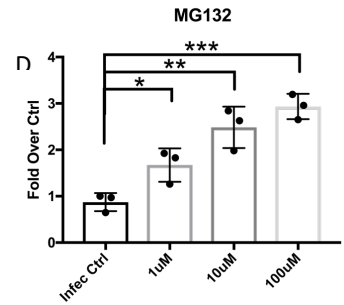
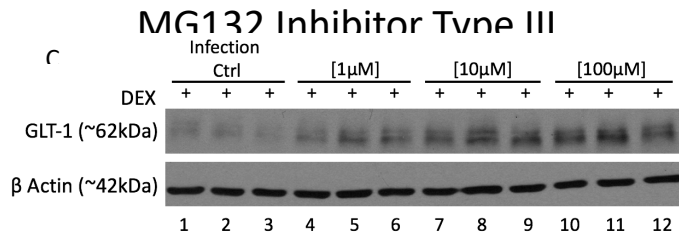
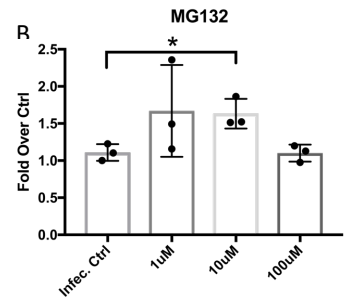
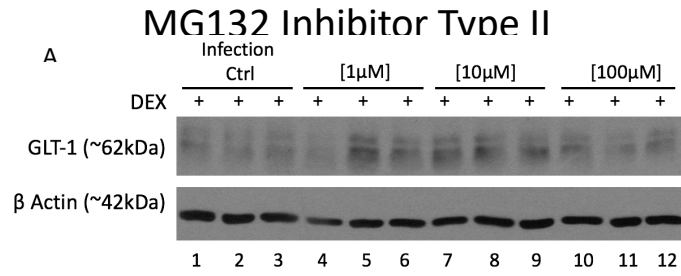


Figure 4.4.3: Downregulation of GLT-1 in Primary Cultured Astrocytes is Mediated by a Degradative Pathway. Astrocytes were infected with **(A)** Type I, **(B)** Type II, or **(C)** Type III *T. gondii* at a multiplicity of infection (MOI) of 1 or 10. Cells were harvested at 24h post-infection for RNA purification followed by qPCR analysis to assess GLT-1 mRNA levels. GAPDH was used as a housekeeping gene to normalize data. Relative fold changes were normalized to the uninfected (mock) samples treated with dexamethasone (DEX). Astrocytes were infected with Type I *T. gondii* at a multiplicity of infection (MOI) of 10. Uninfected (mock) astrocytes with dexamethasone (DEX) were used as controls. **(D/E)** An HSP90b inhibitor (17-allylamino-17-demethoxygeldanamycin (17AAG)) was used at concentrations: 10, 100, or 1000 nM. **(F/G)** A proteasome inhibitor (MG132) was used at concentrations: 1, 10, or 100 μ M. **(H/I)** A deubiquitinase inhibitor (N-Ethylmaleimide (NEM)) was used at concentrations: 2, 20, or 200mM. Cells were harvested at 24 hours post-infection. GLT-1 (~62kDa); GAPDH (~40kDa) is a positive loading control; (+) indicates cells were treated with DEX 72h pre-infection and the duration of infection. Inhibitors were given 3h post-invasion.



Supplementary Figure 4.4.3: *MG132 Control Test with Type II and III*

Astrocytes were infected with **(A)** Type II, **(B)** Type III, or **(C)** untreated at a multiplicity of infection (MOI) of 1 or 10. Cells were harvested at 24h post-infection for subsequent western blot analysis. Where indicated, the proteasome inhibitor (MG132) was used at concentrations: 1, 10, or 100 μ M. GLT-1 (~62kDa); GAPDH (~40kDa) is a positive loading control; (+) indicates cells were treated with DEX 72h pre-infection and the duration of infection. Inhibitors were given 3h post-invasion.



CHAPTER FIVE
Summary and Conclusions

5.1 Summary and Conclusions

In this dissertation I have given extensive background on the forms the parasite can differentiate into, the human populations most impacted by infection, and manipulation strategies to evade the immune response. Work in Chapter Two focused on understanding the biology of the parasite recrudescence process. We showed that ME49EW bradyzoites in mature tissue cysts are a dormant yet diverse population, and that host cells play a role in what form the parasite can differentiate into. Our work demonstrates that in fibroblasts, parasites only follow the bradyzoite-to-tachyzoite differentiation pathway. Murine astrocytes not only can follow this programming, but also undergo bradyzoite-to-bradyzoite development and a reversion of tachyzoites back to bradyzoites. Even though our work resolves parasite development by single cell transcriptomics, additional work still needs to investigate the host factors that are implicated in mediating these recrudescence pathways.

In addition, I have also covered the immune response and emphasized the importance of a continuous pro-inflammatory response in the CNS that is primarily mediated by a heterogeneous mix of T cells. As there are high levels of glutamate in the *T. gondii* infected brain [82], Chapter Three examined how tissue-derived signals influence protective immunity. Our findings demonstrate that there is a population of CD8⁺ T cells that can interact with glutamate via the expression of

group 1 metabotropic glutamate receptors, and this interaction leads to enhanced IFN γ and perforin production of activated T cells. In addition, we report that this population is distinct and defined by a memory and proliferating phenotype.

Although the cause for increased glutamate concentration in the CNS is due to a downregulation of GLT-1, the mechanisms that lead to this are largely unknown [65]. The last body chapter begins to dissect the mechanisms that lead to GLT-1 downregulation. Although there is a lot of work that still needs to be done, our initial findings demonstrate that direct parasite invasion of astrocytes downregulates GLT-1, and this mechanism may be mediated by parasite factors that promote transporter degradation.

Although the studies highlighted in this dissertation have very specific questions in mind, and although each of these topics are tied to one another through the parasite, it is important to think of the system as a whole and consider the dynamic relationship T cells and astrocytes have with one another. When *T. gondii* makes it into the CNS approximately 1 week post infection, a pro-inflammatory response has already been initiated in the periphery but not yet in the brain. The pro-inflammatory mediator, IFN γ , will cause an upregulation of integrins expressed on endothelial cells to increase cell adhesion and subsequent diapedesis of immune cells, however the blood brain barrier (BBB) prevents this cytokine (and others) from traversing into the CNS. This results in the susceptibility to brain infection.

Although neurons are the primary target for parasites to infect and encyst in, a lack of IFN γ priming of astrocytes also makes them vulnerable to infection [5]. This initial susceptibility may be a cause for the observed GLT-1 downregulation during chronic infection. This is supported by work highlighted in Chapter Four that demonstrates that direct invasion of primary cultured astrocytes leads to the downregulation of GLT-1. As astrocytic GLT-1 expression is mediated in part by neuronal export of miR-124 via exosomes [151, 152], my contributions do not exclude the possibility that neuronal-astrocytic communication is being disrupted during infection. In addition, a pro-inflammatory environment can also lead to GLT-1 downregulation, however this may be unlikely in *T. gondii* infection as GLT-1 downregulation is focal and patchy, but the presence of inflammatory mediators are found globally within the CNS.

It is not until astrocytes and other glial cells mediate CNS-immune cell infiltration by the production of chemokines such as CXCL9-11. This allows for CXCR3⁺CD8⁺ T cells to traverse the BBB and provide support to resident brain cells. The release of T cell-derived IFN γ into the brain microenvironment instructs astrocytes to protect themselves by promoting the upregulation of immunity-related GTPases [12]. These molecules will bind to and disrupt the parasitophorous vacuole, making the parasite susceptible to lysosomal degradation. Moreover, the absence of T cells or IFN γ not only allow for parasite reactivation, but cause astrocytes to become infected, where IFN γ depletion studies in mice demonstrate that ~30% of

the infected population in the CNS are astrocytes [5]. Taken together, this demonstrates a synergetic relationship T cells and astrocytes have in order to control CNS *T. gondii* infection.

5.2 References

1. Nissapatorn, V., *Toxoplasma gondii* and HIV: a never-ending story. *Lancet HIV*, 2017. **4**(4): p. e146-e147.
2. Maldonado, Y.A. and J.S. Read, *Diagnosis, Treatment, and Prevention of Congenital Toxoplasmosis in the United States*. *Pediatrics*, 2017. **139**(2).
3. Schwarz, J.A., et al., *A novel rhoptry protein in Toxoplasma gondii bradyzoites and merozoites*. *Mol Biochem Parasitol*, 2005. **144**(2): p. 159-66.
4. Hehl, A.B., et al., *Asexual expansion of Toxoplasma gondii merozoites is distinct from tachyzoites and entails expression of non-overlapping gene families to attach, invade, and replicate within feline enterocytes*. *BMC Genomics*, 2015. **16**(1): p. 66.
5. Cabral, C.M., et al., *Neurons are the Primary Target Cell for the Brain-Tropic Intracellular Parasite Toxoplasma gondii*. *PLoS Pathog*, 2016. **12**(2): p. e1005447.
6. Takács, A.C., I.J. Swierzy, and C.G. Lüder, *Interferon- γ restricts Toxoplasma gondii development in murine skeletal muscle cells via nitric oxide production and immunity-related GTPases*. *PLoS One*, 2012. **7**(9): p. e45440.
7. Mercer, H.L., et al., *Toxoplasma gondii dense granule protein GRA24 drives MyD88-independent p38 MAPK activation, IL-12 production and induction of protective immunity*. *PLoS Pathog*, 2020. **16**(5): p. e1008572.
8. Scanga, C.A., et al., *Cutting edge: MyD88 is required for resistance to Toxoplasma gondii infection and regulates parasite-induced IL-12 production by dendritic cells*. *J Immunol*, 2002. **168**(12): p. 5997-6001.
9. Debierre-Grockiego, F., et al., *Activation of TLR2 and TLR4 by glycosylphosphatidylinositols derived from Toxoplasma gondii*. *J Immunol*, 2007. **179**(2): p. 1129-37.
10. Mahmoudzadeh, S., et al., *The role of IL-12 in stimulating NK cells against Toxoplasma gondii infection: a mini-review*. *Parasitol Res*, 2021. **120**(7): p. 2303-2309.
11. Gazzinelli, R., et al., *Simultaneous depletion of CD4+ and CD8+ T lymphocytes is required to reactivate chronic infection with Toxoplasma gondii*. *J Immunol*, 1992. **149**(1): p. 175-80.

12. Hunn, J.P., et al., *The immunity-related GTPases in mammals: a fast-evolving cell-autonomous resistance system against intracellular pathogens*. Mamm Genome, 2011. **22**(1-2): p. 43-54.
13. Engin, A.B., et al., *Oxidative stress and tryptophan degradation pattern of acute Toxoplasma gondii infection in mice*. Parasitol Res, 2012. **111**(4): p. 1725-30.
14. Kudo, M., et al., *The role of IFN-gamma and Toll-like receptors in nephropathy induced by Toxoplasma gondii infection*. Microbiol Immunol, 2004. **48**(8): p. 617-28.
15. Gazzinelli, R.T., et al., *In the absence of endogenous IL-10, mice acutely infected with Toxoplasma gondii succumb to a lethal immune response dependent on CD4+ T cells and accompanied by overproduction of IL-12, IFN-gamma and TNF-alpha*. J Immunol, 1996. **157**(2): p. 798-805.
16. Wilson, E.H., et al., *A critical role for IL-10 in limiting inflammation during toxoplasmic encephalitis*. J Neuroimmunol, 2005. **165**(1-2): p. 63-74.
17. Gao, X., et al., *The Role and Function of Regulatory T Cells in Toxoplasma gondii-Induced Adverse Pregnancy Outcomes*. J Immunol Res, 2021. **2021**: p. 8782672.
18. Harris, T.H., et al., *Generalized Levy walks and the role of chemokines in migration of effector CD8+ T cells*. Nature, 2012. **486**(7404): p. 545-8.
19. Carrithers, M.D., et al., *Differential adhesion molecule requirements for immune surveillance and inflammatory recruitment*. Brain, 2000. **123** (Pt 6): p. 1092-101.
20. Sa, Q., et al., *VCAM-1/ α 4 β 1 integrin interaction is crucial for prompt recruitment of immune T cells into the brain during the early stage of reactivation of chronic infection with Toxoplasma gondii to prevent toxoplasmic encephalitis*. Infect Immun, 2014. **82**(7): p. 2826-39.
21. Wilson, E.H., et al., *Behavior of parasite-specific effector CD8+ T cells in the brain and visualization of a kinesis-associated system of reticular fibers*. Immunity, 2009. **30**(2): p. 300-11.
22. Kivisäkk, P., et al., *T-cells in the cerebrospinal fluid express a similar repertoire of inflammatory chemokine receptors in the absence or presence of CNS inflammation: implications for CNS trafficking*. Clin Exp Immunol, 2002. **129**(3): p. 510-8.

23. Schluter, D., et al., *Phenotype and regulation of persistent intracerebral T cells in murine Toxoplasma encephalitis*. J Immunol, 2002. **169**(1): p. 315-22.
24. Strack, A., et al., *Regulation of the kinetics of intracerebral chemokine gene expression in murine Toxoplasma encephalitis: impact of host genetic factors*. Glia, 2002. **40**(3): p. 372-7.
25. Dubey, J.P., *Tissue cyst tropism in Toxoplasma gondii: a comparison of tissue cyst formation in organs of cats, and rodents fed oocysts*. Parasitology, 1997. **115 (Pt 1)**: p. 15-20.
26. Dubey, J.P. and J.K. Frenkel, *Feline toxoplasmosis from acutely infected mice and the development of Toxoplasma cysts*. J Protozool, 1976. **23**(4): p. 537-46.
27. Weiss, L.M. and J.P. Dubey, *Toxoplasmosis: A history of clinical observations*. Int J Parasitol, 2009. **39**(8): p. 895-901.
28. Remington, J.S., *Toxoplasmosis in the adult*. Bull N Y Acad Med, 1974. **50**(2): p. 211-27.
29. Dellacasa-Lindberg, I., N. Hitziger, and A. Barragan, *Localized recrudescence of Toxoplasma infections in the central nervous system of immunocompromised mice assessed by in vivo bioluminescence imaging*. Microbes Infect, 2007. **9**(11): p. 1291-8.
30. Odaert, H., et al., *Stage conversion of Toxoplasma gondii in mouse brain during infection and immunodepression*. Parasitol Res, 1996. **82**(1): p. 28-31.
31. Reiter-Owona, I., et al., *Is stage conversion the initiating event for reactivation of Toxoplasma gondii in brain tissue of AIDS patients?* J Parasitol, 2000. **86**(3): p. 531-6.
32. Roos, D.S., et al., *Molecular tools for genetic dissection of the protozoan parasite Toxoplasma gondii*. Methods Cell Biol, 1994. **45**: p. 27-63.
33. Fox, B.A., et al., *Type II Toxoplasma gondii KU80 knockout strains enable functional analysis of genes required for cyst development and latent infection*. Eukaryot Cell, 2011. **10**(9): p. 1193-206.
34. Hong, D.P., J.B. Radke, and M.W. White, *Opposing Transcriptional Mechanisms Regulate Toxoplasma Development*. mSphere, 2017. **2**(1).

35. Huang, S., et al., *Toxoplasma gondii* AP2IX-4 Regulates Gene Expression during Bradyzoite Development. *mSphere*, 2017. **2**(2).
36. Radke, J.B., et al., *ApiAP2* transcription factor restricts development of the *Toxoplasma* tissue cyst. *Proc Natl Acad Sci U S A*, 2013. **110**(17): p. 6871-6.
37. Radke, J.B., et al., *Transcriptional repression by ApiAP2 factors is central to chronic toxoplasmosis*. *PLoS Pathog*, 2018. **14**(5): p. e1007035.
38. Farhat, D.C., et al., *A MORC-driven transcriptional switch controls Toxoplasma developmental trajectories and sexual commitment*. *Nat Microbiol*, 2020. **5**(4): p. 570-583.
39. Bohne, W., et al., *Cloning and characterization of a bradyzoite-specifically expressed gene (hsp30/bag1) of Toxoplasma gondii, related to genes encoding small heat-shock proteins of plants*. *Mol Microbiol*, 1995. **16**(6): p. 1221-30.
40. Kim, S.K. and J.C. Boothroyd, *Stage-specific expression of surface antigens by Toxoplasma gondii as a mechanism to facilitate parasite persistence*. *J Immunol*, 2005. **174**(12): p. 8038-48.
41. Ferguson, D.J., *Use of molecular and ultrastructural markers to evaluate stage conversion of Toxoplasma gondii in both the intermediate and definitive host*. *Int J Parasitol*, 2004. **34**(3): p. 347-60.
42. Saraf, P., et al., *On the determination of Toxoplasma gondii virulence in mice*. *Exp Parasitol*, 2017. **174**: p. 25-30.
43. Jeffers, V., et al., *A latent ability to persist: differentiation in Toxoplasma gondii*. *Cell Mol Life Sci*, 2018. **75**(13): p. 2355-2373.
44. Ferguson, D.J. and W.M. Hutchison, *An ultrastructural study of the early development and tissue cyst formation of Toxoplasma gondii in the brains of mice*. *Parasitol Res*, 1987. **73**(6): p. 483-91.
45. Watts, E., et al., *Novel Approaches Reveal that Toxoplasma gondii Bradyzoites within Tissue Cysts Are Dynamic and Replicating Entities In Vivo*. *mBio*, 2015. **6**(5): p. e01155-15.
46. Radke, J.R., et al., *A change in the premitotic period of the cell cycle is associated with bradyzoite differentiation in Toxoplasma gondii*. *Mol Biochem Parasitol*, 2003. **131**(2): p. 119-27.

47. Dubey, R., et al., *Differential Roles for Inner Membrane Complex Proteins across Toxoplasma gondii and Sarcocystis neurona Development*. mSphere, 2017. **2**(5).
48. Ouologuem, D.T. and D.S. Roos, *Dynamics of the Toxoplasma gondii inner membrane complex*. J Cell Sci, 2014. **127**(Pt 15): p. 3320-30.
49. Jerome, M.E., et al., *Toxoplasma gondii bradyzoites form spontaneously during sporozoite-initiated development*. Infect Immun, 1998. **66**(10): p. 4838-44.
50. Radke, J.R., et al., *The transcriptome of Toxoplasma gondii*. BMC Biol, 2005. **3**: p. 26.
51. Denton, H., et al., *Enzymes of energy metabolism in the bradyzoites and tachyzoites of Toxoplasma gondii*. FEMS Microbiol Lett, 1996. **137**(1): p. 103-8.
52. Cerutti, A., N. Blanchard, and S. Besteiro, *The Bradyzoite: A Key Developmental Stage for the Persistence and Pathogenesis of Toxoplasmosis*. Pathogens, 2020. **9**(3).
53. Dubey, J.P., *Unexpected oocyst shedding by cats fed Toxoplasma gondii tachyzoites: in vivo stage conversion and strain variation*. Vet Parasitol, 2005. **133**(4): p. 289-98.
54. Dzierszynski, F., et al., *Dynamics of Toxoplasma gondii differentiation*. Eukaryot Cell, 2004. **3**(4): p. 992-1003.
55. Waldman, B.S., et al., *Identification of a Master Regulator of Differentiation in Toxoplasma*. Cell, 2020. **180**(2): p. 359-372 e16.
56. Tanaka, N., et al., *Use of human induced pluripotent stem cell-derived neurons as a model for Cerebral Toxoplasmosis*. Microbes Infect, 2016. **18**(7-8): p. 496-504.
57. Halonen, S.K., G.A. Taylor, and L.M. Weiss, *Gamma interferon-induced inhibition of Toxoplasma gondii in astrocytes is mediated by IGTP*. Infect Immun, 2001. **69**(9): p. 5573-6.
58. Hidano, S., et al., *STAT1 Signaling in Astrocytes Is Essential for Control of Infection in the Central Nervous System*. mBio, 2016. **7**(6).

59. Rani, S., et al., *Toxoplasma gondii* tissue cyst formation and density of tissue cysts in shoulders of pigs 7 and 14 days after feeding infected mice tissues. *Vet Parasitol*, 2019. **269**: p. 13-15.
60. Ten Hoeve, A.L., M.A. Hakimi, and A. Barragan, *Sustained Egr-1 Response via p38 MAP Kinase Signaling Modulates Early Immune Responses of Dendritic Cells Parasitized by Toxoplasma gondii*. *Front Cell Infect Microbiol*, 2019. **9**: p. 349.
61. Xue, Y., et al., *A single-parasite transcriptional atlas of Toxoplasma gondii reveals novel control of antigen expression*. *Elife*, 2020. **9**.
62. Bechmann, I., I. Galea, and V.H. Perry, *What is the blood-brain barrier (not)?* *Trends Immunol*, 2007. **28**(1): p. 5-11.
63. Kawakami, N., et al., *Live imaging of effector cell trafficking and autoantigen recognition within the unfolding autoimmune encephalomyelitis lesion*. *J Exp Med*, 2005. **201**(11): p. 1805-14.
64. Constantin, G., *Chemokine signaling and integrin activation in lymphocyte migration into the inflamed brain*. *J Neuroimmunol*, 2008. **198**(1-2): p. 20-6.
65. Becker, T.C., et al., *Interleukin 15 is required for proliferative renewal of virus-specific memory CD8 T cells*. *J Exp Med*, 2002. **195**(12): p. 1541-8.
66. Ku, C.C., et al., *Control of homeostasis of CD8+ memory T cells by opposing cytokines*. *Science*, 2000. **288**(5466): p. 675-8.
67. Schluns, K.S., et al., *Interleukin-7 mediates the homeostasis of naïve and memory CD8 T cells in vivo*. *Nat Immunol*, 2000. **1**(5): p. 426-32.
68. Araki, K., et al., *mTOR regulates memory CD8 T-cell differentiation*. *Nature*, 2009. **460**(7251): p. 108-12.
69. Araki, Y., et al., *Genome-wide analysis of histone methylation reveals chromatin state-based regulation of gene transcription and function of memory CD8+ T cells*. *Immunity*, 2009. **30**(6): p. 912-25.
70. Youngblood, B., et al., *Effector CD8 T cells dedifferentiate into long-lived memory cells*. *Nature*, 2017. **552**(7685): p. 404-409.
71. Pizzolla, A., et al., *Resident memory CD8(+) T cells in the upper respiratory tract prevent pulmonary influenza virus infection*. *Sci Immunol*, 2017. **2**(12).

72. Steffen, J., et al., *Type 1 innate lymphoid cells regulate the onset of Toxoplasma gondii-induced neuroinflammation*. Cell Rep, 2022. **38**(13): p. 110564.
73. Ploix, C.C., et al., *CNS-derived CCL21 is both sufficient to drive homeostatic CD4+ T cell proliferation and necessary for efficient CD4+ T cell migration into the CNS parenchyma following Toxoplasma gondii infection*. Brain Behav Immun, 2011. **25**(5): p. 883-96.
74. Norose, K., et al., *CXCL10 is required to maintain T-cell populations and to control parasite replication during chronic ocular toxoplasmosis*. Invest Ophthalmol Vis Sci, 2011. **52**(1): p. 389-98.
75. Noor, S., et al., *CCR7-dependent immunity during acute Toxoplasma gondii infection*. Infect Immun, 2010. **78**(5): p. 2257-63.
76. Bhadra, R., et al., *Control of Toxoplasma reactivation by rescue of dysfunctional CD8+ T-cell response via PD-1-PDL-1 blockade*. Proc Natl Acad Sci U S A, 2011. **108**(22): p. 9196-201.
77. O'Brien, C.A., et al., *IL-10 and ICOS Differentially Regulate T Cell Responses in the Brain during Chronic Toxoplasma gondii Infection*. J Immunol, 2019. **202**(6): p. 1755-1766.
78. McGovern, K.E., et al., *SPARC coordinates extracellular matrix remodeling and efficient recruitment to and migration of antigen-specific T cells in the brain following infection*. Sci Rep, 2021. **11**(1): p. 4549.
79. Landrith, T.A., et al., *CD103(+) CD8 T Cells in the Toxoplasma-Infected Brain Exhibit a Tissue-Resident Memory Transcriptional Profile*. Front Immunol, 2017. **8**: p. 335.
80. Peterson, A.R., et al., *Targeted overexpression of glutamate transporter-1 reduces seizures and attenuates pathological changes in a mouse model of epilepsy*. Neurobiol Dis, 2021. **157**: p. 105443.
81. Hotz, A.L., et al., *Loss of glutamate transporter eaat2a leads to aberrant neuronal excitability, recurrent epileptic seizures, and basal hypoactivity*. Glia, 2022. **70**(1): p. 196-214.
82. David, C.N., et al., *GLT-1-Dependent Disruption of CNS Glutamate Homeostasis and Neuronal Function by the Protozoan Parasite Toxoplasma gondii*. PLoS Pathog, 2016. **12**(6): p. e1005643.

83. Bai, W. and Y.G. Zhou, *Homeostasis of the Intraparenchymal-Blood Glutamate Concentration Gradient: Maintenance, Imbalance, and Regulation*. Front Mol Neurosci, 2017. **10**: p. 400.
84. Levite, M., *Glutamate, T cells and multiple sclerosis*. J Neural Transm (Vienna), 2017. **124**(7): p. 775-798.
85. Javidi, E. and T. Magnus, *Autoimmunity After Ischemic Stroke and Brain Injury*. Front Immunol, 2019. **10**: p. 686.
86. Hayashi, K., et al., *LAT1 is a critical transporter of essential amino acids for immune reactions in activated human T cells*. J Immunol, 2013. **191**(8): p. 4080-5.
87. Siska, P.J., et al., *Fluorescence-based measurement of cystine uptake through xCT shows requirement for ROS detoxification in activated lymphocytes*. J Immunol Methods, 2016. **438**: p. 51-58.
88. Mak, T.W., et al., *Glutathione Primes T Cell Metabolism for Inflammation*. Immunity, 2017. **46**(6): p. 1089-1090.
89. Pacheco, R., et al., *Group I metabotropic glutamate receptors mediate a dual role of glutamate in T cell activation*. J Biol Chem, 2004. **279**(32): p. 33352-8.
90. Levite, M., *Neurotransmitters activate T-cells and elicit crucial functions via neurotransmitter receptors*. Curr Opin Pharmacol, 2008. **8**(4): p. 460-71.
91. Ganor, Y., et al., *Human T cells express a functional ionotropic glutamate receptor GluR3, and glutamate by itself triggers integrin-mediated adhesion to laminin and fibronectin and chemotactic migration*. J Immunol, 2003. **170**(8): p. 4362-72.
92. Pouloupoulou, C., et al., *Modulation of voltage-gated potassium channels in human T lymphocytes by extracellular glutamate*. Mol Pharmacol, 2005. **67**(3): p. 856-67.
93. Miglio, G., F. Varsaldi, and G. Lombardi, *Human T lymphocytes express N-methyl-D-aspartate receptors functionally active in controlling T cell activation*. Biochem Biophys Res Commun, 2005. **338**(4): p. 1875-83.
94. Buschler, A. and D. Manahan-Vaughan, *Metabotropic glutamate receptor, mGlu5, mediates enhancements of hippocampal long-term potentiation*

- after environmental enrichment in young and old mice.* Neuropharmacology, 2017. **115**: p. 42-50.
95. Takeuchi, T., A.J. Duzkiewicz, and R.G. Morris, *The synaptic plasticity and memory hypothesis: encoding, storage and persistence.* Philos Trans R Soc Lond B Biol Sci, 2014. **369**(1633): p. 20130288.
 96. Chiocchetti, A., et al., *Group I mGlu receptor stimulation inhibits activation-induced cell death of human T lymphocytes.* Br J Pharmacol, 2006. **148**(6): p. 760-8.
 97. Liu, Y., et al., *Transcriptional landscape of the human cell cycle.* Proc Natl Acad Sci U S A, 2017. **114**(13): p. 3473-3478.
 98. Zhou, Y. and N.C. Danbolt, *Glutamate as a neurotransmitter in the healthy brain.* J Neural Transm (Vienna), 2014. **121**(8): p. 799-817.
 99. Huang da, W., B.T. Sherman, and R.A. Lempicki, *Systematic and integrative analysis of large gene lists using DAVID bioinformatics resources.* Nat Protoc, 2009. **4**(1): p. 44-57.
 100. Sherman, B.T., et al., *DAVID: a web server for functional enrichment analysis and functional annotation of gene lists (2021 update).* Nucleic Acids Res, 2022.
 101. Saugstad, J.A., et al., *RGS4 inhibits signaling by group I metabotropic glutamate receptors.* J Neurosci, 1998. **18**(3): p. 905-13.
 102. Gonzalez, N.M., et al., *Schrödinger's T Cells: Molecular Insights Into Stemness and Exhaustion.* Front Immunol, 2021. **12**: p. 725618.
 103. Farsakoglu, Y., B. McDonald, and S.M. Kaech, *Motility Matters: How CD8(+) T-Cell Trafficking Influences Effector and Memory Cell Differentiation.* Cold Spring Harb Perspect Biol, 2021. **13**(8).
 104. Yao, C., et al., *Single-cell RNA-seq reveals TOX as a key regulator of CD8(+) T cell persistence in chronic infection.* Nat Immunol, 2019. **20**(7): p. 890-901.
 105. Chung, H.K., B. McDonald, and S.M. Kaech, *The architectural design of CD8+ T cell responses in acute and chronic infection: Parallel structures with divergent fates.* J Exp Med, 2021. **218**(4).

106. Kaech, S.M., et al., *Selective expression of the interleukin 7 receptor identifies effector CD8 T cells that give rise to long-lived memory cells*. Nat Immunol, 2003. **4**(12): p. 1191-8.
107. Buggert, M., et al., *T-bet and Eomes are differentially linked to the exhausted phenotype of CD8+ T cells in HIV infection*. PLoS Pathog, 2014. **10**(7): p. e1004251.
108. Kaech, S.M. and W. Cui, *Transcriptional control of effector and memory CD8+ T cell differentiation*. Nat Rev Immunol, 2012. **12**(11): p. 749-61.
109. Wilson, E.H. and C.A. Hunter, *Immunodominance and recognition of intracellular pathogens*. J Infect Dis, 2008. **198**(11): p. 1579-81.
110. Shallberg, L.A., et al., *Impact of secondary TCR engagement on the heterogeneity of pathogen-specific CD8+ T cell response during acute and chronic toxoplasmosis*. PLoS Pathog, 2022. **18**(6): p. e1010296.
111. Avecilla, V., M. Doke, and Q. Felty, *Contribution of Inhibitor of DNA Binding/Differentiation-3 and Endocrine Disrupting Chemicals to Pathophysiological Aspects of Chronic Disease*. Biomed Res Int, 2017. **2017**: p. 6307109.
112. Yokota, Y., et al., *Development of peripheral lymphoid organs and natural killer cells depends on the helix-loop-helix inhibitor Id2*. Nature, 1999. **397**(6721): p. 702-6.
113. Boos, M.D., et al., *Mature natural killer cell and lymphoid tissue-inducing cell development requires Id2-mediated suppression of E protein activity*. J Exp Med, 2007. **204**(5): p. 1119-30.
114. Yang, C.Y., et al., *The transcriptional regulators Id2 and Id3 control the formation of distinct memory CD8+ T cell subsets*. Nat Immunol, 2011. **12**(12): p. 1221-9.
115. Wu, T., et al., *The TCF1-Bcl6 axis counteracts type I interferon to repress exhaustion and maintain T cell stemness*. Sci Immunol, 2016. **1**(6).
116. Lee, K., et al., *Distinct biochemical properties of the class I histone deacetylase complexes*. Curr Opin Chem Biol, 2022. **70**: p. 102179.
117. Bhaskara, S., et al., *Histone deacetylases 1 and 2 maintain S-phase chromatin and DNA replication fork progression*. Epigenetics Chromatin, 2013. **6**(1): p. 27.

118. Lei, M., *The MCM complex: its role in DNA replication and implications for cancer therapy*. *Curr Cancer Drug Targets*, 2005. **5**(5): p. 365-80.
119. Arbel, M., et al., *PCNA Loaders and Unloaders-One Ring That Rules Them All*. *Genes (Basel)*, 2021. **12**(11).
120. Chen, Y., et al., *Subunit Interaction Differences Between the Replication Factor C Complexes in Arabidopsis and Rice*. *Front Plant Sci*, 2018. **9**: p. 779.
121. Li, Z. and X. Xu, *Post-Translational Modifications of the Mini-Chromosome Maintenance Proteins in DNA Replication*. *Genes (Basel)*, 2019. **10**(5).
122. Fry, A.M., et al., *Cell cycle regulation by the NEK family of protein kinases*. *J Cell Sci*, 2012. **125**(Pt 19): p. 4423-33.
123. Peres de Oliveira, A., et al., *Checking NEKs: Overcoming a Bottleneck in Human Diseases*. *Molecules*, 2020. **25**(8).
124. Sysel, A.M., V.E. Valli, and J.A. Bauer, *Immunohistochemical quantification of the cobalamin transport protein, cell surface receptor and Ki-67 in naturally occurring canine and feline malignant tumors and in adjacent normal tissues*. *Oncotarget*, 2015. **6**(4): p. 2331-48.
125. Scholzen, T. and J. Gerdes, *The Ki-67 protein: from the known and the unknown*. *J Cell Physiol*, 2000. **182**(3): p. 311-22.
126. Tiwari, A., et al., *Penetration of CD8(+) Cytotoxic T Cells into Large Target, Tissue Cysts of Toxoplasma gondii, Leads to Its Elimination*. *Am J Pathol*, 2019. **189**(8): p. 1594-1607.
127. Suzuki, Y., et al., *Removal of Toxoplasma gondii cysts from the brain by perforin-mediated activity of CD8+ T cells*. *Am J Pathol*, 2010. **176**(4): p. 1607-13.
128. Hays, S.A., K.M. Huber, and J.R. Gibson, *Altered neocortical rhythmic activity states in Fmr1 KO mice are due to enhanced mGluR5 signaling and involve changes in excitatory circuitry*. *J Neurosci*, 2011. **31**(40): p. 14223-34.
129. Leibowitz, A., et al., *Blood glutamate scavenging: insight into neuroprotection*. *Int J Mol Sci*, 2012. **13**(8): p. 10041-66.
130. Bergersen, K.V., et al., *Targeted Transcriptomic Analysis of C57BL/6 and BALB/c Mice During Progressive Chronic Toxoplasma gondii Infection*

- Reveals Changes in Host and Parasite Gene Expression Relating to Neuropathology and Resolution.* Front Cell Infect Microbiol, 2021. **11**: p. 645778.
131. Collingridge, G.L., et al., *Metabotropic glutamate receptors, 5 years on.* Neuropharmacology, 2017. **115**: p. 1-3.
 132. Rondard, P. and J.P. Pin, *Dynamics and modulation of metabotropic glutamate receptors.* Curr Opin Pharmacol, 2015. **20**: p. 95-101.
 133. Chang, J.T., et al., *Asymmetric T lymphocyte division in the initiation of adaptive immune responses.* Science, 2007. **315**(5819): p. 1687-91.
 134. Reiner, S.L., F. Sallusto, and A. Lanzavecchia, *Division of labor with a workforce of one: challenges in specifying effector and memory T cell fate.* Science, 2007. **317**(5838): p. 622-5.
 135. Badovinac, V.P., B.B. Porter, and J.T. Harty, *Programmed contraction of CD8(+) T cells after infection.* Nat Immunol, 2002. **3**(7): p. 619-26.
 136. Chu, H.H., et al., *Continuous Effector CD8(+) T Cell Production in a Controlled Persistent Infection Is Sustained by a Proliferative Intermediate Population.* Immunity, 2016. **45**(1): p. 159-71.
 137. Sung, J.H., et al., *Chemokine guidance of central memory T cells is critical for antiviral recall responses in lymph nodes.* Cell, 2012. **150**(6): p. 1249-63.
 138. Kastenmüller, W., et al., *Peripheral prepositioning and local CXCL9 chemokine-mediated guidance orchestrate rapid memory CD8+ T cell responses in the lymph node.* Immunity, 2013. **38**(3): p. 502-13.
 139. Malek, T.R. and I. Castro, *Interleukin-2 receptor signaling: at the interface between tolerance and immunity.* Immunity, 2010. **33**(2): p. 153-65.
 140. Boyman, O. and J. Sprent, *The role of interleukin-2 during homeostasis and activation of the immune system.* Nat Rev Immunol, 2012. **12**(3): p. 180-90.
 141. Mitchell, D.M., E.V. Ravkov, and M.A. Williams, *Distinct roles for IL-2 and IL-15 in the differentiation and survival of CD8+ effector and memory T cells.* J Immunol, 2010. **184**(12): p. 6719-30.

142. Hand, T.W., et al., *Differential effects of STAT5 and PI3K/AKT signaling on effector and memory CD8 T-cell survival*. Proc Natl Acad Sci U S A, 2010. **107**(38): p. 16601-6.
143. Kim, E.H., et al., *Signal integration by Akt regulates CD8 T cell effector and memory differentiation*. J Immunol, 2012. **188**(9): p. 4305-14.
144. Toma, G., et al., *Transcriptional Analysis of Total CD8(+) T Cells and CD8(+)CD45RA(-) Memory T Cells From Young and Old Healthy Blood Donors*. Front Immunol, 2022. **13**: p. 806906.
145. Pacheco, R., et al., *Glutamate released by dendritic cells as a novel modulator of T cell activation*. J Immunol, 2006. **177**(10): p. 6695-704.
146. Park, Y.H. and H.W. Nam, *Clinical features and treatment of ocular toxoplasmosis*. Korean J Parasitol, 2013. **51**(4): p. 393-9.
147. Hu, Y.Y., et al., *GLT-1 Upregulation as a Potential Therapeutic Target for Ischemic Brain Injury*. Curr Pharm Des, 2017. **23**(33): p. 5045-5055.
148. Du, J., et al., *Toxoplasma gondii virulence factor ROP18 inhibits the host NF- κ B pathway by promoting p65 degradation*. J Biol Chem, 2014. **289**(18): p. 12578-92.
149. Sha, L., et al., *Pharmacologic inhibition of Hsp90 to prevent GLT-1 degradation as an effective therapy for epilepsy*. J Exp Med, 2017. **214**(2): p. 547-563.
150. Peng, Y.C., et al., *Hsp90 β inhibitors prevent GLT-1 degradation but have no beneficial efficacy on absence epilepsy*. J Asian Nat Prod Res, 2019. **21**(9): p. 905-915.
151. Huang, W.Y., et al., *miR-124 upregulates astrocytic glutamate transporter-1 via the Akt and mTOR signaling pathway post ischemic stroke*. Brain Res Bull, 2019. **149**: p. 231-239.
152. Morel, L., et al., *Neuronal exosomal miRNA-dependent translational regulation of astroglial glutamate transporter GLT1*. J Biol Chem, 2013. **288**(10): p. 7105-16.